Department of Medicine and Surgery

PhD program in Neuroscience, XXXII Cycle

Curriculum in Experimental Neuroscience

The role of Neurofilament Light Chain as a serum biomarker in chemotherapy-induced peripheral neurotoxicity rat models

Candidate: **Dr. GIULIA FUMAGALLI**

Registration number: **730593**

Tutor: **Prof. Guido Cavaletti**

Coordinator: **Prof. Guido Cavaletti**

ACADEMIC YEAR: 2018/2019

TABLE OF CONTENTS

ABSTRACT

In last decades, the improvement in anticancer therapy permitted the increase in the treatment efficacy, but on the other side, serious side effects became evident. Among these, Chemotherapy Induced Peripheral Neurotoxicity (CIPN) is the most prevalent neurological complication.

CIPN is predominantly a sensory and length-dependent neuropathy: the damage arises at limb extremities with a distal to-proximal-progression. Each chemotherapy drug exerts a toxic activity targeting different structure of the peripheral nervous system: the axon and the neuronal cell body.

Nowadays the monitoring of CIPN onset and progression in treated patients represents an unmet clinical need: there is difficulty in performing a detailed neurological examination and there is the need for an early detection of CIPN in order to prevent permanent damage. At the moment no serum biomarkers are available.

Neurofilaments Light Chain (NfL) are the major intermediate filaments in neurons which are specifically expressed in axons. NfL are important for neuronal structural stability and they are released into the interstitial fluid and blood after damage of the axonal membrane.

Blood NfL concentration is useful for clinical diagnostic evaluation in neurological disorders such as Alzheimer's and Huntington's diseases, Amyotrophic Lateral Sclerosis and Multiple Sclerosis. A recent study indicated NfL as a marker of axonal damage in patients with Charcot Marie Tooth, an inherited neuropathy, reporting an increase of NfL concentration in serum.

The aim of this project was to study the axonal damage and to investigate NfL as a specific axonal damage biomarker for CIPN onset and progression in preclinical models.

Among the conventional drugs associated to CIPN, cisplatin (CDDP), paclitaxel (PTX) and vincristine (VCR), which belong respectively to the platinum, taxanes and vinca alkaloids

classes of anticancer drugs, were studied. These drugs have different putative targets involved in the establishment of CIPN (dorsal root ganglia for CDDP and axons for PTX and VCR).

In order to pursue the aim, two different protocols were performed.

In the first study, female Wistar rats were divided in CTRL arm, which remained untreated, CDDP- (2 mg/kg i.p 2qwx4 ws) and PTX- (10 mg/kg i.v q7dx4 ws) treated groups.

At the end of the treatment, neurophysiological analyses were performed and morphological analyses were conducted on collected peripheral nerves. An important nerve degeneration and fiber loss were demonstrated in caudal nerves of PTX-treated animals compared to CTRL and CDDP-treated ones. Moreover, the analysis of caudal nerves demonstrated that the damage was more severe at distal level progressing from distal to proximal level in accord with the length-dependent features of CIPN.

Regarding CDDP-treated rats, a milder axonopathy was detected. Furthermore, PTX-treated group showed a massive macrophage infiltration in the caudal nerves whereas it was absent in CDDP-treated animals.

Interestingly, NfL quantification in serum samples collected at the end of treatment showed a significant increase of their concentration only in PTX-treated animals, according to the more severe axonal damage, whereas the levels of NfL in CDDP ones remained similar to the CTRL arm.

Given these interesting results, a second experiment using PTX- (10 mg/kg i.v q7dx4 ws) and VCR- (0.2 mg/kg i.v. q7dx4 ws) treated animals was performed. In particular, the aim of this second experiment was to assess a weekly time course in order to compare the progression of CIPN pathology and the serum NfL concentration. The analyses and sample collection were performed at different weekly time points and at the end of treatment.

Morphological and neurophysiological investigations indicated a length-dependent damage progression during the weeks of treatment in both PTX- and VCR-treated groups. The loss of

fibers was more important in PTX-treated group from the second week of treatment until the end of treatment, in particular at distal level. After 4 weeks of treatment, also VCR-treated group evidenced a severe damage in nerves.

In addition, a more abundant macrophage infiltration was detected in caudal nerves of PTX-treated animals at each time point compared to VCR ones.

These results were correlated with the progressive increase of NfL concentration during the weeks of treatment, which was anyway higher in PTX-treated animals compared to VCR ones, according to the more severe axonal damage.

In conclusion, PTX-treated animals presented a higher axonal damage compared to VCR-treated group, which was length-dependent according to CIPN pathophysiology. NfL concentration in serum samples of PTX- and VCR-treated groups correlated with the progression of the damage, although the levels were higher in PTX-treated one. NfL concentration in CDDP-treated animals was comparable to the CTRL arm.

These results demonstrated that NfL dosage may be used as an important serum biomarker for monitoring CIPN pathology and for an early detection in order to prevent severe damage.

INTRODUCTION

1. CHEMOTHERAPY INDUCED PERIPHERAL NEUROTOXICITY (CIPN)

In the last few years, the improvement in anticancer therapy permitted the increase in the treatment efficacy, but on the other side, serious side-effects became evident. Among these, CIPN is the most prevalent neurological complication and it affects most of the patients exposed to cancer treatment (Velasco et al., 2010; Cavaletti et al., 2015a; Cavaletti et al., 2015b).

In particular, the anticancer drugs associated to CIPN are commonly used for breast, colorectal, head and neck, lung, ovarian, hematological and testicular cancer (Park et al., 2013).

Several clinical features are related to the use of different anticancer drugs, which have a different chemical structure and mechanism of action. The antineoplastic drugs commonly associated to CIPN include: the platinum derivatives (like cisplatin, oxaliplatin and carboplatin), the vinka alkaloids (vincristine and vinblastine), the taxanes (paclitaxel and docetaxel), the proteasome inhibitors (bortezomib and carfilzomib), the epothilones (ixabepilone) and immunomodulatory drugs (thalidomide) (Wolf et al., 2008; Brewer et al., 2016). These drugs are summarized in **Tab 1**.

Drug name	Type of cancer treated	Mechanism of action	Neuropathy incidence
Platinum-based drugs	Lung, ovarian, bladder, germ cells, testicular, colorectal cancer.	Cancer cell DNA-cross-linking.	70-100 %
Taxanes	Breast, ovarian, lung, prostate, pancreatic cancer.	Cancer cell microtubule formation impairment.	11-87 %
Thalidomide and its analogs	Multiple myeloma.	Antiangiogenesis, immunomodulation.	20-60 %
Ixabepilone	Breast cancer.	Tubulin malformation.	60-65 %

Bortezomib	Multiple myeloma.	Proteasome inhibition.	20-30 %
Vinca alkaloids	Lung, brain, bladder, testicular cancer.	Cancer cell microtubule formation.	Up to 20 %

Tab. 1. Characteristics of neurotoxicity-inducing drugs routinely used in clinical practice (Banach et al., 2016).

CIPN can be characterized by severe and long lasting symptoms, which may affect patient daily activities and impact on the quality of life, leading to anticancer treatment modification or even withdrawal, and may affect overall survival (Miltenburg et al., 2014; Carozzi et al., 2015; Cavaletti et al., 2015; Cavaletti et al., 2015b).

CIPN is predominantly a sensory and length-dependent neuropathy: the symptoms include numbness, sensory loss, tingling, pins and needles sensation, "stocking-and-glove" distribution characterized by hyperalgesia or allodynia in hands or feet and neuropathic pain. Neuropathy may significantly impacts patient daily activities: for example difficulty in buttoning up their clothes due to the lack of correct touch sensation or inability to take items from the fridge because of cold hypersensitivity (Hopkins et al., 2016).

The damage is usually dose-dependent, it begins at limb extremities and then progresses from the distal to the proximal region according to the pathophysiology of a length-dependent neuropathy (Carozzi et al., 2014; Seretny et al., 2014; Brewer et al., 2015).

Sometimes symptoms may persist or even develop few months after the discontinuation of the chemotherapy: this phenomenon is called coasting (Stillman et al., 2006).

Rarely there can be a damage of motor fibers, which may results in a motor neuropathy, or an autonomic impairment (Argyriou et al., 2012; Cavaletti et al., 2015).

The main clinical features of CIPN are summarized in **Table 2.**

Drug	Typical Symptoms/Signs
Platinum	
Cisplatin	Early reduction/loss deep tendon reflexes. Distal, symmetric, upper- and lower-limb impairment/loss of all sensory modalities. Sensory ataxia and gait imbalance are frequent. Neuropathic pain can be present, but is it not frequent. Coasting phenomenon is frequent.
Carboplatin	Similar to cisplatin but milder.
Oxaliplatin	**Acute:** cold-induced transient paresthesias in mouth, throat and limb extremities; cramps/muscle spasm in throat muscle, jaw spasm. **Chronic:** very similar to cisplatin.
Bortezomib	Reduction/loss deep tendon reflexes. Mild to moderate, distal symmetric loss of all sensory modalities occurs. Small myelinated and unmyelinated fibers are markedly affected, leading to severe neuropathic pain. Mild distal weakness in lower limbs is possible.
Taxanes (paclitaxel, docetaxel)	Reduction/loss deep tendon reflexes. Myalgia syndrome is frequent (as an atypical neuropathic pain?). Distal, symmetric, upper- and lower-limb impairment/loss of all sensory modalities. Gait unsteadiness is possible because of proprioceptive loss. Distal, symmetric weakness in lower limbs is generally mild.
Epothilones (epothilone, ixabepilone, sagopilone)	Signs and symptoms are similar to taxanes, but neuropathic pain is less frequent, and recovery is reportedly faster.
Vinca alkaloids (vincristine, other compounds)	Reduction/loss deep tendon reflexes. Neuropathic pain/paresthesia at limb extremities is relatively frequent. Distal, symmetric, upper- and lower-limb impairment/loss of all sensory modalities.

	Distal, symmetric weakness in lower limbs progressing to foot drop.
	Autonomic, symptoms may be severe.
Thalidomide	Reduction/loss deep tendon reflexes.
	Relatively frequent neuropathic pain at limb extremities.
	Mild to moderate, distal, symmetric loss of all sensory modalities.
	Weakness is rare.

Tab. 2. Typical clinical features of CIPN associated with conventional chemotherapy (Cavaletti et al., 2015).

The toxic activity of chemotherapy drugs targets different structures of the peripheral nervous system (PNS): the axon (length-dependent axonopathy) or cell body of dorsal root ganglia (DRG) neurons (neuronopathy) (Carozzi et al., 2015).

The major susceptibility to the action of noxious exogenous agents of PNS is due to a low efficiency in the action of the blood-nervous tissue barrier and the complexity of the processes involved in peripheral nerve repair and regeneration (Allodi et al., 2012).

In particular, DRG are characterized by the presence of fenestrated capillaries and for this reason they are more sensitive to circulating molecules and constitute the major drugs entry site in PNS (Englander, 2013; Cavaletti et al., 2015).

Chemotherapy drugs predominantly affect large myelinated fibers, but also small myelinated or unmyelinated fibers could be involved, depending on the drug employed (Starobova and Vetter, 2017).

The mechanism of action of antineoplastic drugs is relatively understood, whereas the mechanisms of axonal and nerve cell damage remain unclear. Several neurotoxic mechanisms have been proposed: mitochondrial damage, impairment of axonal transport, oxidative stress, and the involvement of transporters (Canta et al., 2015; Cavaletti et al., 2015; Starobova and Vetter, 2017).

Recent findings make neuroinflammation an attractive target responsible for the symptoms of CIPN. In fact, pro-inflammatory cytokines play an important role in symptoms of peripheral neuropathic pain and hyperalgesia. For example, in rat models of constriction injury, the axonal damage leads to an inflammatory reaction and consequently to neuropathic pain (Bennet et al., 2000). In particular, inflammatory cells as macrophages infiltrate the site and also an increase in inflammatory cytokines occurs (Cleeland et al., 2003). In different rodent models, the pain is associated to a pro-inflammatory immune response when animals are treated with chemotherapy agents including taxanes and vinca alkaloids (Lees et al., 2017).

Other clinical and genetic factors may increase the risk of CIPN onset and its severity: the specific antineoplastic drug used, the duration of exposure, cumulative dose, pre-existing history of neuropathy, combined therapies and genetic polymorphisms (Kerckhove et al., 2017).

Also age, sex (female), race (black), history of diabetes, obesity, physical inactivity and metastatic versus non metastatic cancer represent other possible associated risk factors (Bakogeorgos and Georgouilias, 2017; Kim and Johnson, 2017).

Therefore, CIPN pathophysiology is still under investigation. The use of laboratory models is needed to understand the mechanisms and to investigate any possible preventive and treatment strategies (Stillman et al., 2006; Flatters et al., 2017).

In this project, studies with three different agents (cisplatin, paclitaxel and vincristine) belonged respectively to platinum compounds, taxanes and vinca alkaloids were analyzed.

1.1 Cisplatin (CDDP)

CDDP (cis-dichlorodiammineplatinum II) is the first developed platinum-based drug for chemotherapy. Its clinical experimentation stared in 1972 with The National Cancer Institute (NCI) and it was then approved by the Food and Drug Administration (FDA) for the treatment of urogenital tumours in 1978.

CDDP is mostly used for testicular, ovarian, small cell lung, bladder, stomach, and head and neck cancers (Rabik et al., 2007).

CDDP has a central platinum ion surrounded by 4 ligands, 2 amino and 2 hydrochloric acid groups (Fig.1). It is an alkylating agent (Renshaw and Thomson, 1967; Howle and Gale, 1970; Drobnik et al., 1973) that induces apoptosis in cancer cells forming platination adducts: it binds proteins and DNA, interacting with endogenous nucleophiles sites of purine bases and forming inter-strand and intra-strand DNA-protein and DNA-DNA crosslinks (Maheswari et al., 2000; Podratz et al., 2010; Butler et al., 2013; Üstün et al., 2018).

Among the main toxicities of CDDP (nephrotoxicity, severe nausea, vomiting, neuropathy and ototoxicity), neurotoxicity is the main side effect and a dose-limiting factor (Miltenburg et al., 2014). Neurotoxicity is due to the accumulation of CDDP in the DRG which results in large myelinated axon degeneration and nerve fiber axonopathy (Sharawy et al., 2015).
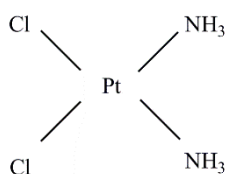

Fig.1. Cisplatin (Carozzi et al., 2015)

1.2 Paclitaxel (PTX)

In 1960 the NCI started a screening program in order to find new and effective anticancer drugs. After 22 years, PTX entered clinical trials and demonstrated good cytotoxicity activity and was finally approved by the FDA for treatment against ovarian and breast cancers (Kampan et al., 2015).

PTX is a taxane-derived antineoplastic agent principally used for lung, breast and ovarian cancers. PTX consists of two molecules: a taxane ring with a four-membered oxetane side ring at positions C4 and C5 and a homochiral ester side chain at C13 (Fig.2).

Normally, microtubules undergo a process of dynamic instability, which consists in depolymerization and repolymerization. PTX is a microtubule-binding drug, in particular, it binds to the heterodimer β-tubulin and it arrests cell cycle in the G_0/G_1 and G_2/M phases stabilizing microtubules and suppressing dynamic instability. In dividing cells, such as proliferating cancer cells, this loss of dynamicity interferes with mitosis and leads to apoptosis (Gornstein et al., 2013; Dugget et al., 2016; Gornstein et al., 2016).

Neurons are not dividing cells, but they are nevertheless vulnerable to PTX. Indeed, the treatment with PTX affects the peripheral nervous system leading to a sensory axonal neurotoxicity, but the mechanisms involved are not completely understood (Carozzi et al., 2015).
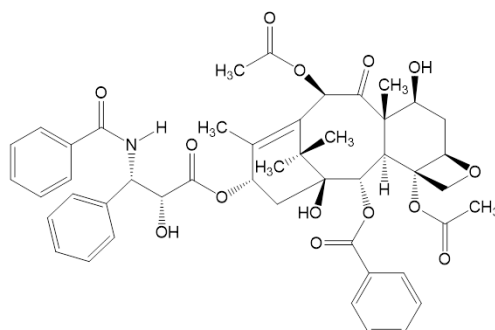

Fig.2. Paclitaxel (Carozzi et al., 2015)

1.3 Vincristine (VCR)

VCR (Fig.3) belongs to vinca alkaloid family, a class of agents derived from the plant Catharanthus roseus (Van de Velde et al., 2017), which has been gradually applied in the treatment of various tumors since 1963 (Yang et al., 2015). VCR is used for a variety of hematologic cancers such as Hodgkin's lymphoma, non-Hodgkin's lymphoma and leukemia (Khalilzadeh et al., 2018). VCR arrests dividing cells in metaphase: its mechanism of action consists in preventing the polymerization by binding to the β-subunit of tubulin heterodimers. These subunits are also components of nerve fiber axons underling the correlation with the establishment of neurotoxicity (Mora et al., 2016).

VCR clinical use is characterized by three categories of dysfunctions: sensory, motor, and autonomic neuropathy.

The most common side effects are peripheral sensory and motor nerve neuropathy characterized by numbness, paresthesia, impaired balance, weakened tendon reflexes, and altered gait. Otherwise, autonomic dysfunctions including constipation, paralytic ileus, urinary retention and orthostatic hypotension can occur (Madsen et al., 2019).
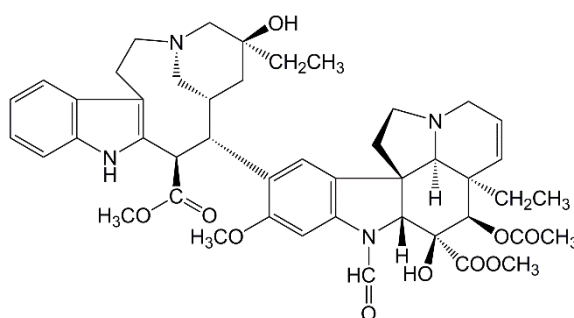

Fig.3. Vincristine (Carozzi et al., 2015)

1.4 Clinical need: assessment and monitoring CIPN

Neuroaxonal damage and loss result in severe or in some cases permanent disability. Grading of CIPN still represents an unmet clinical need: it is therefore important to assess CIPN in a simple and effective reproducible manner.

Usually the assessment method is based on objective and subjective evaluations. Objective assessment includes a bedside clinical examination and nerve conduction studies (NCS) in order to reveal sensory or motor abnormalities. However, these observations have some limitations.

For example, conventional NCS is useful to evaluate CIPN onset, but it only gives information about the involvement of large myelinated fibers whereas it does not detect any alteration in small fibers (Themistocleous et al., 2014).

An emerging and promising diagnostic tool is represented by the magnetic resonance neurography, which allows to visualize axonal alteration and demyelination (Wessig et al., 2011).

Recently, subjective evaluations are used in order to classify the patient perception of CIPN severity in neurotoxicity grading scales such as the National Cancer Institute Common Toxicity Criteria scale and the Eastern Cooperative Oncology Group scale (Cavaletti et al., 2010; Miltenburg and Boogerd, 2014).

These scales are simple to use but they usually underestimate the severity and the frequency of symptoms and therefore, they are not satisfactory for evaluating CIPN (Cavaletti et al., 2010).

Other scales combine both clinical assessments and neurophysiological parameters: for example, the Total Neuropathy Score combines observations from grading of symptoms, signs, nerve conduction studies, and quantitative sensory tests, providing a single measure to quantify neuropathy (Cornblath et al., 1999).

However, scales composed by objective and subjective items are not always unambiguously described and they lead to a variable interpretation.

Different self-reported questionnaires (Patient Reported Outcome Measures, PROM) have been developed and they seem to overcome the limitation of the patient interview, being more accurate and sensitive compared to the clinician-reported ones (Hershman et al., 2011; Alberti et al., 2014).

However, better instruments are required in order to overcome the evidence in underestimate the severity and frequency of CIPN and these methods need to achieve simplicity, responsiveness, reproducibility and meaningfulness (Cavaletti et al., 2010). The ability to readily detect and supervise such damage would be an important advantage in the assessment of disease activity and in monitoring treatment response and prognosis. In view of this scenario, the possible use of a biomarker able to reflect axonal injury would be useful for reaching individual therapeutic decisions and monitoring drug effects in clinical trials.

The possible use of cerebrospinal fluid (CSF) proteins MRI and metabolic imaging have been involved despite several limitations (Khalil et al., 2018).

Neurofilaments (Nfs) are gaining increasing attention as a possible biomarker of neuroaxonal injury.

1.5 Biomarkers

A biomarker is defined by the World Health Organization as "any substances, structure or process that can be measured in the body or its products and influence or predict the incidence or outcome disease" (World Health Organization, 2001; Diaz et al., 2018).

In order to identify and monitor disease activity, the use of biomarkers in clinical practice may be useful. Some biomarkers are specific proteins, which are released in blood or CSF after tissue damage. For example, the presence of high protein concentration in CSF may

represent the first diagnostic biomarker for Guillain-Barre syndrome (GBS) (Jacobs and Willison, 2009).

Recently, studies indicated that the levels of glial protein markers S100-B and glial fibrillary acidic protein (GFAP) were higher in CSF of patients with GBS. In fact, GFAP is a cytoskeletal protein expressed in Schwann cells which expression is increased after Wallerian degeneration. Moreover, elevated concentration of tau protein was associated with poor outcomes (Notturno et al., 2008; Petzold et al., 2009).

In a recent study, Trostchansky suggested that lipid products can be dosed in blood and used as prognostics indicators of ALS due to their high presence at CNS and their capacity to cross the blood brain barrier (Trostchansky, 2019).

Vakilian and colleagues indicated that plasma levels of the enzyme BACE1 might be a valuable blood-based biomarker to use in preference to other invasive diagnostic methods such as CSF analysis in patients with Alzheimer Disease (Vakilian et al., 2019).

In recent years, studies regarding the pharmacogenomic approach have been conducted in order to obtain a possible marker for identifying patients at high or low risk of CIPN development. Different genes have been identified on the basis of mechanistic hypotheses relevant to cancer cells. In particular, genes involved in drug distribution, metabolism and detoxification, DNA repair and cancer-cell resistance have been studied (Cavaletti et al., 2011).

Among the studied genes, different polymorphisms in GSTP1, GSTM1, GSTM3, ERCC1, AGXT, ABCB1, CYP2C8, CYP3A5 and ITGB3 genes were found to be correlate with CIPN assessment and severity (Cavaletti et al., 2011; Cliff et al., 2017). Moreover, Argyriou and colleagues reviewed several studies and indicated specific genes for each chemotherapy treatment: CCNH, XRCC1, SCNA and TAC1 genes in platinum-related CIPN; PKNOX1, CBS and CYP17A1 genes in bortezomib-related CIPN; ABCB1, TUBB2A, GPR177 and

ERPHA genes in taxane-related CIPN; and CEP72 in vincristine-related CIPN (Argyriou et al., 2017). Despite the efforts in the identification of reliable risk factors for the development of severe CIPN, the prediction of neurological course is still an unmet clinical need. In fact, these collected data are inconsistent: most biomarkers are supported by a single study or have conflicted evidence regarding their efficacy. Therefore, there is the need of a methodological improvement in clinical trials to obtain reliable results.

Cavaletti and colleagues investigated the rate of a soluble factor, the nerve growth factor (NGF), which belongs to neurotrophin family, in plasma of rats treated with CDDP. Using a commercially available ELISA kit, they observed relevant changes in NGF circulating levels of CDDP-treated animals, which decreased during the treatment (Cavaletti et al., 2002a). In another work conducted on rats treated with two different doses of oxaliplatin, they showed a dose-dependent reduction of NGF levels in plasma (Cavaletti et al., 2002b).

In a further study with plasma samples of patients treated with CDDP or PTX, a decrease of NGF levels compared to baseline values was detected. Moreover, NGF levels were correlated with CIPN severity. Although these interesting results, NGF levels were not efficient predictors of the final patient outcome (Cavaletti et al., 2004).

In contrast with these precedent works, Velasco and collaborators reported a change of NGF levels in serum of CIPN patients. However, in this case, CDDP- and PTX-treated patients with worse CIPN presented higher NGF serum levels (Velasco et al., 2017).

Currently, no blood biomarkers are available for a reliable assessment and detection of peripheral nerve damage, particularly in CIPN (Jacobs and Willison, 2009). Serum parameter could be an important indicator due to its feasibility as a routine test (Velasco et al., 2017).

2. NEUROFILAMENTS

The neuronal cytoskeleton is composed by three structures: the actin microfilaments, microtubules and intermediate filaments. In particular, intermediate filaments (Ifs) are neuron specific proteins with a 10 nm diameter, which have an important role in supporting the axon and dendrite outgrowth, stabilization and function. Neurons express different If proteins classified on the basis of their developing stage or their localization in the nervous system. Among them, the α-internexin is expressed more abundantly during the development of the nervous system and persists during the adult stage of neurons in cerebellum, whereas peripherin is expressed in lower motor, autonomic and sensory neurons. Neurofilaments (Nfs) become the major components of the mature neuronal cytoskeleton both in CNS and PNS (Al-Chalabi et al., 2003; Perrot et al., 2008; Perrot et al., 2009).

Nfs are particular abundant in axons where they have a critical role in increasing the axonal caliber of myelinated axons and consequently they are essential for electrical impulse transmission and for nerve conduction velocity (Yuan et al., 2012).

Neurofilament subunits are classified according to their molecular weight in Nf light (NfL, 68 kDa), Nf medium (NfM, 160kDa) and Nf heavy (NfH, 205 kDa) (Perrot et al., 2008).

In the CNS, Nfs are therefore composed by the co-assemble of NfL, NfM, NfH with α-internexin which is replaced in the PNS by peripherin (Yuan et al., 2012) (Fig. 4a).

As all If proteins, all the types of Nfs share a common structure with a non-helical amino and carboxy-terminal regions (the head and tail domains) and a central α-helical rod domain composed of about 310 amino acids. This central rod domain contains highly conserved motifs, which are characteristic for each Nf subtype and essential for assembly, while head and tail domains are less conserved. The head domain is short and characterized by the presence of Ser and Thr. The tail domain allows to identify the Nf proteins: NfL has a short

tail domain with many glutamic acid residues, while NfM and NfH have a longer one, with also several phosphorylation sites Lys-Ser-Pro (Al-Chalabi et al., 2003; Perrot et al., 2008).

In order to obtain the final 10 nm intermediate filament, the first step is the dimerization of NfL with NfM or with NfH. The association of their rod domains forms a tetramer structure, which can exist in two forms: NfL-NfM and NfL-NfH (Heins et al., 1993; Cohlberg et al., 1995). The combination of tetramers forms protofilaments, which finally constitute the If (Perrot et al., 2008) (Fig.4b).

Therefore, NfL is essential for the assembly of Nfs and constitutes their core. NfM and NfH are around this core and with their tail domains form lateral projections which are important for the formation of cross-bridges and for the stabilization of the filament network. In particular, NfH is also important for the interaction with the other cytoskeletal elements (Hirokawa et al., 1984; Hisanga et al., 1988; Al-Chalabi et al., 2003).

Nfs are exposed to several post-translational modifications such as phosphorylation, glycolisation, nitration, oxidation and ubiquitylation. In particular, phosphorylation is the most important and it regulates Nf function in a dynamic way. The amino-terminal head domains and the carboxy-terminal domains are the phosphorylation sites and this post-translational modification could regulate the Nf assembly. Indeed, the phosphorylation by protein kinase A (PKA), protein kinase C (PKC) and protein kinase N (PKN) of NfL and NfM head domains prevents the assembly or leads to the disassembly (Al-Chalabi et al., 2003; Perrot et al., 2008).

Nf could be degraded by non-specific proteases like lysosomal cathepsin D, trypsin and α-chemotrypsin, but also post-translational modifications can regulate proteolysis of Nf. The most important role in the degradation of Nf is represented by calcium activated proteases which show specificity with If. Many pathological states induce an increase of free calcium within the axon leading to a massive proteolysis of Nfs (Nelson et al., 1982; Perrot et al.,

2008). In normal conditions, Nfs are highly stable and their turnover is low. Indeed, abnormal

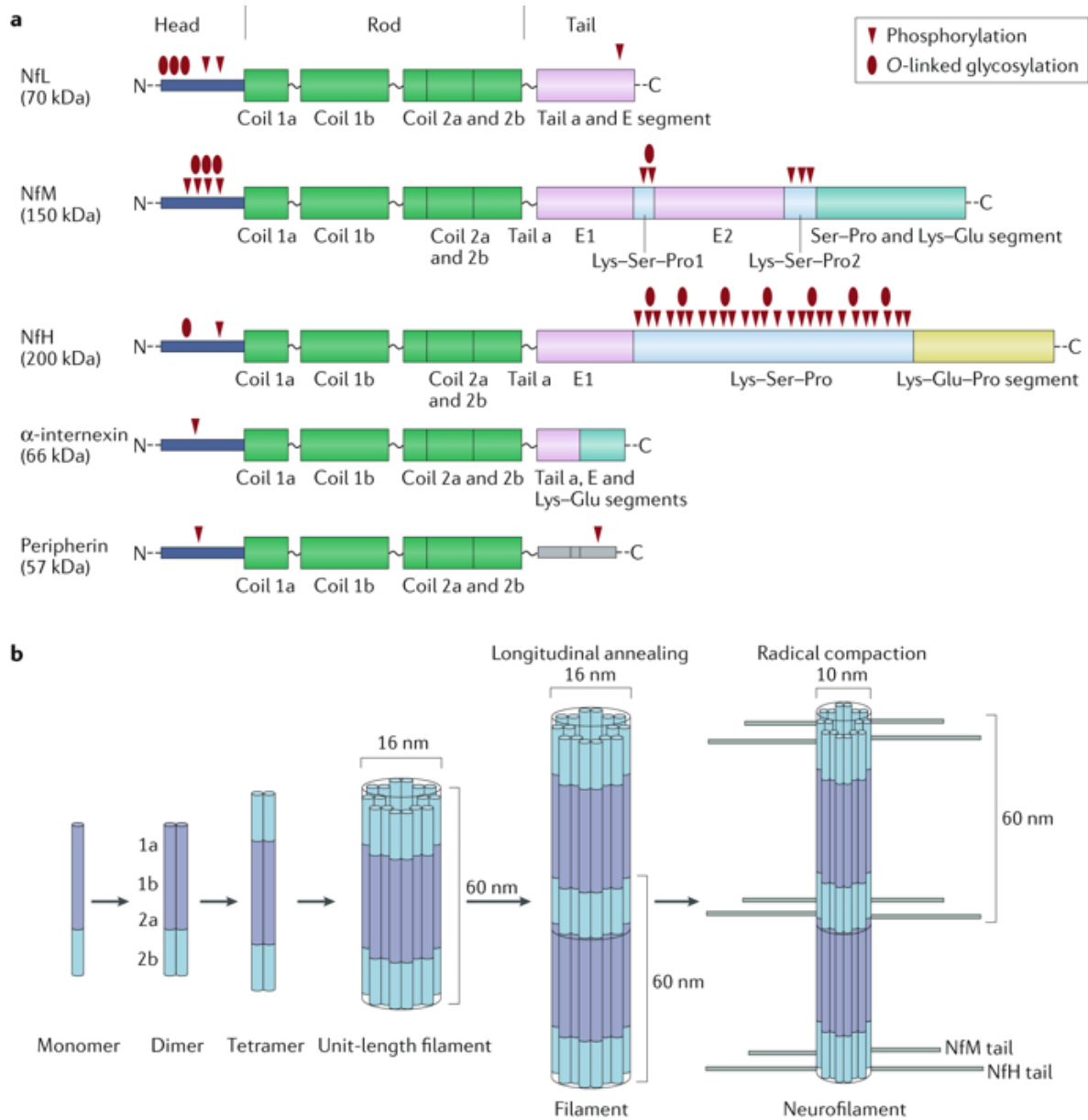Nf accumulations are found in several neuropathological diseases.

Fig.4. Structure and assembly of Neurofilaments. a) Domain structure of Neurofilament subunits. b) Neurofilament assembly (Khalil et al., 2018).

2.1 Nf as an axonal damage biomarker

The emerging concept of the possible use of Nfs as biomarkers in neuroaxonal injury is due to their exclusively expression in neurons and their abnormal accumulation as a result of axonal damage in several diseases. Indeed, many pathological processes are characterized by the release of Nf into the extracellular fluid, CSF and peripheral blood and consequently, an abnormal accumulation of Nf is a pathological hallmark (Khalil et al., 2018).

The measurement of Nf concentration is useful for clinical diagnostic evaluation in neurological disorders of the CNS such as Alzheimer's, Huntington's and Parkinson's diseases, ALS and Multiple Sclerosis (Perrot et al., 2009; Novakova et al., 2017; Khalil et al., 2018).

Several works indicated the association of NfL concentration between CSF and serum samples of patients with ALS, Alzheimer's disease and GBS. CSF and serum measurements were highly correlated supporting the feasibility of quantifying NfL both in CSF and serum samples as a measure of axonal injury (Gaiottino et al., 2013; Lu et al., 2015). This strong correlation between CSF and blood NfL suggests that blood NfL is a valid surrogate marker for CSF NfL, due to the redistribution of the NfL protein trough the blood-brain barrier (Lu et al., 2015).

Kucharz and colleagues showed that monitoring NfL levels in CSF and plasma of animal models of Huntington's disease may be a valid biomarker. The NfL levels in CSF were 9-fold higher than in serum, confirming the CNS origin of the serum NfL (Soylu-Kucharz et al., 2017).

Also in patients with Multiple Sclerosis, CSF NfL concentration was associated with the number of lesions evidenced by the MRI and interestingly, NfL concentration decreased after the therapy, indicating an important role of the biomarker in monitoring the course of the disease (Novakova et al., 2017).

Less is known about biomarkers for PNS. Recently, Sandelius and colleagues published the results of a study conducted on patients affected by demyelinating and axonal forms of an inherited neuropathy (Charcot-Marie-tooth disease, CMT). In this work plasma NfL concentration was used in order to validate NfL as a potential biomarker in this peripheral neuropathy. They reported an increase of plasma NfL concentration in patients with CMT compared to age-matched healthy controls (Sandelius et al., 2018), (Fig.5).
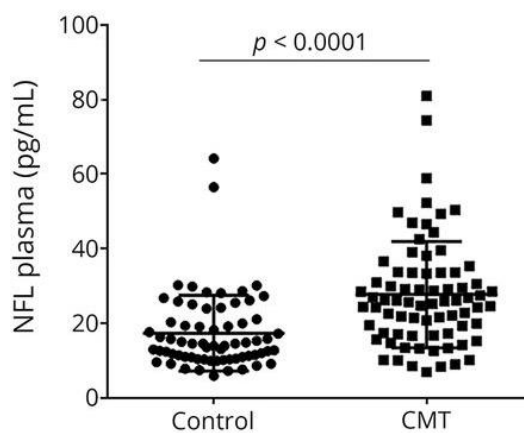

Fig.5. Plasma NfL concentration in patients with Charcot-Marie-tooth (CMT). The graph indicates an increase of plasma NfL concentration in patients affected by CMT compared to the control group (Sandelius et al., 2018).

2.2 NfL detection

NfL is the most abundant component of Nf and it is also the most soluble subunit. Kuhle and colleagues compared two highly sensitive assays in order to measure the two subunits of the Nf: the NfL and NfH. They demonstrated a better performance of NfL in discriminating patients with Multiple Sclerosis from control, compared with the assay for NfH detection (Kuhle et al., 2013). Moreover, an advantage in the use of NfL compared to NfH was observed in ALS samples: a potential inconsistent result due to the aggregation of NfH was found in measuring plasma whereas it was not detected in NfL quantification. NfH plasma concentration showed also a decline as the disease advanced, whereas blood NfL levels in ALS samples were significantly higher and maintained a correlation with the temporal course of the pathology (Gaiottino et al., 2013; Lu et al., 2014).

In the past three decades, several studies were conducted in order to develop sensitive immunoassay technologies for Nf detection (Fig.6). First-generation immunoassays were semi-quantitative and based on electrophoretic protein separation. They reliably demonstrated the presence of Nf in CSF and blood of different diseases (Petzold, 2005).

The sandwich ELISA technology belongs to the second-generation assays. It produced quantitative data of NfH and NfL concentration in CSF and also in serum and plasma, but they highlighted the need for improved assay standardization (Norgren et al., 2003; Petzold et al., 2003).

The electrochemiluminiscence (ECL) technology is a third-generation assay and represented an important improvement in analytical sensitivity. In fact, ECL based assays are highly sensitive and require a very small sample volume (Khule et al., 2017).

Only the introduction of single-molecule-assay (Simoa) has permitted the detection of NfL in blood samples across a whole range of concentrations. Simoa technology is a fourth-generation technology. In Nf quantification it is 126-fold and 25-fold more sensitive than ELISA and ECL assays respectively. This method is based on single-molecule arrays and it allows the counting of singulated capture microscopic beads that carry the sandwich antibody complexes (Kuhle et al., 2016; Disanto et al., 2017; Khalil et al., 2018).

Simoa restricts the analysis in femtoliter-sized wells whereas the analog immunoassays perform the reaction in relatively large volume (50-100 µl). A camera detects active or inactive wells, which correspond to the presence or absence of single enzyme molecules. This greater sensitivity allows the use of low quantities of labeling reagent which decreases nonspecific interactions (Kuhle et al., 2016). Simoa assay will be described in detail in *Materials and Methods* section.
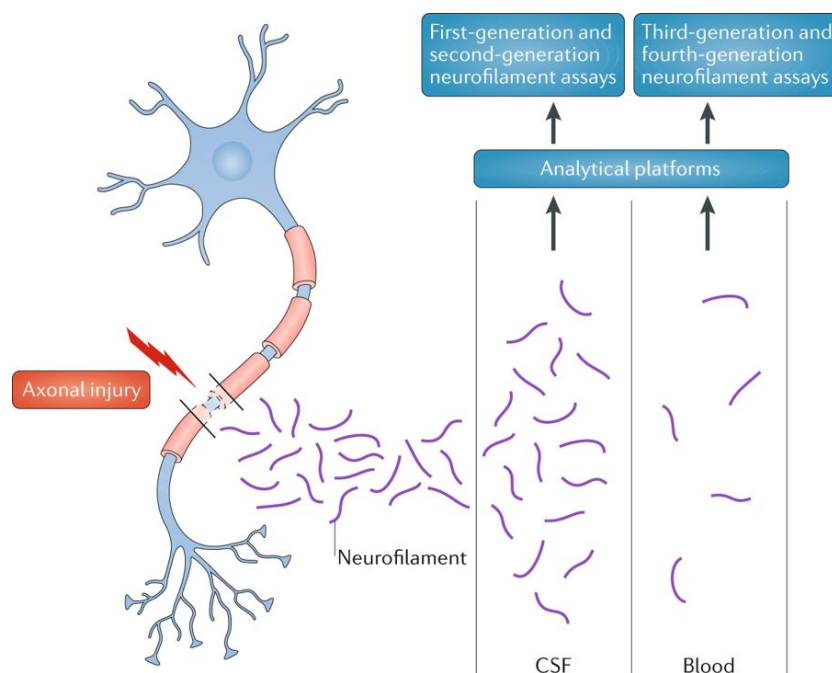

Fig.6. Neurofilament release and detection. First-generation (immunoblots) and second-generation (ELISA) assays can detect neurofilaments in CSF but have limited sensitivity for detection in the blood. Third-generation (ECL) and in particular fourth-generation (Simoa) assays can reliably measure NfL blood levels and they are able to detect a whole range of concentrations (Khalil et al., 2018).

AIM OF THE WORK

The possible use of NfL as a biomarker in neuroaxonal injury is due to its exclusive expression in neurons and its abnormal accumulation as a result of axonal damage in several diseases. The measurement of NfL concentration in blood or CSF is useful for clinical diagnostic evaluation in neurological disorders of the CNS, whereas less is known about biomarkers for PNS.

The ability to readily detect and supervise axonal damage would be an important advantage in the assessment of CIPN activity and in monitoring treatment response and prognosis.

Therefore, the aim of this study was to investigate the possible role of serum NfL as an axonal damage biomarker in preclinical models of peripheral neuropathies induced by different anticancer drugs. In particular, the attention has been focused on CDDP, PTX and VCR, which have different putative targets involved in the onset of the pathology.

SKILLS

Before undergoing the experiments for this work, during my PhD program I have acquired important skills necessary to perform animal studies. In particular, I took part in different experimental studies which gave arise to several publications such as "Ghrelin agonist HM01 attenuates chemotherapy-induced neurotoxicity in rodent models" (attached at the end of this thesis).

In this paper, we used HM01, a synthetic, brain penetrable, non-peptidic, ghrelin receptor agonist in different animal models of chemotherapy-induced neurotoxicity. Several studies have demonstrated that ghrelin can inhibit activation of microglia and secretion of proinflammatory cytokines, both processes involved in the development and maintenance of neuropathic pain in animal models.

In this work, three antineoplastic agents for the development of CIPN were used: cisplatin and bortezomib in rat models and oxaliplatin in a mouse model. The positive effects of HM01, administered per os at doses of 3‑30 mg/kg, showed that cisplatin-induced mechanical hypersensitivity was significantly reduced by HM01. In the preventive setting, HM01 blocked bortezomib-induced hyperalgesia and intraepidermal nerve fiber density (IENFD) reduction at all doses tested. In the therapeutic setting, significant effect was observed, but only at the highest dose. Moreover, the animals treated with bortezomib alone showed a reduction in fiber density while the co-administration of HM01 prevented this loss.

In the oxaliplatin model, HM01 prevented the decrease in nerve conduction velocity and attenuated the reduction in IENFD.

In this work I have dealt with the animal manipulation, in particular I have performed several drug administrations (intraperitoneally, intravenously and gavage administrations). I have participated in neurophysiological investigations and in sample collection procedure. I have

also dealt with the preparation of semithin sections of nerve samples in order to perform morphometric and morphological analyses.

MATERIALS AND METHODS

1. ANIMALS AND HUSBANDRY

All the procedures were approved by Animal Care and Use Committee of the University of Milano-Bicocca. The experiments were performed in conformity with the institutional and governmental guidelines for humane treatment of laboratory animals set forth in the Guide for the Care and Use of Laboratory Animals (Office of Laboratory Animal Welfare) as well as with the Italian D.L.vo n. 26/2014 and the European Union directive 2010/63/UE.

Adult female Wistar rats (n= 8, 12 or 14 per group, 175-200 g at the beginning of the study, Envigo, Udine, Italy) were assigned to control or treated groups on the base of neurophysiology studies in order to ensure homogeneity.

The animals were housed 2/3 per cage in a certified and limited access animal facility under constant temperature (21 °C $\pm$ 2) and humidity (50% $\pm$ 20). Artificial lighting provided a 12 h light/12 h dark (7 a.m.–7 p.m.) cycle. Animal health condition was monitored daily and the body weight was recorded twice a week. Animals were sacrificed under deep anesthesia with CO_2 in order to collect samples.

2. DRUG AND FORMULATIONS

CDDP (Accord Healthcare Limited, Middlesex, UK) was dosed in saline solution at 2 mg/kg and administered intraperitoneally (i.p., 1 ml/kg) two times a week for 4 weeks.

PTX (LC laboratories, Woburn, MA, USA) was formulated in 10% Tween80, 10% EtOH 100% and 80% saline solution and injected at 10 mg/kg intravenously (i.v., 1 ml/kg) once a week for 4 weeks.

VCR (TEVA Pharma B.V., Mijdrecht, Netherlands) was prepared in water and injected at 0.2 mg/kg intravenously (i.v., 1 ml/kg) once a week for 4 weeks. All dosing solutions were made fresh on each administration day.

3. EXPERIMENTAL DESIGN

3.1 Study 1

In the first study, 24 rats were assigned to three different groups of 8 rats each: control group (CTRL) which remained untreated, CDDP-treated group which received 2 mg/kg CDDP (i.p.) two times a week for 4 weeks and PTX-treated group which received 10 mg/kg PTX (i.v.) once a week for 4 weeks.

At the end of treatment, neurophysiological studies, behavioral test (Dynamic Aesthesiometer Test) and sample collection (tissue and blood) were performed.

3.2 Study 2

A second study was performed in order to investigate the time course of the pathology in PTX- and VCR-treated rats. In this second experimental design, 40 rats were assigned to three different groups of 12/14 rats each: control group (CTRL) which remained untreated, PTX-treated group which received 10 mg/kg PTX (i.v.) once a week for 4 weeks and VCR-treated group which received 0.2 mg/kg VCR (i.v.) once a week for 4 weeks. At different time points (after 1, 2 and 4 weeks of treatment), neurophysiological studies and sample collection (tissue and blood) were performed. The behavioral test (Dynamic Aesthesiometer Test) was performed after 2 weeks of treatment and at the end of treatment.

4. ASSESSMENT OF CIPN

4.1 Mechanical threshold determinations: Dynamic aesthesiometer test

This test was performed in order to detect the presence of mechanical allodynia.

The mechanical nociceptive threshold was assessed using a Dynamic Plantar Aesthesiometer (No 37450; Ugo Basile Biological Instruments), which generated a linearly increasing mechanical force. The dynamic test was performed after 2 weeks of treatment and at the end

of treatment. Before testing, rats were placed in a Plexiglas chamber ($28 \times 40 \times 35$ cm, wire mesh floor) in which the animals performed a 15-minute acclimatization period before testing. A servo-controlled mechanical stimulus, represented by a pointed metallic filament of 0.5 mm diameter, was positioned under the plantar surface of the hind paw. This stimulus exerted a progressively increasing punctate pressure, reaching up to 50 g within 20 seconds. The pressure leads to a clear spontaneous hind paw withdrawal response, which was recorded automatically. The mechanical threshold was assessed on both the hind paws alternatively every 2 minutes. The result was expressed as a mean value of 6 measures.

The results are expressed in grams and they represented the maximal pressure (the mechanical nociceptive threshold index) tolerated by the animals. A response was considered positive when the animal exhibited nocifensive behaviors, for example brisk paw withdrawal, licking, or shaking of the paw. Otherwise, if paw movement appeared to be associated with grooming or locomotion, the measure was repeated after a delay of 1 minute. The cut-off was set at 30 seconds, after which the mechanical stimulus was automatically stopped in order to avoid any damage for the animal. Mechanical measurements were assessed by a single experimenter who was blind to the treatment groups (Chiorazzi et al., 2018; Meregalli et al., 2018a).

4.2 Nerve conduction studies

Baseline nerve conduction studies were performed prior to drug administration. Animals were then randomly assigned to one of the study treatment groups with similar mean values.

The neurophysiological analyses were also conducted at different time points: after 1 and 2 weeks of drug administration and at the end of treatment.

During all recording sessions, animals were anesthetized with 2% isoflurane and placed on a warm heating pad with rectal temperature monitored and maintained between 37.0 and 41.0 °C.

Sensory conduction studies (Sensory Nerve Action Potential [SAP] and Nerve Conduction Velocity [NCV]) of caudal and hind limb digital nerves were obtained; motor conduction studies of caudal nerve (Compound Motor Action Potential [CMAP] and NCV) were also performed.

In the sensory caudal nerve set up recording cathode and anode, ground electrode and stimulating anode and cathode were placed respectively at 1 cm, 2 cm, 3 cm, 5 cm 6 cm from the base of the tail for the recording at the proximal level. The same distance was used from the tip of the tail for the recording at distal level.

The digital nerve response was recorded in the hind limb placing the recording cathode in front of the patellar bone and the recording anode behind the ankle bone; stimulating anode and cathode were placed at the tip and base of the fourth toe, respectively; the ground electrode was inserted subcutaneously in the sole.

Stimulation of each nerve segment was performed, with increasing voltage, until the maximal response had been achieved.

NCV and SAP were assessed orthodromically.

Latencies were measured from stimulus onset and peak-to-peak amplitudes were calculated. NCV was calculated dividing the response latency time by the distance between the anode electrodes of the stimulating and recording dipole.

In the motor caudal nerve set up recording anode and cathode were placed in the caudal muscle at 11 cm and 12 cm respectively from the base of the tail. Ground electrode was placed at 6 cm from the base of the tail; distal stimulation was performed placing cathode and anode respectively at 5 cm and 6 cm from the base of the tail and proximal stimulation was then obtained repositioning them at 1 cm and 2 cm, respectively.

Filters were kept between 20 Hz and 3 KHz for sensory recordings and between 20 Hz and 2 KHz for motor recordings; sweep was kept at 0.5 msec. A Myto II EMG device (EBN Neuro,

Florence, Italy) and Stainless-steel subdermal needle electrodes [Ambu Neuroline (Ambu, Ballerup, Denmark)] were employed for both recording and stimulation (Chiorazzi et al., 2018; Meregalli et al., 2018a).

5. SAMPLE COLLECTION AND ANALYSIS

5.1 Pathological evaluation of peripheral nerves

Animals were sacrificed under deep anesthesia with CO_2. Sciatic and caudal nerves were isolated and dissected out without stretching. The samples were fixed by immersion in 3% glutaraldehyde in 0.12 M phosphate buffer solution and post fixed in OsO_4, epoxy resin embedded. These nerves were used for morphological and morphometric analysis.

Specimens were cut, and 1-μm-semithin sections were obtained and then stained with toluidine blue. The nerves were finally examined with a Nikon Eclipse E200 light microscope (Leica Microsystems GmbH, Wetzlar, Germany).

For morphometric analysis, 60 X pictures of three randomly selected different fields of each nerve section were taken using a Nikon Eclipse E200 light microscope (Leica Microsystems GmbH, Wetzlar, Germany). Nerves of three animals per group were analyzed using an automatic image analyzer compiled by Immagini e Computer SNC (Milan, Italy), which recognizes the fibers and measures their external diameter. Data were then analyzed with GraphPad Prism statistical package (GraphPad Software, San Diego, CA) (Canta et al., 2016).

5.2 Immunohistochemical (IHC) characterization of the infiltrating cells in nerves

Sciatic and caudal nerves of three animals per group were dissected in order to investigate the macrophage infiltration in peripheral nerves. The collected samples were fixed in 10% formalin overnight (o/n), paraffin embedded, and 3-μm-thick slices were cut with a Leica RM2265 microtome (Microsystems GmbH, Wetzlar, Germany). Immunohistochemistry was

performed using anti-CD68 antibody (CD68 Biorad MCA341GA, Segrate, Milan, Italy) to detect macrophage infiltrating cells, anti-iNOS antibody (Biorbyt orb13614, Cambridge, UK), and anti-ARG1 antibody (Biorbyt orb394005, Cambridge, UK) to discriminate M1 (pro-inflammatory) from M2 (anti-inflammatory) macrophages. Paraffin sections were deparaffinized with xylene, rehydrated and heated in a steamer for 20 min (1 mM EDTA pH 8 or 10 mM Citrate Buffer pH 5) to retrieve antigens. Endogenous peroxidase activity was quenched by incubation in 3% H_2O_2 for 10 min at RT. The slides were washed in PBS and incubated in blocking solution (5% NGS or 3% BSA) for 1 h at RT. Then, the sections were incubated with anti-CD68 antibody (1:300 in 1% NGS), anti-ARG1 (1:50 in 1% BSA), or anti-iNOS (1:500 in 1% BSA) o/n at 4 °C. The following day, the slides were washed and incubated with secondary anti-mouse (1:200, Millipore, Burlington, MA) or antirabbit antibody (1:200, Perkin Elmer, Milan, Italy) for 1 h at RT. The antigen-antibody complex was visualized by incubating the sections with 3,3-diaminobenzidine hydrochloride (Sigma, St. Louis, MO) dissolved in PBS with 10 μl of 3% H_2O_2. Negative controls were incubated only with the secondary antibody. Semi-quantitative assessment of macrophage infiltration was performed in the caudal nerve of animals sacrificed after 1 and 2 weeks from the beginning of the experiment and after the end of treatment. The analysis was performed by the same blinded examiner by scoring + for a rare presence of infiltration (1‑5 macrophages/section); ++ for a robust presence of infiltration (5-20); +++ for a more robust infiltration (20‑30 macrophages/section); and ++++ for a very high infiltration (> 30 macrophages/section) (Meregalli et al., 2018a).

5.3 Skin biopsy: intraepidermal nerve fiber (IENF) density evaluation

At sacrifice, hind paw skin specimens were collected separating the plantar glabrous skin, which included epidermis and dermis, from the underlying metatarsal bones. 5-mm round

samples from each animals were obtained and immediately fixed in 2% PLP (paraformaldehyde-lysine and periodate sodium) for 24 hours at 4° C.

Footpads were dissected out and were washed in phosphate buffer (PB) and placed in cryoprotectant (20% glycerol, 20% PB, 60% H_2O) solution. Tissue blocks were cut using a freezing microtome at 20 µm intervals. Three sections from each footpad were randomly selected.

Immunohistochemical staining was performed using a free-floating protocol. The sections were rinsed in phosphate buffer TBS (2 x 10 min). In order to bleach melanin, sections were incubated in 0.25% potassium permanganate for 15 min at RT, washed in TBS (1 x 10 min) and incubated in 5% oxalic acid for 2 min. After 2 washes in TBS (2 x 10 min), the sections were placed in blocking solution (TBS with 0.1% triton X-100, 4% normal serum) for 1 h at RT. Sections were incubated with rabbit polyclonal antiprotein gene product 9.5 (PGP 9.5; Gene Tex, Irvine, CA, USA) (1:200 in TBS with 0.05 % triton X-100, 2% normal serum) over night at room temperature in 96 well tissue culture plates on a horizontal tabletop shaker at 50 rolls per min. The following day, sections were washed in phosphate buffer (TBS) (2 x 10 min) and then incubated with goat anti-rabbit Ab (Vector Labs, Burlingame, CA) for 1h. After 2 washes in TBS (2 x 10 min), the sections were placed in 33% methanol/PBS with 3.3 % H_2O_2 for 30 min. Bound immunoglobulin was visualized by the ABC kit (Vector labs, Burlinggame, CA), an avidin biotin mix. The sections were then incubated in SG substrate kit, which contains the peroxidase substrate for 2 min, followed by a wash in PBS (10 min). After the mounting, counterstaining and coverslipping, the total number of PGP 9.5-positive IENF in each section was counted, the length of the epidermis was measured and the linear density of IENF/mm was obtained by the same blinded examiner (Canta et al., 2016).

5.4 Blood collection and Neurofilament Light analyses

Blood samples were collected from the tail vein of control and treated rats 2 days after the drug administration. Serum was obtained through centrifugation at 4 °C, 3500 g for 15 min. Serum was then aliquoted and stored at -80 °C pending NfL quantification. For these analyses, we had a collaboration with The Sahlgrenska Academy at the University of Gothenburg, Mölndal, Sweden and with Disarm Therapeutics, Cambridge, MA, USA.

Serum NfL concentrations were measured with the NF-Light assay from Uman Diagnostics and transferred onto the Simoa platform with a home-brew kit (Quanterix Corp, Boston, MA). 2.7 μm diameter paramagnetic carboxylated beads (Quanterix) were activated by adding 5% (vol/vol) 10 mg/mL 1-ethyl-3-(3-dimethylaminopropyl) carbodiimide (Quanterix) to a magnetic beads solution containing 1.4×10^6 beads/μL. After 30 minute of incubation at RT, the beads were washed with a magnetic separator and then incubated for 2 h at RT with 0.3 mg/mL of the capture antibody (UD1, UmanDiagnostics). After the incubation, the beads were washed, and a blocking solution was added. After 3 washes, the conjugated beads were suspended and stored at 4 °C. The beads were then diluted at a concentration of 2,500 beads/μL. The detection antibody (1 mg/mL, UD2, UmanDiagnostics) was biotinylated by adding 3% (vol/vol) 3.4 mmol/L EZ-Link NHS-PEG4-Biotin (Quanterix), followed by a 30-minute incubation at RT. Free biotin was removed with spin filtration (Amicon Ultra-2, 50 kDa, Sigma, St. Louis, MO), and the biotinylated antibody was stored at 4 °C. The serum samples were assayed in duplicate on a Simoa HD-1 instrument (Quanterix) using a 2-step assay dilution protocol: after the aspiration of the diluent from 100 μL conjugated beads (2,500 beads/μL), 20 μL biotinylated antibody (0.1 μg/mL) and 100 μL of 4-fold diluted sample (or undiluted calibrator) were added to the pellet. For both samples and calibrator, the same diluent was used (phosphate-buffered saline; 0.1% Tween20; 2% bovine serum albumin; 10 μg/mL TRU Block [Meridian Life Science, Inc, Memphis, TN]).

The beads were washed, followed by the incubation with 100 μL streptavidin-conjugated β-galactosidase (150 pmol/L).

Before reading, 25 μL resorufin β-D-galactopyranoside was added. The calibrator curve was constructed by use of the standard from the NfL ELISA (NF-Light, UmanDiagnostics) in triplicate. The average repeatability of the assay was assessed by measurements of quality control samples and the coefficient of variation was 6.2% for a sample with a mean NfL concentration of 50.7 pg/ml, and 12.3% for a sample with a mean NfL concentration of 22.6 pg/ml.

All measurements were performed by board-certified laboratory technicians in one round of experiments using one batch of reagents (Rohrer et al., 2016).

6. STATISTICAL EVALUATION

For the statistical analysis, GraphPad Prism4 statistical package (GraphPad Software, San Diego, CA) was used. In particular, the changes in body weight were statistically evaluated using the analysis of variance (ANOVA) followed by the Tukey post hoc test (significance level set at $p < 0.05$).

To compare the behavioral, IENF density, neurophysiological and NfL data, 2-sided Mann-Whitney U test (to compare pairs of data samples) or Kruskal-Wallis test (for multiple comparisons) followed by the Dunn's post-hoc test were used to evaluate data not showing a normal distribution (significance level set at $p < 0.05$).

RESULTS

In order to evaluate the possible role of NfL in CIPN models, two different experiments were conducted.

1. STUDY 1 (Cisplatin and Paclitaxel Study)

In the first study, rats were divided in three groups: the CTRL arm, CDDP- and PTX-treated animals. All the analyses were conducted at the end of the experiment (4 weeks of treatment for both the anticancer drugs). The aim was to evidence any possible difference in axonal damage using drugs that induce CIPN acting on different targets (the cell body of DRG or the axon).

1.1 Body weight changes

The body weight was recorded twice a week during all the experiment in order to assess animal health condition and to adjust the drug dose before the treatment. At every experimental point the mean of the body weight of all the animals composing each group is represented. Only CDDP-treated animals showed a significant decrease in the body weight, whereas no significant changes was noticed in PTX-treated group compared to the untreated controls (Fig.7).
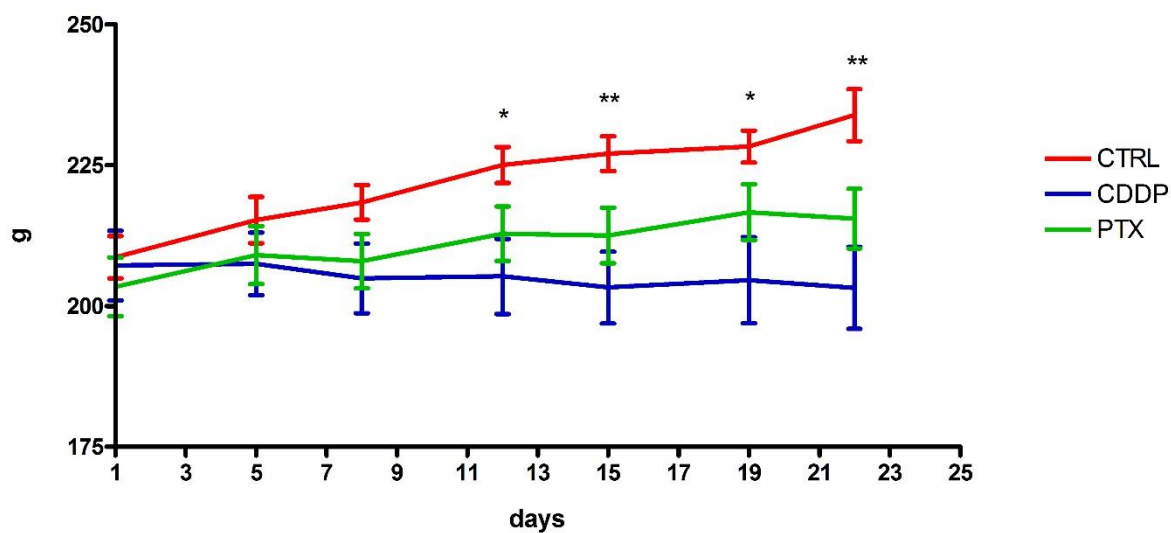
Fig.7. Animal Body Weight. Cisplatin (CDDP) treatment induced a significant decrease in daily body weight, whereas paclitaxel (PTX)-treated animals did not have a significant decrease. The results are expressed as mean ± SD of the body weight of all the animals for each group. Statistical evaluations were obtained using the one-way analysis of variance (ANOVA), followed by the Tukey post hoc-test. *$p<0.05$ for PTX vs CTRL; **$p<0.01$ for PTX vs CTRL.

1.2 Mechanical nociceptive threshold evaluation

In order to detect the presence of changes in the mechanical threshold, the Dynamic Aesthesiometer test was performed at the end of treatment. Only PTX-treated group showed allodynia compared to CTRL (Fig.8).
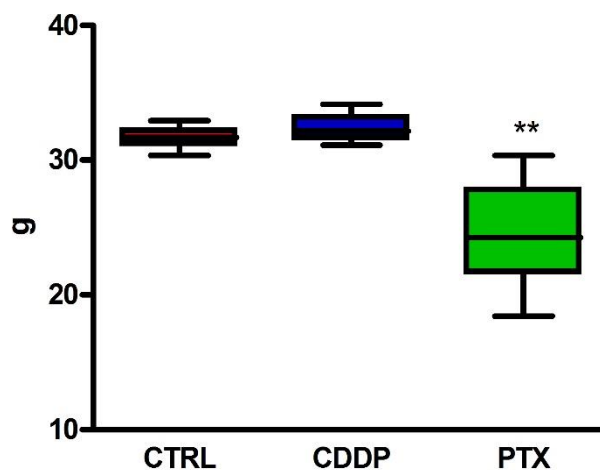
Fig.8. Dynamic test. The graphic shows the maximal pressure (expressed in grams) tolerated by the animals related to mechanical stimuli in controls (CTRL), cisplatin (CDDP)- and paclitaxel (PTX)-treated rats at the end of treatment. Statistical evaluations were obtained using the Kruskal-Wallis test followed by the Dunn's post-hoc test. **p<0.01 for PTX vs CTRL.

1.3 Pathology assessment

At the end of the treatment, animals were sacrificed and samples were collected for different evaluations:

- ✓ morphological and morphometric analyses on nerves;
- ✓ macrophage infiltration on nerves;
- ✓ intraepidermal nerve fiber density on the hind paw.

1.3.1 Morphological and morphometric studies on peripheral nerves

Peripheral nerves (caudal nerves) were dissected and processed for morphological and morphometric investigations. The morphological analysis indicated a marked nerve degeneration only in PTX-treated rats according to the drug putative target (the axons). This damage progressed from distal to proximal level of caudal nerve according to the length-dependent neuropathy. The distal part of caudal nerve presented a huge loss of fibers confirming a context of axonopathy. Regarding to the CDDP-treated group, a few degenerated fibers were observed at distal level (Fig.9).
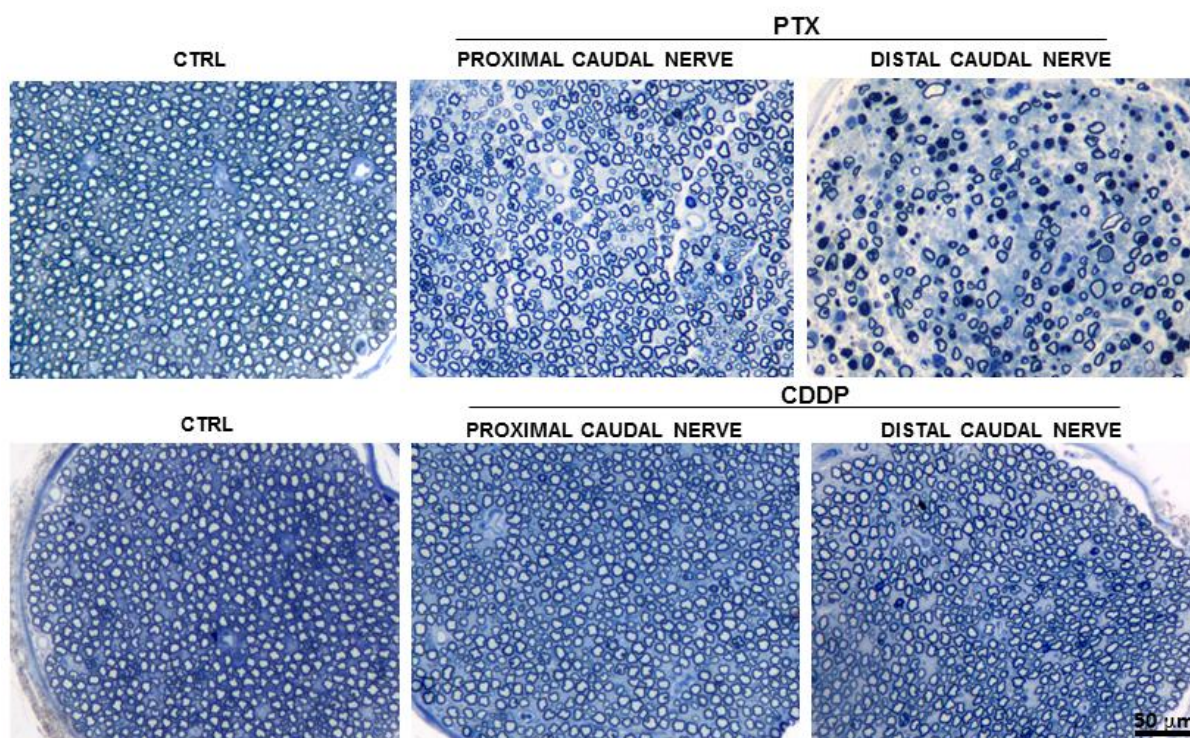
Fig.9. Morphological examination of caudal nerves at proximal and distal level. Severe axonopathy induced by paclitaxel (PTX) administration was evident in the caudal nerve if compared to control arm (CTRL) and cisplatin (CDDP)-treated animals. Scale bar 50 μm.

The morphometric analysis (Fig.10A), obtained using an automatic image analyzer, showed a loss of fibers of larger diameter in both CDDP- and PTX-treated animals. Anyway, this loss was more severe in PTX-treated group confirming the previous results. Size frequency data

were normalized based on the density of fibers. Moreover, Fig.10B confirms these data showing a reduction in the mean of fiber diameter in CDDP- and PTX-treated animals compared to CTRL.
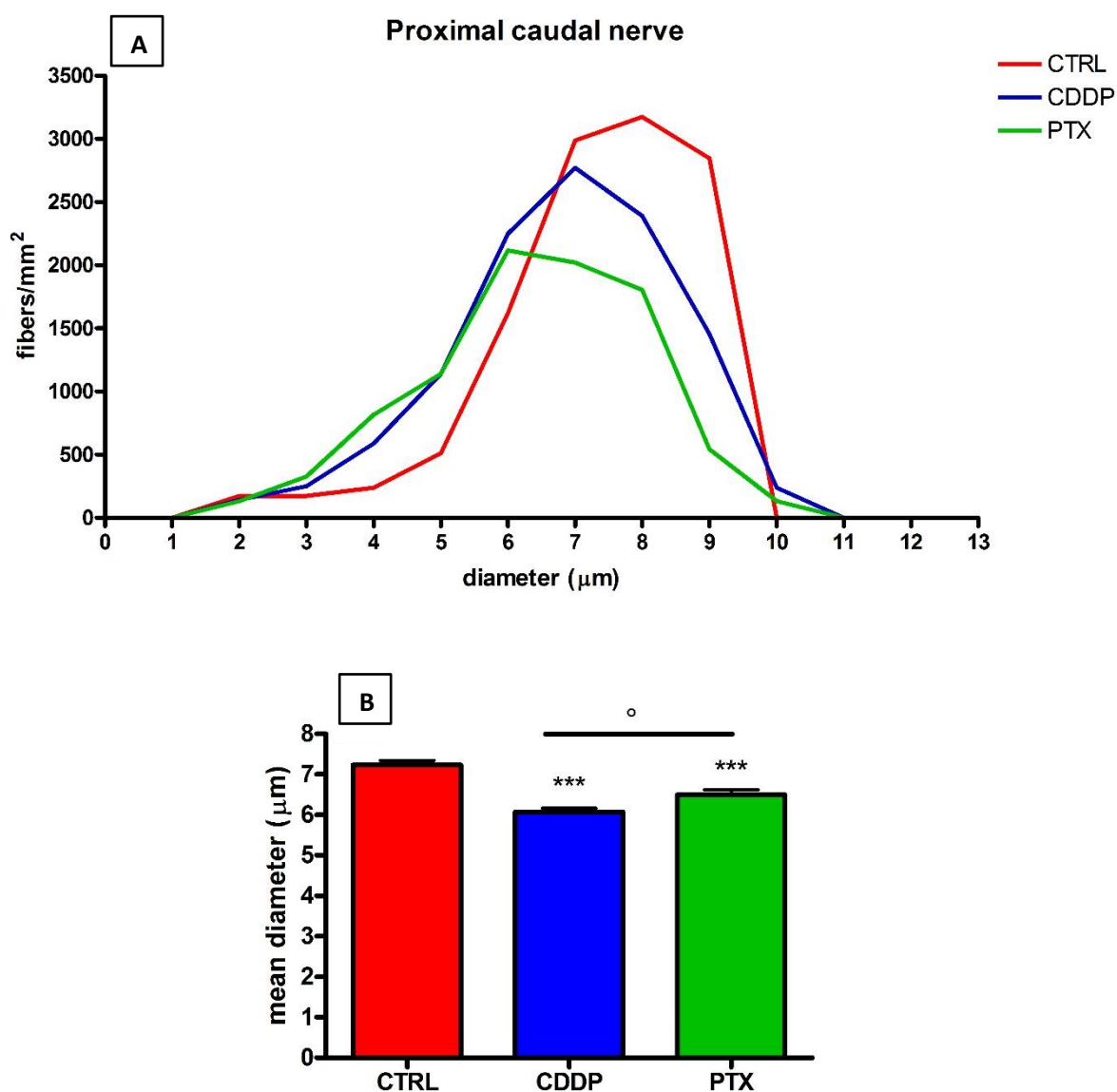
Fig.10. A) Morphometric analysis of caudal nerves at proximal level. The frequency distribution is normalized for the density of fibers for each group. The loss of fibers with larger diameter was higher in paclitaxel (PTX)- and cisplatin (CDDP)-treated animals compared to the controls (CTRL). **B) Mean of fiber diameter.** The graph confirms a reduction of mean fiber diameter in CDDP- and PTX-treated animals compared to CTRL. Statistical evaluations were obtained using the one-way analysis of variance (ANOVA), followed by the Tukey post hoc-test. ***$p<0.001$ for CDDP, PTX vs CTRL; ° $p<0.05$ for CDDP vs PTX.

1.3.2 Macrophage infiltration

In order to investigate the possible role of neuroinflammation in the assessment of axonal damage, immunohistochemical analyses were performed on peripheral nerves. In particular the possible role of macrophages was studied. The IHC analysis for CD68 showed a robust macrophage infiltration in caudal nerves of PTX-treated animals at the end of treatment. To further characterize infiltrating CD68$_+$ cells, an IHC for iNOS (pro-inflammatory macrophages) and for ARG1 (anti-inflammatory macrophages) was performed, evidencing that all infiltrating cells were iNOS positive. A semi-quantitative analysis on anti-CD68 stained sections confirmed these observations. Otherwise, IHC analysis on CDDP samples resulted negative (Fig.11). IHC analysis on sciatic nerves evidenced no macrophage infiltration (Fig.12).
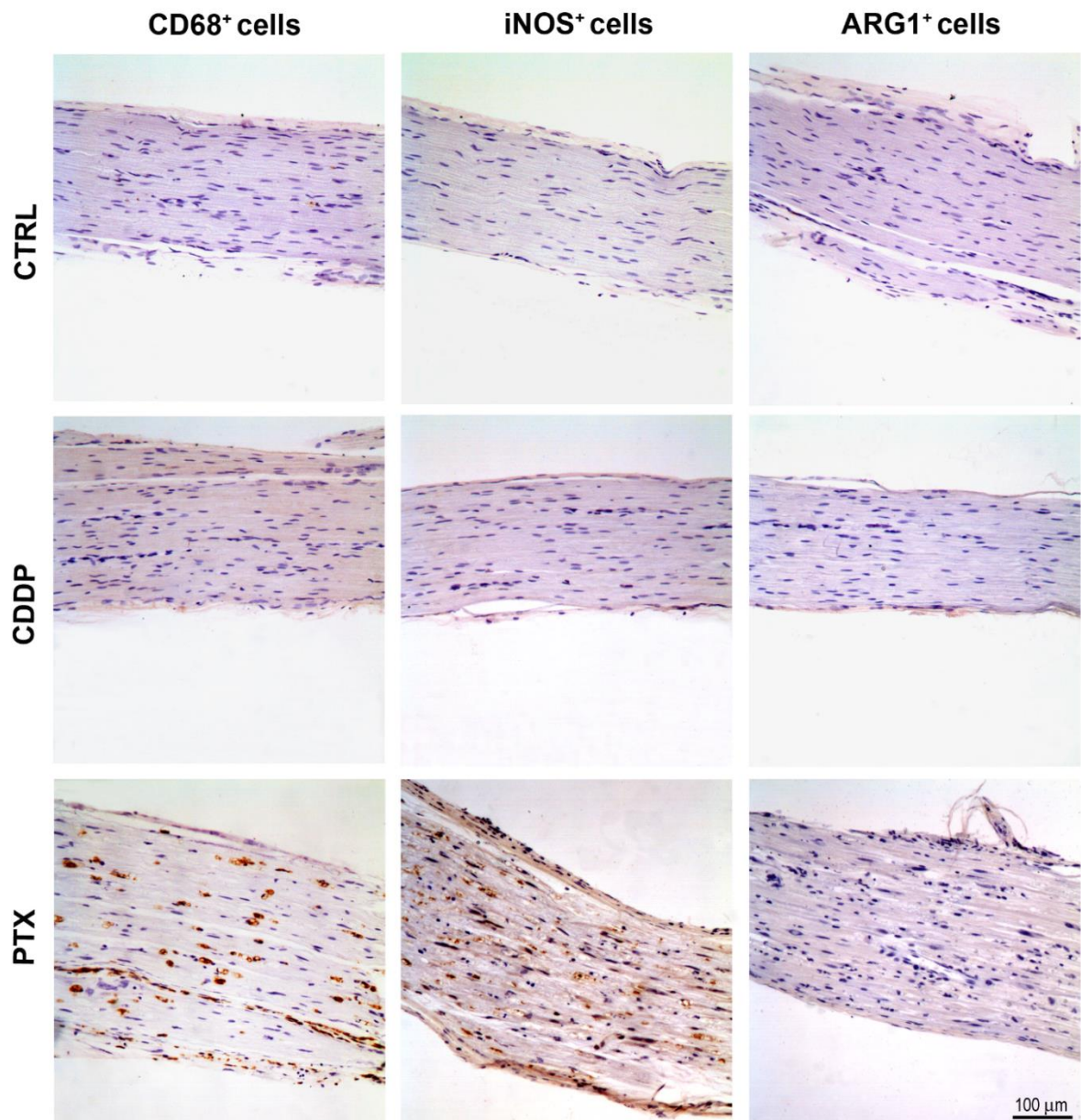
Fig.11. Macrophage infiltration in caudal nerves. Immunohistochemistry for CD68: caudal nerves in paclitaxel (PTX)-treated rats show a massive macrophage infiltration. Most infiltrating macrophages (CD68+) are iNOS+ pro-inflammatory M1 type whereas a very limited amount of them are ARG1+ anti-inflammatory M2 type. Sections collected from cisplatin (CDDP)-treated animals resulted negative. Scale bar 100 μm.
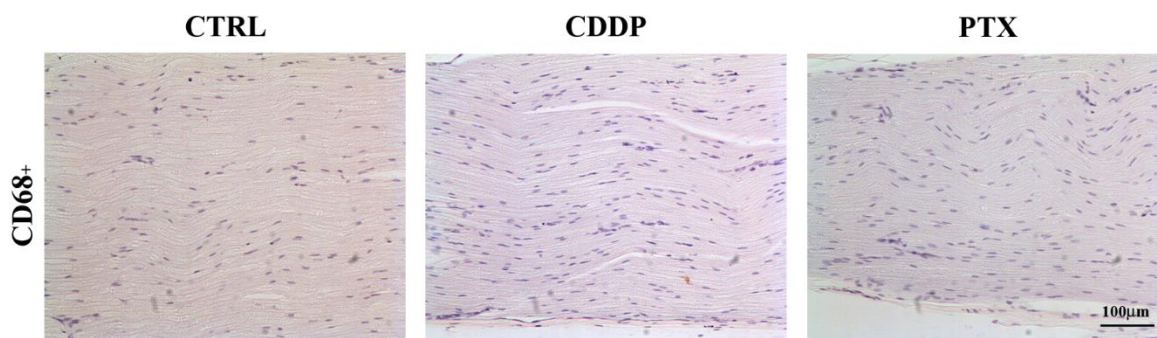
Fig.12. Macrophage infiltration in sciatic nerves. Immunohistochemistry for CD68: all the samples resulted negative. Scale bar 100 μm.

1.3.3 IENF density

Among the collected samples, also hind paw skin was harvested and immunohistochemical staining was performed in order to detect intraepidermal nerve fibers density.

At the end of treatment, the animals treated with CDDP and PTX showed a statistically significant reduction in IENF density compared to CTRL (Fig.13, 14).
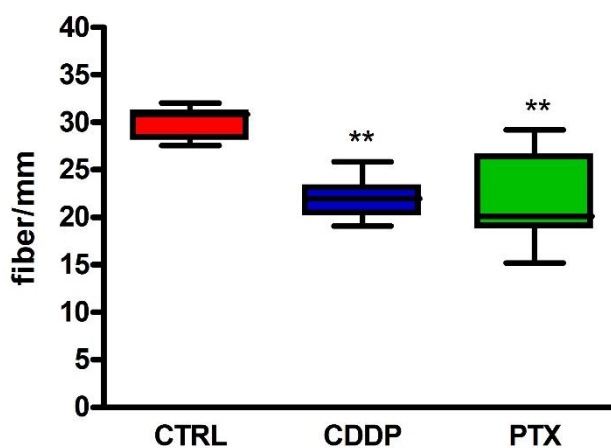
Fig.13. Intraepidermal nerve fiber density. Treatment with cisplatin (CDDP) and paclitaxel (PTX) induced a statistically significant reduction in IENF density when compared to CTRL. Statistical evaluations were obtained using the Kruskal-Wallis test followed by the Dunn's post-hoc test. **p<0.01 for CDDP, PTX vs CTRL.

End of treatment
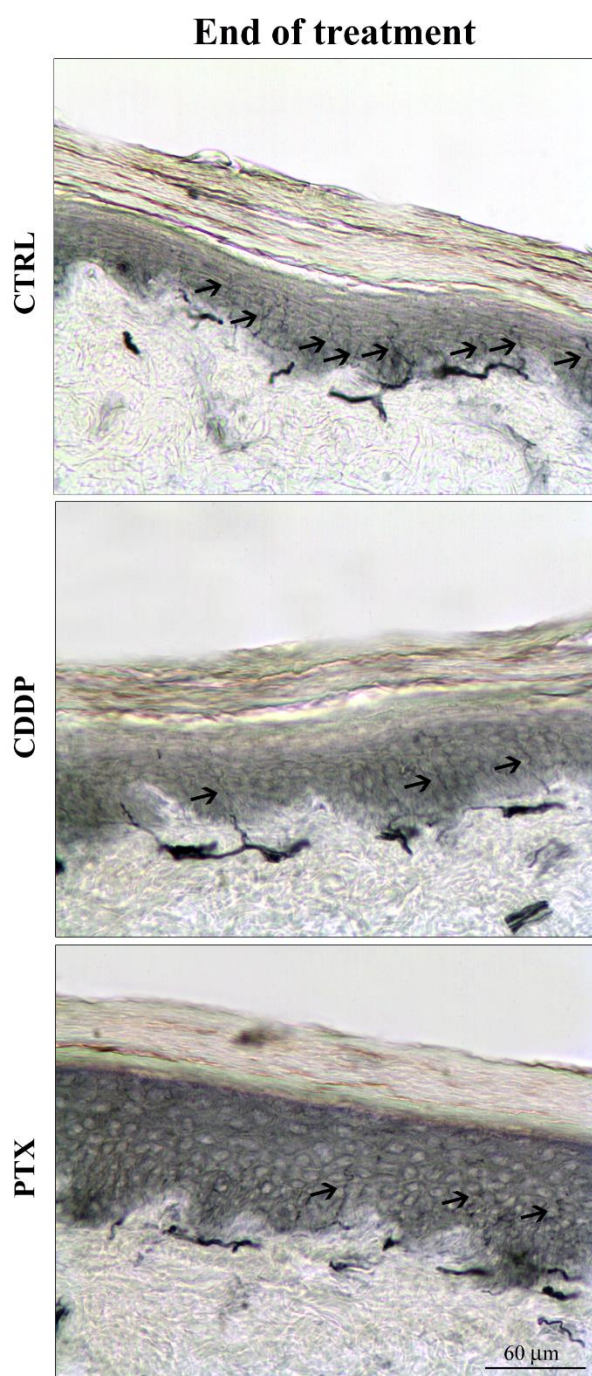
Fig.14. Skin biopsy. A representative image of skin biopsy samples of cisplatin (CDDP)- and paclitaxel (PTX)-treated animals. In CDDP- and PTX-treated animals, a reduction in intraepidermal nerve fibers (IENF) density was evidenced (fibers indicated by arrows). Scale bar 60 μm.

1.4 Nerve conduction studies

Nowadays, the neurophysiological studies are the gold standard in the investigation of the pathology in patients. In order to assess the axonal damage, the study was conducted on different peripheral nerves (caudal nerve and digital nerve). In particular, the caudal nerve was studied at proximal and distal levels in order to evaluate the length-dependent pathology (Fig.15).

Regarding to PTX-treated group, at the end of the experiment, a significant decrease in proximal caudal amplitude ($p < 0.01$) was detected (A); no significant changes in NCV was observed at proximal level (B). At distal level, in most animals it was not possible to record the tracks due to the important damage and loss of fibers evidenced also by the morphological observations (C, D).

Regarding to CDDP-treated rats, a reduction in caudal distal amplitude and NCV was observed (C, D), whereas no significant differences were evidenced at proximal level (A, B). Finally, no statistically significant differences were observed in the amplitude and NCV of digital nerve in both groups (E, F).
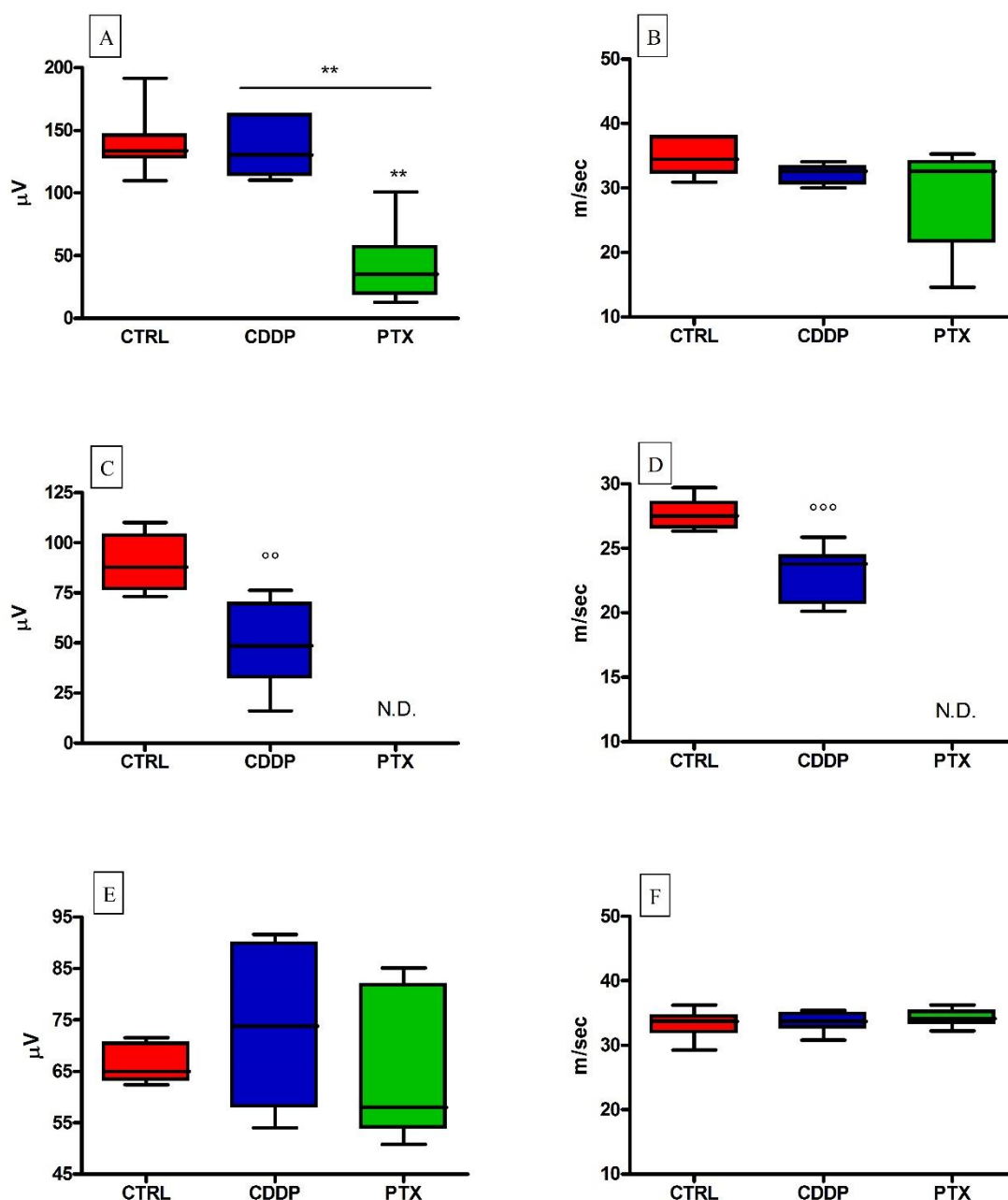
Fig.15. Nerve conduction studies. The graph reports the amplitude and the velocity obtained from caudal nerve at proximal (A,B) and distal (C,D) level and from digital nerve (E,F) of controls (CTRL), cisplatin (CDDP)- and paclitaxel (PTX)-treated rats. A) PTX-treated animals presented a significant decrease in amplitude compared to CTRL and CDDP-treated group. B) No significant alterations in velocity. C,D) Regarding to PTX-treated rats, it was not possible to record the tracks (not detectable, N.D.). A reduction in amplitude and NCV was detected in CDDP-treated samples. E,F) No significant alteration was reported in the digital nerve. Statistical evaluations were obtained using the Kruskal-Wallis test followed by the Dunn's post-hoc test and the Mann-Whitney test. **p<0.01 for PTX vs CTRL, CDDP (Kruskal-Wallis test). °°p<0.01, °°°p<0.001 for CDDP vs CTRL (Mann-Whitney test).

47

1.5 Serum NfL concentration

In order to investigate the possible role of NfL as a serum biomarker of axonal damage, at the end of the treatment, blood was collected from the tail vein and serum was obtained. NfL analyses were conducted using a Simoa Technologies Assay (Quanterix) as previously described. The quantification indicated an increase in NfL concentration only in PTX-treated rats while the CDDP-treated group was similar to the CTRL arm (Fig.16).
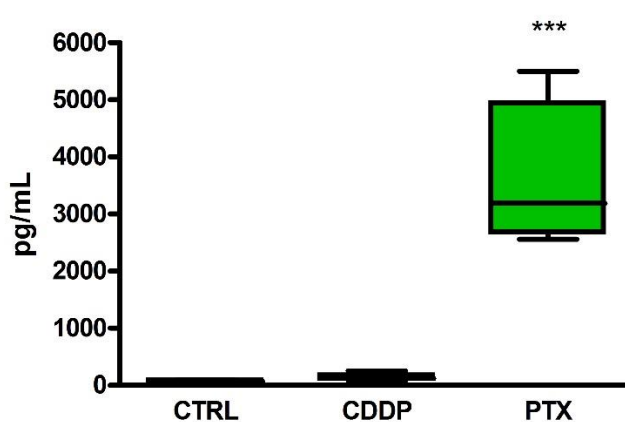

Fig.16. Serum Neurofilament Light (NfL) concentration. Data collected indicate that paclitaxel (PTX)-treated animals had an important increase in NfL concentration. In cisplatin (CDDP)-treated group the NfL levels remained unchanged compared to the CTRL one. Statistical evaluations were obtained using the Kruskal-Wallis test followed by the Dunn's post-hoc test. ***$p < 0.001$ for PTX vs CTRL, CDDP.

2. STUDY 2 (Time course of Paclitaxel and Vincristine Study)

In the first experiment, an important axonal damage was detected in PTX-treated animals. This damage correlated with a significant and marked increase of serum NfL level. Otherwise, a mild damage in CDDP-treated rats was observed and no significant difference in NfL concentration was detected compared to the controls. Given these interesting results, a second experiment using PTX and VCR (which also acts on axons) was performed. The aim of this second experiment was to assess a weekly time course in order to observe the progression of the pathology and the serum NfL concentration trend. The treatments lasted four weeks and at different weekly time points, neurophysiological studies and behavioral test were performed. Three animals per group were sacrificed at different time points for samples harvest. Blood from all animals was collected from the tail vein weekly.

2.1 Body weight changes

In order to assess the general toxicity and to adjust the correct dose of drug, body weight variations were recorded twice a week for the duration of treatment. At every experimental point, the mean of the body weight of all the animals composing each group is represented. No significant decrease in body weight was observed in the groups of treatment (PTX and VCR) compared to the untreated controls (CTRL) (Fig.17), suggesting a good tolerability of the treatments.
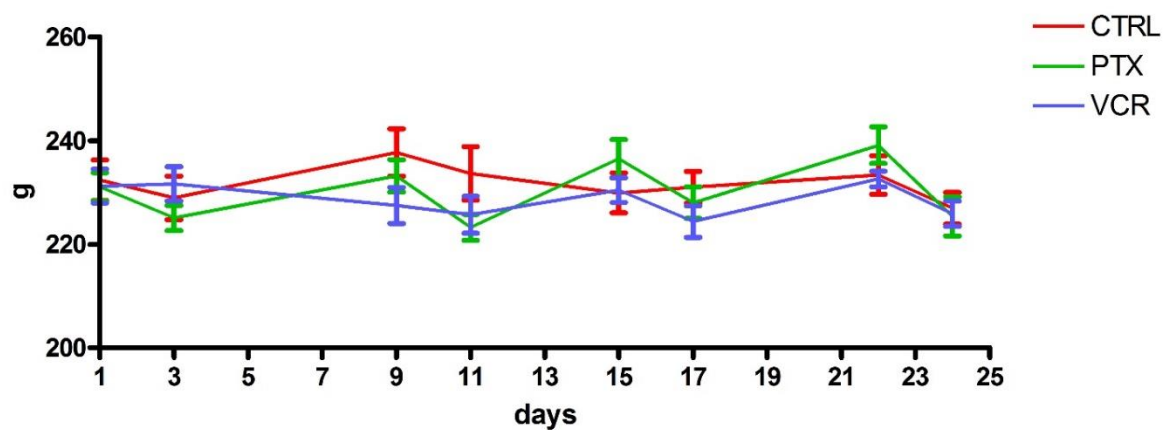
Fig.17. Animal Body Weight. Body weight variations of untreated controls rats (CTRL), paclitaxel (PTX)- and vincristine (VCR)-treated rats. No differences were detected compared to CTRL. The results are expressed as mean ± SD of the body weight of all the animals for each group. Statistical evaluations were obtained using the one-way analysis of variance (ANOVA), followed by the Tukey post-hoc test.

2.2 Mechanical nociceptive threshold evaluation

The Dynamic Aesthesiometer test was used to detect the presence of changes in mechanical threshold and it was performed after two weeks of treatment and at the end of treatment. Only at the end of the treatment both PTX- and VCR-treated groups showed allodynia compared to CTRL (Fig.18).
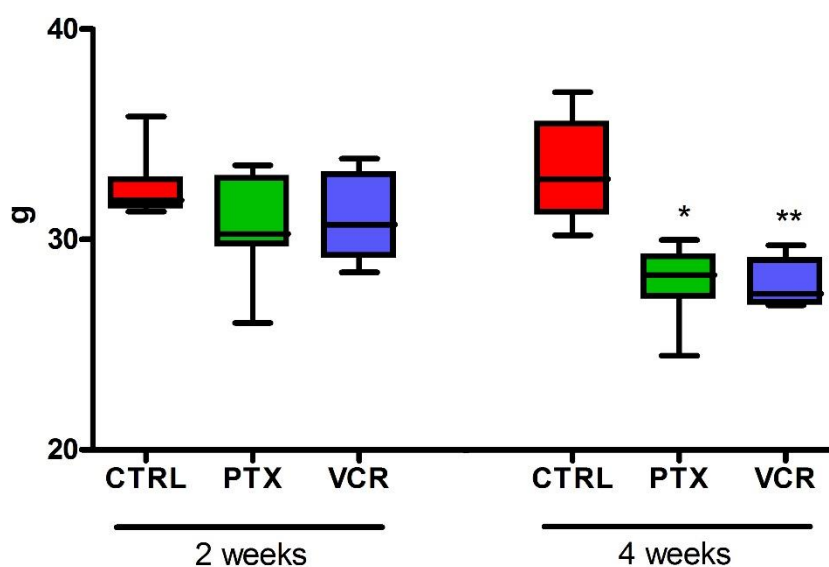
Fig.18. Dynamic test. The graphic shows the maximal pressure (grams) tolerated by the animals related to mechanical stimuli in controls (CTRL), paclitaxel (PTX)- and vincristine (VCR)-treated rats at 2 weeks of treatment and at the end of treatment. Statistical evaluations were obtained using the Kruskal-Wallis test followed by the Dunn's post-hoc test. *p<0.05 for PTX vs CTRL; **p<0.01 for VCR vs CTRL.

2.3 Pathology assessment

At 1, 2 weeks of treatment and at the end of the treatment, three animals per group were sacrified and samples were collected for different studies:

- ✓ morphological an morphometric analysis on nerves;

- ✓ macrophage infiltration on nerves;

- ✓ intraepidermal nerve fiber density on the hind paw.

2.3.1 Morphological and morphometric studies on peripheral nerves

Peripheral nerves (sciatic and caudal nerve) were dissected and processed for morphological and morphometric investigations.

Caudal nerve: proximal level

The morphological analysis indicated only a few degenerated fibers after 1 week of treatment in both groups of treatment. This degeneration increased during the following weeks until the end of treatment in both PTX- and VCR-treated groups, but the loss of fibers was more marked in PTX one (Fig.19).

These observations were confirmed by the morphometric studies (Fig.20 on the left): after 2 weeks of treatment (A) and at the end of treatment (B), the graphs show the loss of fibers of larger diameter in PTX-treated animals. Size frequency data were normalized based on the density of fibers (Fig.20). The graphs on the right (Fig.20) showed the reduction of the mean fiber diameter in PTX- ($p<0.01$) and in VCR- ($p<0.05$) treated rats.
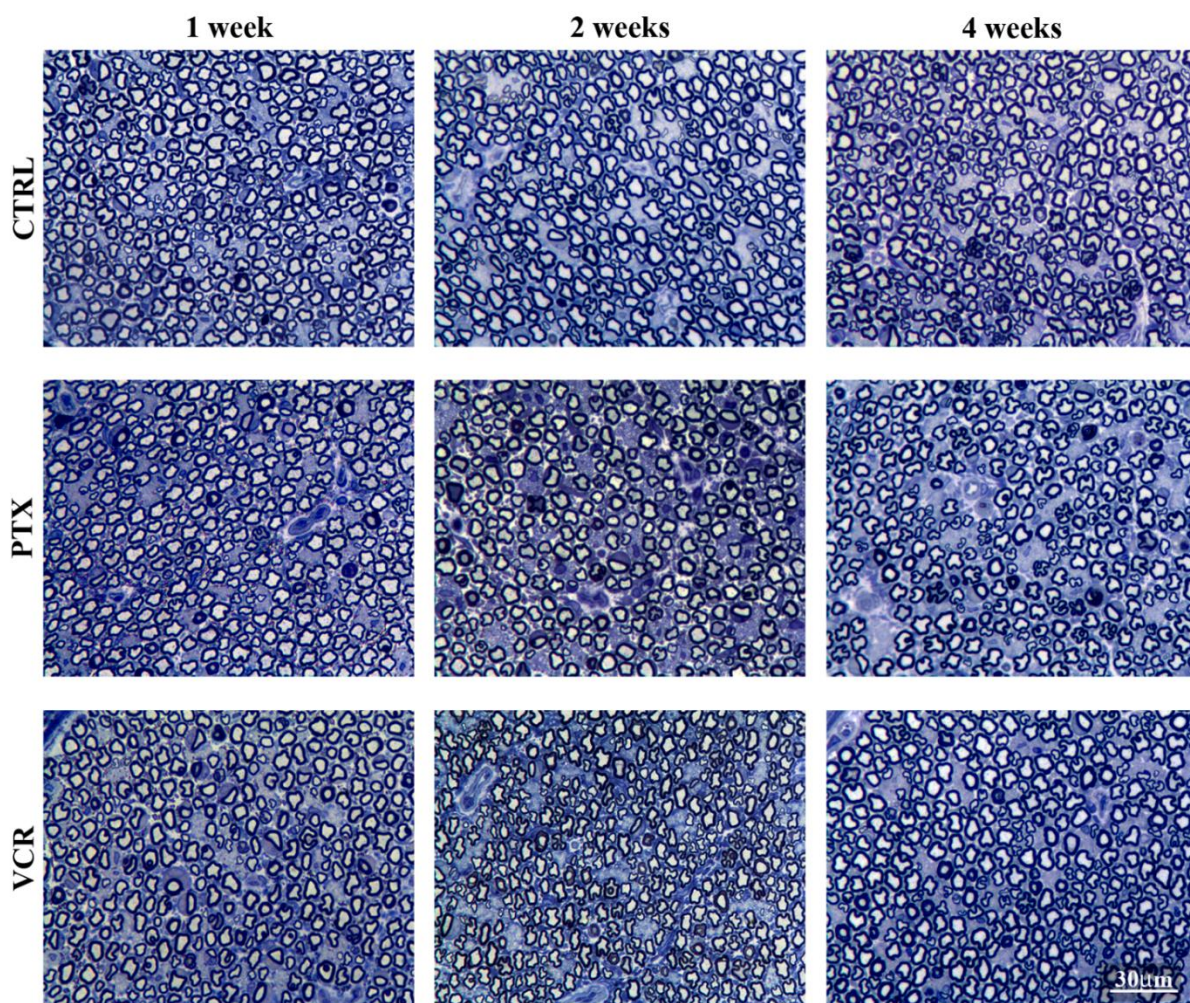
Fig.19. Morphological examination of caudal nerves at proximal level. Time course of fiber loss and degeneration in caudal nerves (proximal level) of paclitaxel (PTX)- and vincristine (VCR)-treated rats compared to the controls (CTRL). The axonopathy was evident from the second week of treatment, especially for PTX-treated animals. Scale bar 30 μm.
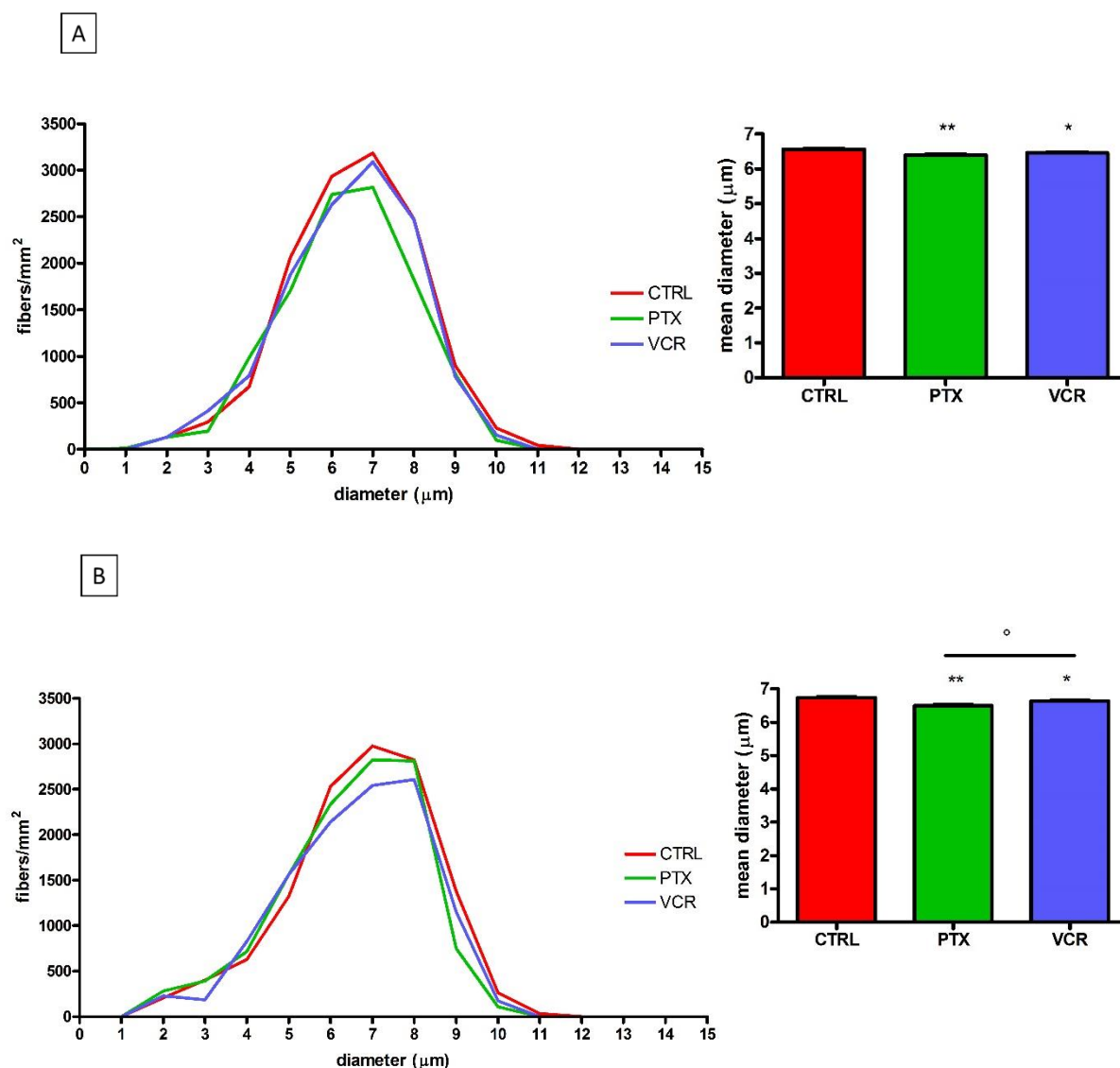
Fig.20. Morphometric analysis of caudal nerves at proximal level (on the left) and the mean of fiber diameter (on the right). The graphs on the left indicates the morphometric analysis after 2 weeks of treatment (A) and at the end of treatment (B) for paclitaxel (PTX)- and vincristine (VCR)-treated groups compared to the controls (CTRL). The frequency distribution is normalized for the total number of fibers for each group. In PTX-treated group there was a loss of fibers with larger diameter after 2 weeks of treatment (A). At the end of treatment (B) the graph indicates a loss of fibers with larger diameter both in PTX- and VCR-treated groups. The graphs on the right shows a reduction in mean fiber diameter in PTX- ($p<0.01$) and VCR- ($p<0.05$) treated animals after 2 weeks of treatment (A) and at the end of treatment (B). Statistical evaluations were obtained using the one-way analysis of variance (ANOVA), followed by the Tukey post hoc-test. **$p<0.01$ for PTX vs CTRL; *$p<0.05$ for VCR vs CTRL; ° $p<0.05$ for VCR vs PTX.

Caudal nerve: distal level

According to the length-dependent neuropathy, at the distal level the caudal nerve presented a more severe axonopathy with a huge loss of fibers than at the proximal level. The degeneration was evident from the second week of treatment especially in PTX-treated animals (Fig.21).
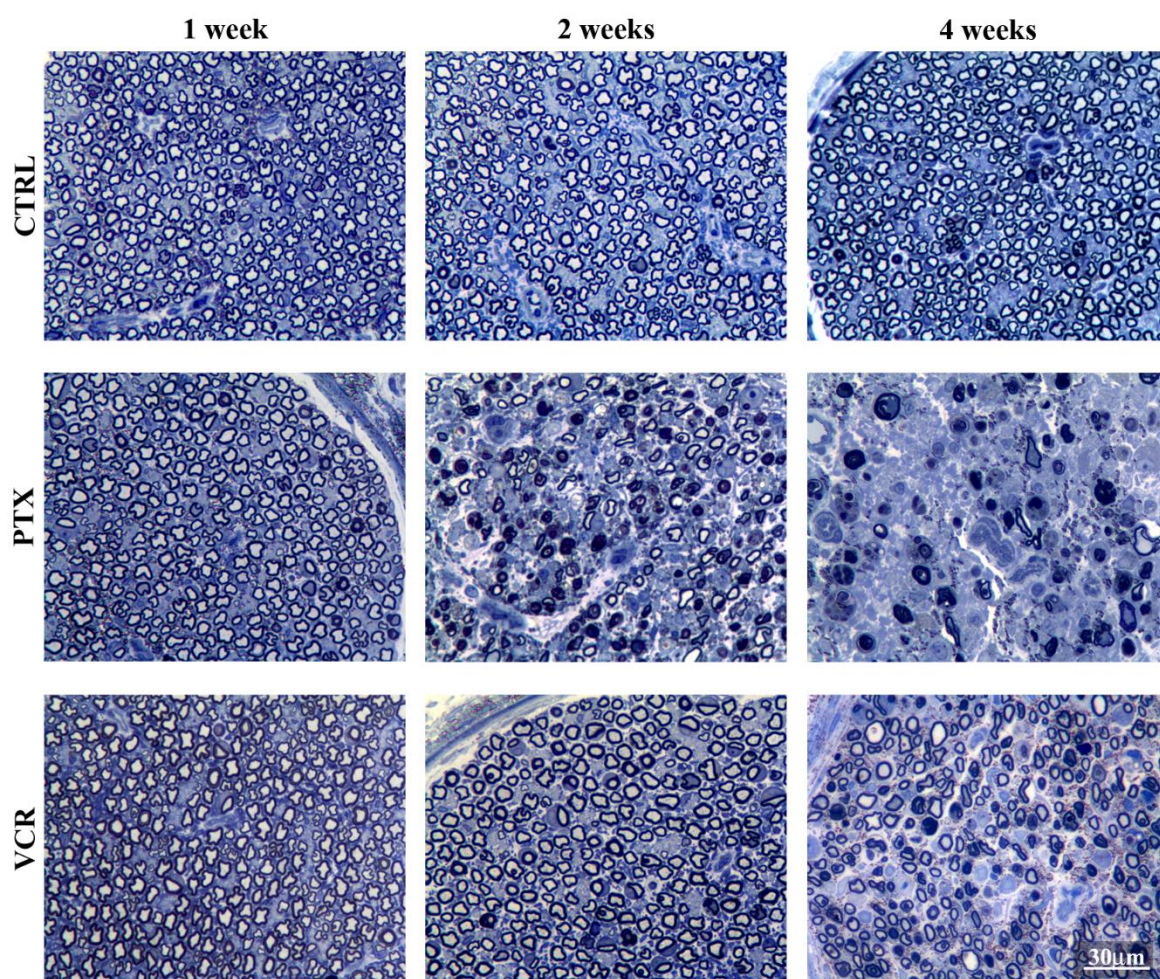

Fig.21. Morphological examination of caudal nerves at distal level. Time course of fiber loss and degeneration in caudal nerves (distal level). Severe axonopathy induced by paclitaxel (PTX) administration was evident in the caudal nerve from the second week of treatment and it got worse at the end of treatment. Regarding to vincristine (VCR), axonopathy was less severe but otherwise important especially at the end of treatment. Scale bar 30 µm.

Sciatic nerve

Regarding the sciatic nerve, the Fig.22 shows that only a few degenerated fibers were present at the end of treatment, in particular in PTX-treated animal nerves. The graphs in Fig.23 on the left confirms a loss of fibers of larger diameter in PTX-treated animals from the second week of treatment (A) until the end of the experiment (B). Size frequency data were normalized based on the density of fibers. On the right, the graphs confirms the observations showing a reduction in fiber diameter in PTX-treated animals compared to VCR-treated rats and CTRL (Fig.23).
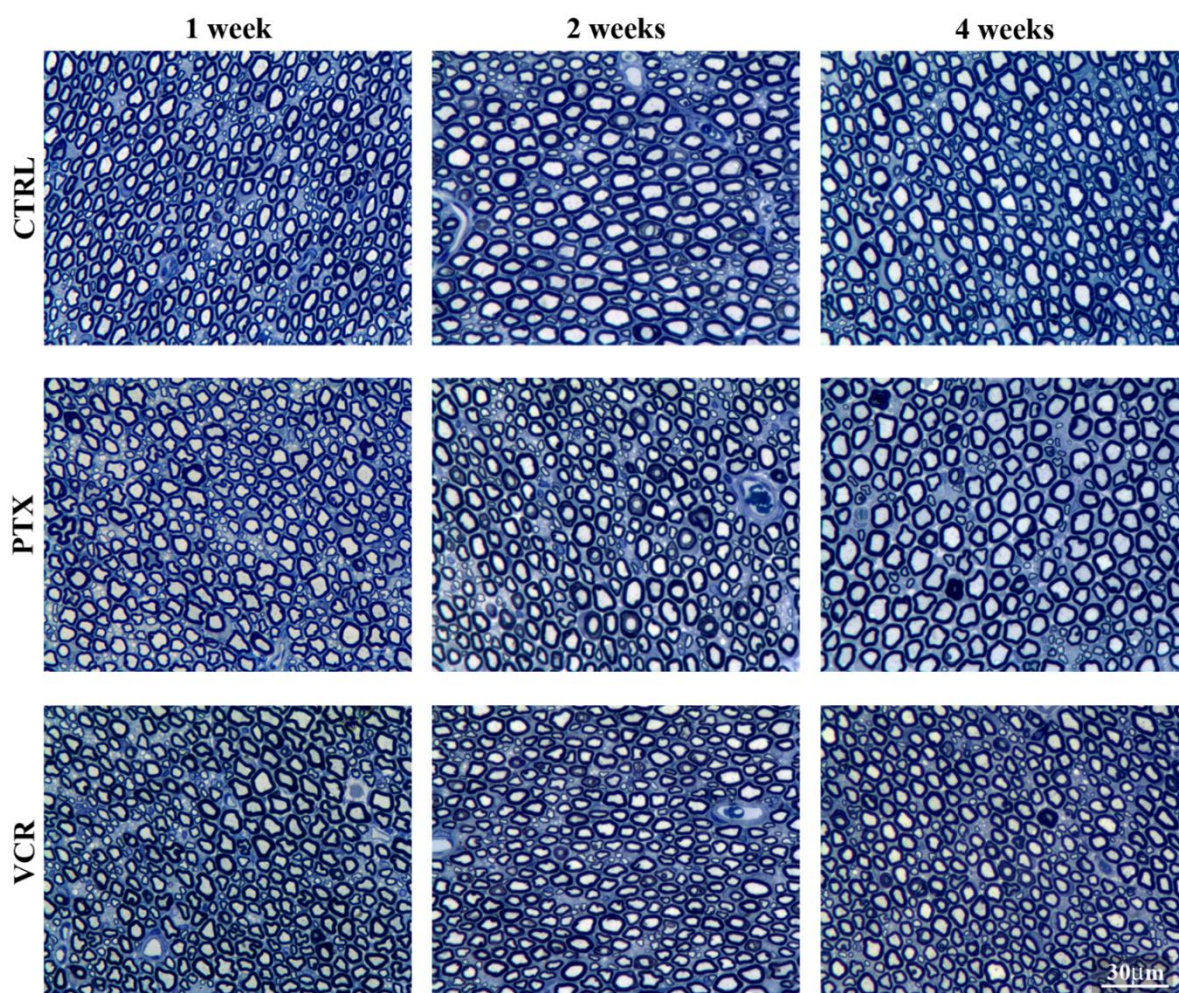
Fig.22. Morphological examination of sciatic nerves. Time course of fiber loss and degeneration in sciatic nerves of paclitaxel (PTX)- and vincristine (VCR)-treated rats compared to the controls (CTRL). Only a few degenerated fibers at the end of treatment were detected. Scale bar 30 μm.
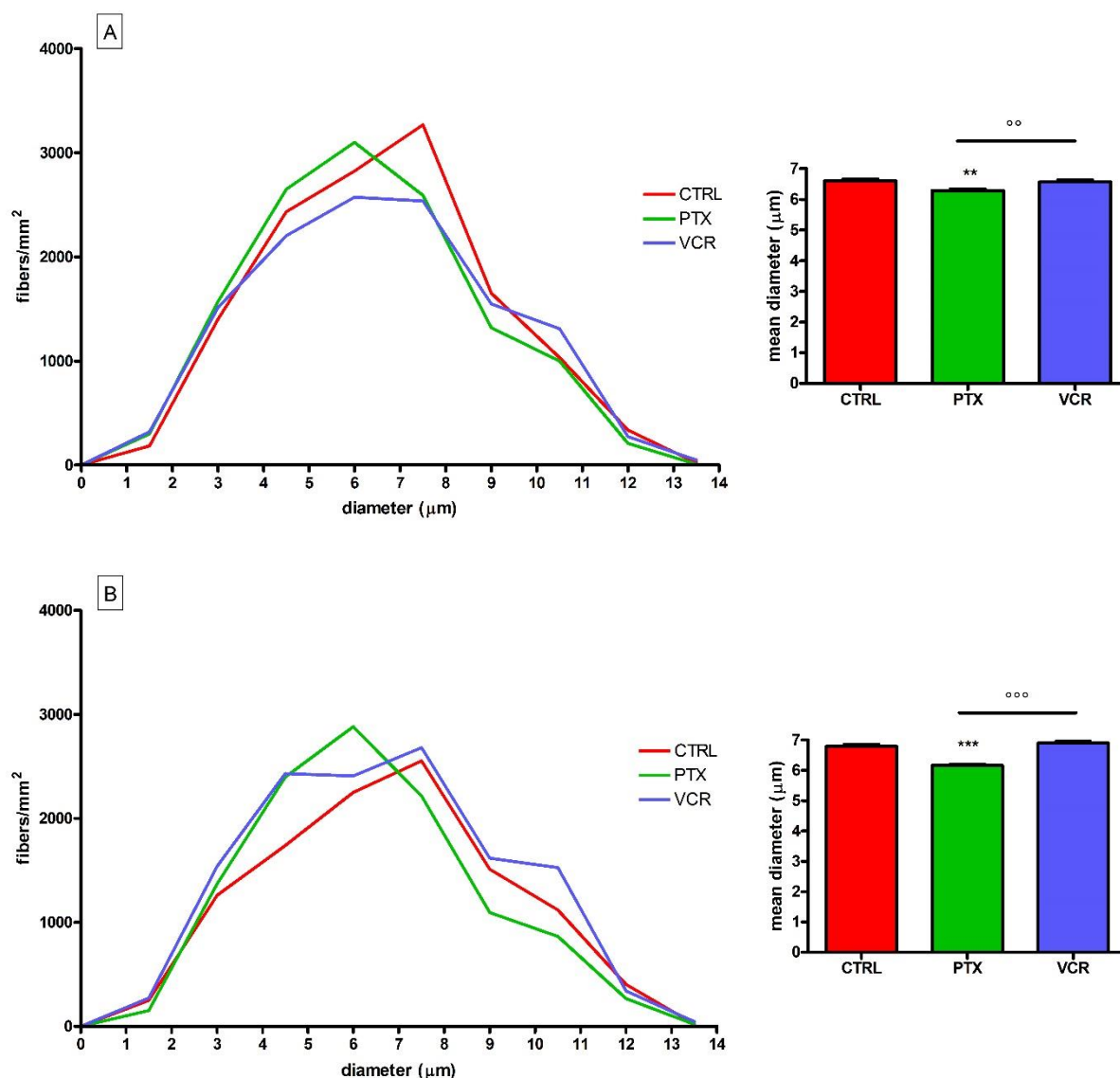
Fig.23. Morphometric analysis of sciatic nerves (on the left) and mean of fiber diameter (on the right). The graphs on the left indicates the morphometric analysis after 2 weeks of treatment (A) and at the end of treatment (B) for paclitaxel (PTX)- and vincristine (VCR)-treated groups compared to the controls (CTRL). The frequency distribution is normalized for the total number of fibers for each group. Only in PTX-treated group there was a loss of fibers with larger diameter after 2 weeks of treatment (A) and at the end of treatment (B). The graphs on the right confirms a reduction in mean fiber diameter in PTX-treated animals after 2 weeks of treatment (A) and at the end of treatment (B). Statistical evaluations were obtained using the one-way analysis of variance (ANOVA), followed by the Tukey post hoc-test. **p<0.01 for PTX vs CTRL; *** for PTX vs CTRL; °° p<0.01 for PTX vs VCR; °°°p<0.001 for PTX vs VCR.

2.3.2 Macrophage infiltration

In order to investigate the possible role of macrophage infiltration in the onset of axonal damage, immunohistochemical analyses were performed on peripheral nerves. The IHC analysis for CD68 showed a robust macrophage infiltration in caudal nerves of PTX-treated animals from the second week of treatment (2weeks) until the end of the experiment.

Macrophage infiltration in caudal nerves of VCR-treated rats started also from the second week of treatment, but it was less severe than in PTX-treated animals. IHC analysis on CTRL samples resulted negative (Fig.24).

A semi-quantitative analysis on anti-CD68 stained sections confirmed these observations (Tab.3).

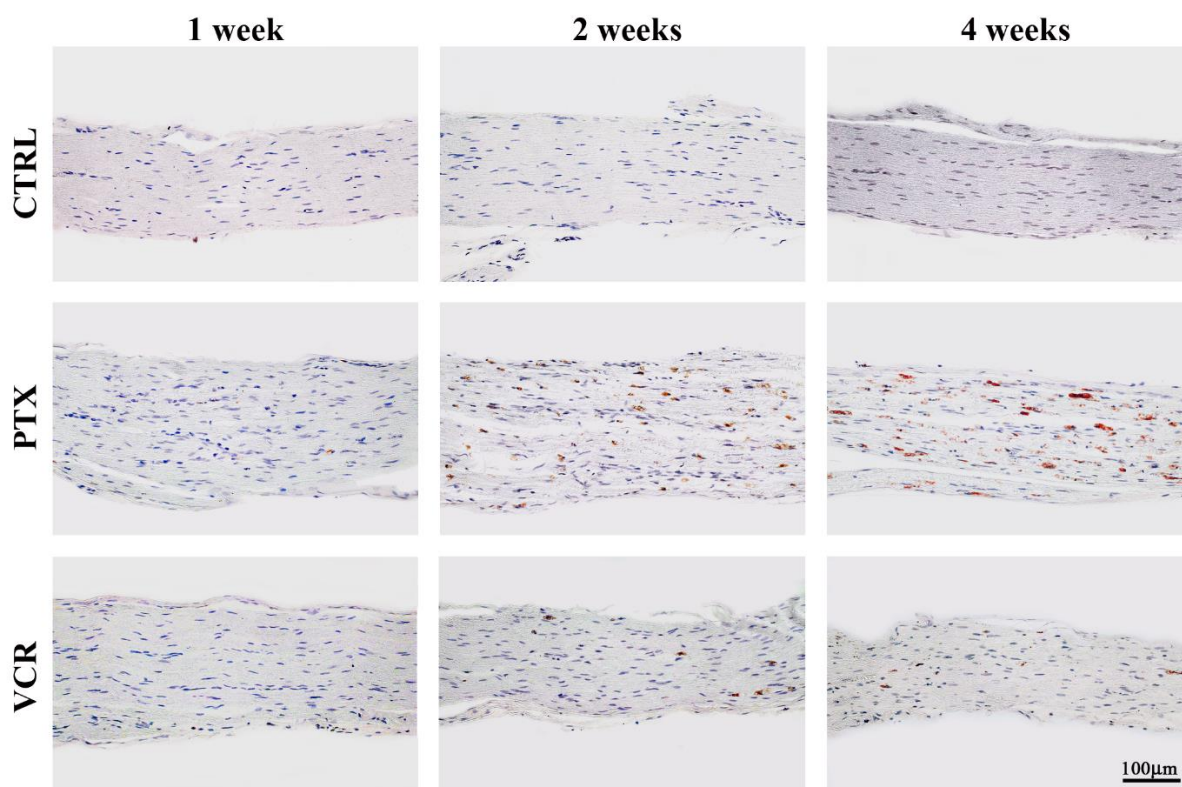Regarding to sciatic nerves, macrophage infiltration was absent in all samples (data not shown).

Fig.24. Macrophage infiltration in caudal nerves. Immunohistochemistry for CD68: caudal nerves of paclitaxel (PTX)-treated rats show a massive macrophage infiltration from the second week of treatment. Macrophage infiltration in vincristine (VCR)-treated rats was less severe than in PTX-treated animals and it started also from the second week of treatment. Scale bar 100 μm.

	1week	2weeks	4weeks
VCR	/	+	+
PTX	+	+++	++++

Tab.3. Semi-quantitative analysis of the immunohistochemical (IHC) results for CD68. A semi-quantitative analysis on anti-CD68 stained sections confirmed the observations obtained from the IHC studies. Macrophage infiltration in paclitaxel (PTX)-treated group started from the 1 week of treatment (+) and progressively increased until the end of the treatment (++++). The infiltration in vincristine (VCR) samples was milder than PTX, it was detected from the 2 weeks of treatment and it remained constant until the end of the treatment (+).

2.3.3 IENF density

The hind paw skin was harvested and immunohistochemical staining was performed in order to detect intraepidermal nerve fibers.

After 2 weeks of treatment and at the end of treatment, the animals treated with PTX and VCR showed a statistically significant reduction in IENF density compared to CTRL (Fig.25, 26).
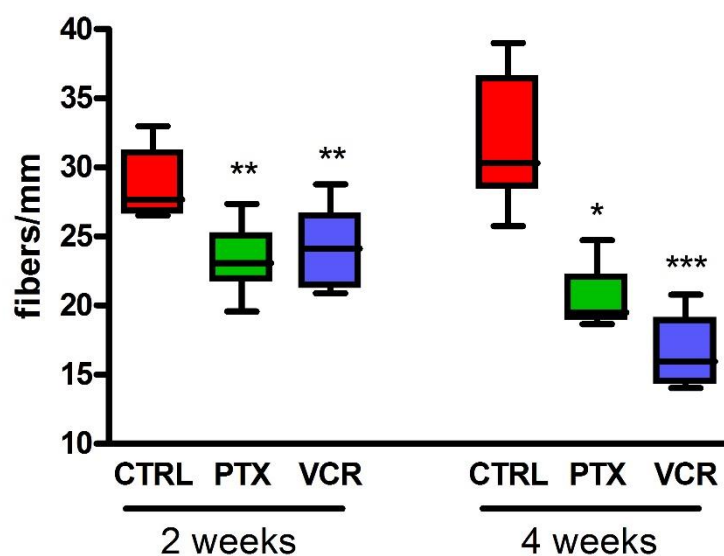

Fig.25. Intraepidermal nerve fiber density. After 2 weeks of treatment and at the end of treatment paclitaxel (PTX) and vincristine (VCR) induced a statistically significant reduction of IENF density when compared to controls (CTRL). Statistical evaluations were obtained using the Kruskal-Wallis test followed by the Dunn's post-hoc test. *p<0.05 for PTX vs CTRL; **p<0.01 for PTX, VCR vs CTRL; ***p<0.001 for VCR vs CTRL.
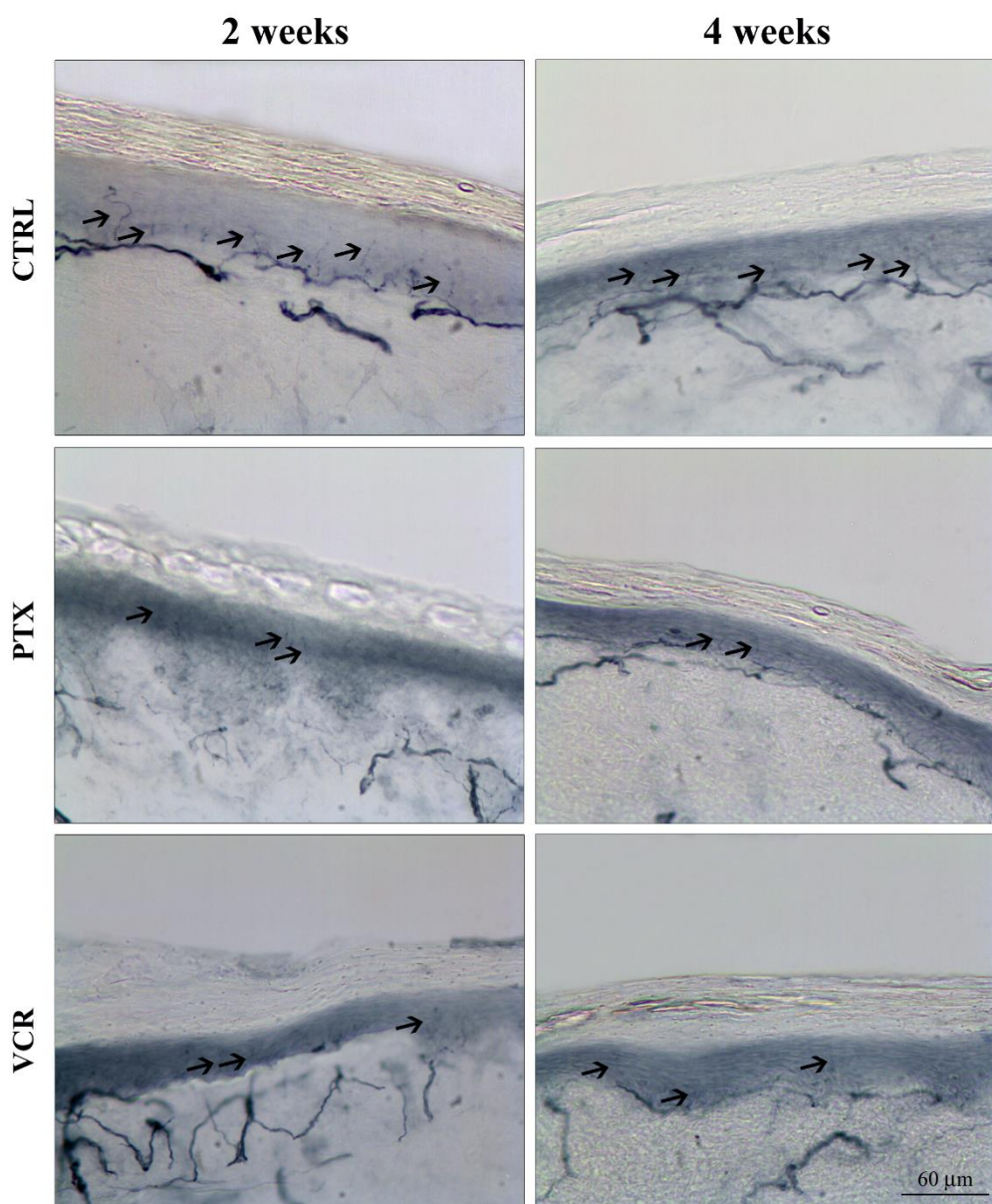
Fig.26. Skin biopsy. A representative image of skin biopsy samples of paclitaxel (PTX)- and vincristine (VCR)-treated animals. In PTX- and VCR-treated animals, a reduction in intraepidermal nerve fibers (IENF) density was evidenced (fibers indicated by arrows) both at 2 and 4 weeks of treatment. Scale bar 60 µm.

2.4 Nerve conduction studies

2.4.1 Sensory nerve conduction studies

In order to assess the axonal damage, the neurophysiological studies were conducted on caudal and digital nerves. In particular, the caudal nerve was studied at proximal and distal level in order to evaluate the length-dependent pathology. The data were obtained after 1, 2 weeks of treatment and at the end of the experiment and they confirmed the pathological observations previously reported.

After two weeks of treatment, both PTX- and VCR-treated groups presented a significant decrease in proximal amplitude ($p<0.001$ and $p<0.01$ respectively), which remained decreased compared to the controls until the end of the experiments ($p<0.01$ and $p<0.05$ respectively) (Fig.27). After 4 weeks of treatment, PTX-treated group showed a statistically significant reduction in proximal NCV compared to the CTRL only after 4 weeks of treatment ($p<0.05$), as reported in Fig.28.

At distal level a significant decrease in amplitude ($p<0.05$) was detected for VCR-treated group, whereas it was not possible to record the track in most animals of PTX-treated group due to the marked damage and loss of fibers. After 4 weeks of treatment, also the tracks of VCR-treated group were not recordable (Fig.29, 30).

Finally, a reduction in digital amplitude was observed only in PTX-treated animals at the end of the experiment ($p<0.05$) (Fig.31). At this level, no differences in NCV were detected (Fig.32).
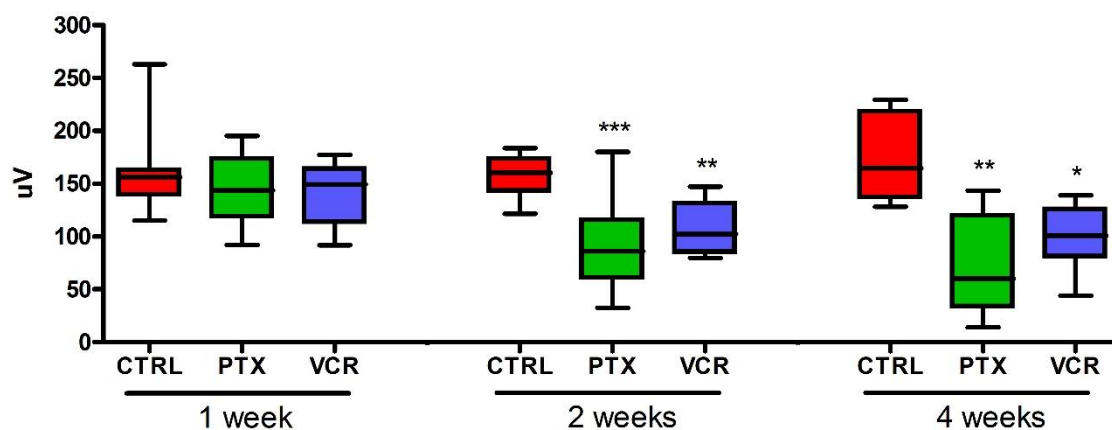
Fig.27. Proximal caudal amplitude. The graph reports the time course of the caudal amplitude at proximal level of paclitaxel (PTX)- and vincristine (VCR)-treated rats compared to controls (CTRL). From the second week of treatment a decrease in amplitude was observed for both the treatment until the end of the experiment. Statistical evaluations were obtained using the Kruskal-Wallis test followed by the Dunn's post-hoc test. *p<0.05 for VCR vs CTRL; **p<0.01 for PTX, VCR vs CTRL; ***p<0.001 for PTX vs CTRL.
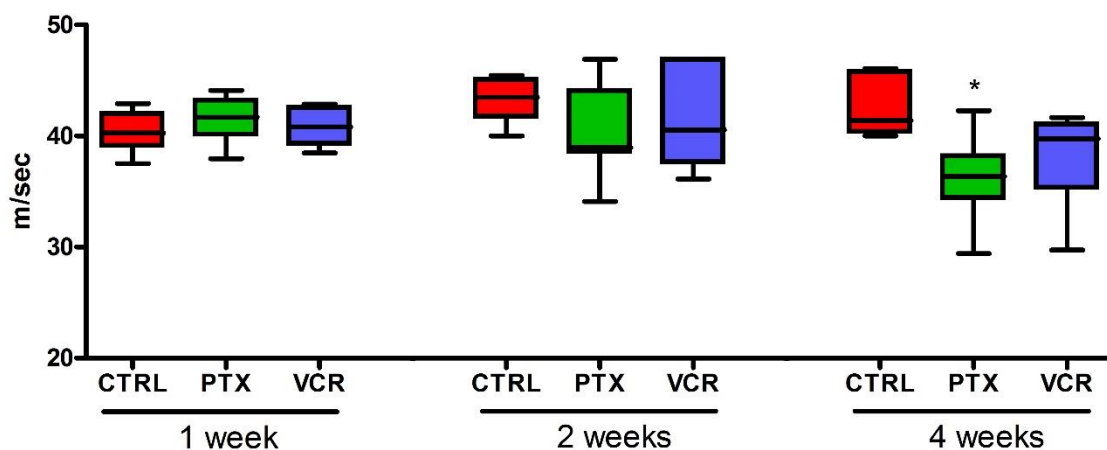

Fig.28. Proximal caudal NCV. The graph reports the time course of the caudal NCV at proximal level of paclitaxel (PTX)- and vincristine (VCR)-treated rats compared to controls (CTRL). At the end of the treatment, a decrease in NCV was detected only in PTX-treated group. Statistical evaluations were obtained using the Kruskal-Wallis test followed by the Dunn's post-hoc test. *p<0.05 for PTX vs CTRL.
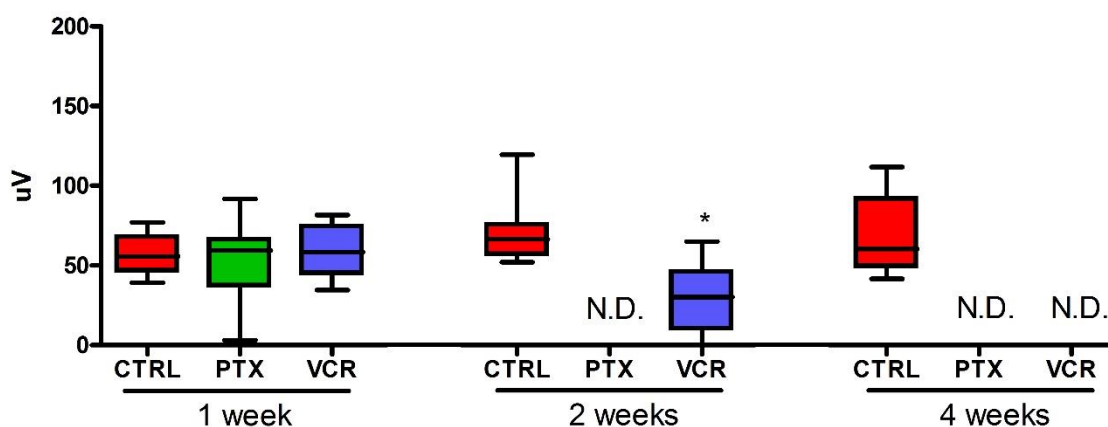
Fig.29. Distal caudal amplitude. The graph reports the time course of the caudal amplitude at distal level of paclitaxel (PTX)- and vincristine (VCR)-treated rats compared to controls (CTRL). At the second week of treatment a decrease in amplitude was observed for VCR-treated group whereas it was not possible to record PTX-treated group tracks (not detectable, N.D.). At the end of treatment, both the tracks were not recordable (N.D.). Statistical evaluations were obtained using the Kruskal-Wallis test followed by the Dunn's post-hoc test. *p<0.05 for VCR vs CTRL.
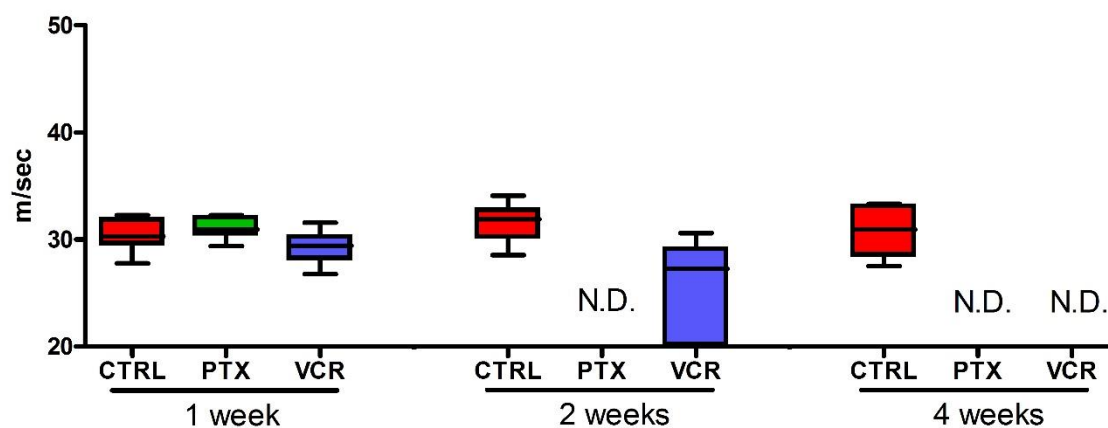

Fig.30. Distal caudal NCV. The graph reports the time course of the NCV at distal level of paclitaxel (PTX)- and vincristine (VCR)-treated rats compared to controls (CTRL). At the second week of treatment PTX-treated group tracks were not recordable (not detectable, N.D.). At the end of the treatment it was not possible to record the tracks for both PTX- and VCR-treated groups (N.D.). Statistical evaluations were obtained using the Kruskal-Wallis test followed by the Dunn's post-hoc test.
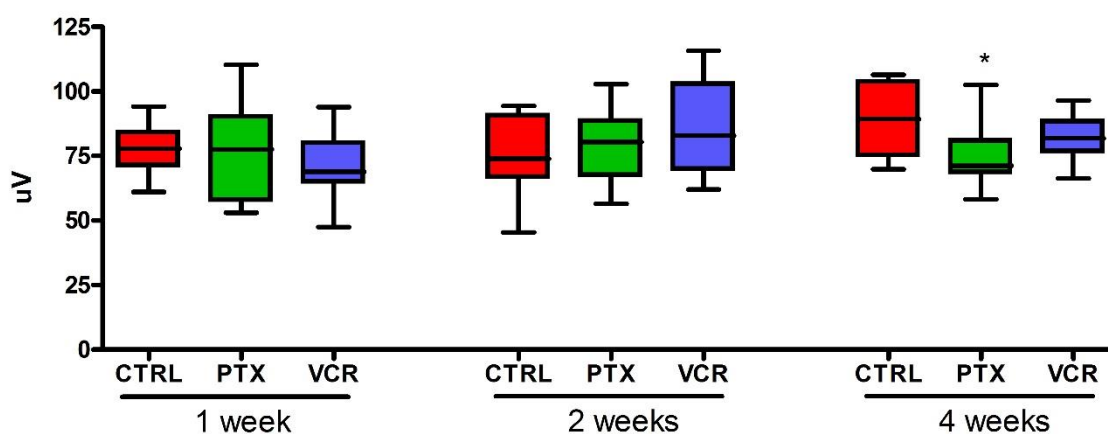
Fig.31. Digital amplitude. The graph reports the time course of the digital amplitude of paclitaxel (PTX)- and vincristine (VCR)-treated rats compared to controls (CTRL). Only at the end of treatment PTX-treated group had a reduction in amplitude. Statistical evaluations were obtained using the Kruskal-Wallis test followed by the Dunn's post-hoc test. *p<0.05 for PTX vs CTRL.
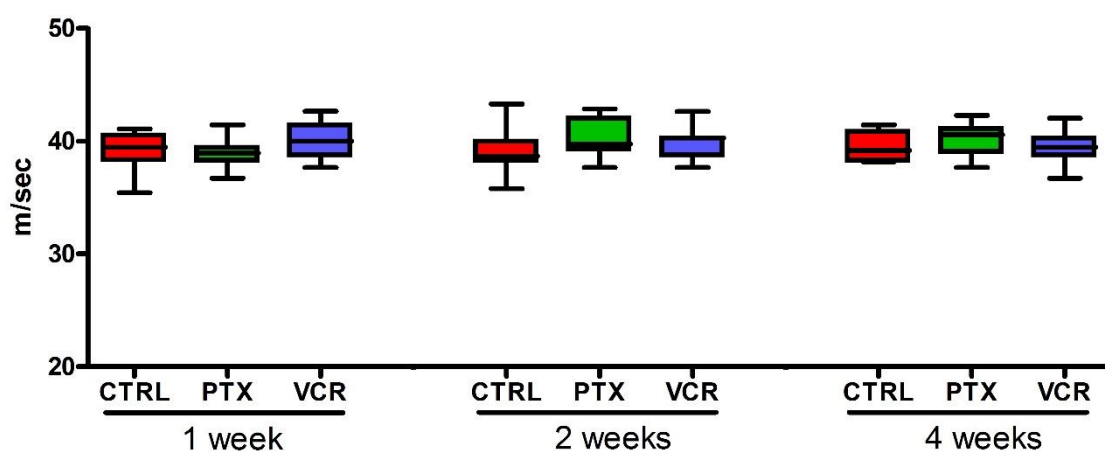

Fig.32. Digital NCV. The graph reports the time course of the NCV of paclitaxel (PTX)- and vincristine (VCR)-treated rats compared to controls (CTRL). No statistically significant differences were observed in both groups. Statistical evaluations were obtained using the Kruskal-Wallis test followed by the Dunn's post-hoc test.

2.4.2 Motor conduction studies

Since patients undergoing VCR chemotherapy regimen, experience not only a progressive sensory neuropathy, but also a motor neurotoxicity, motor conduction studies were

performed. The graph in Fig.33 shows a decrease in motor amplitude from the 1 week of treatment (p<0.001) until the end of the experiment (p<0.01) (Fig.33A) and also a decrease in motor NCV from the 2 weeks of treatment (p<0.01) (Fig.33B).
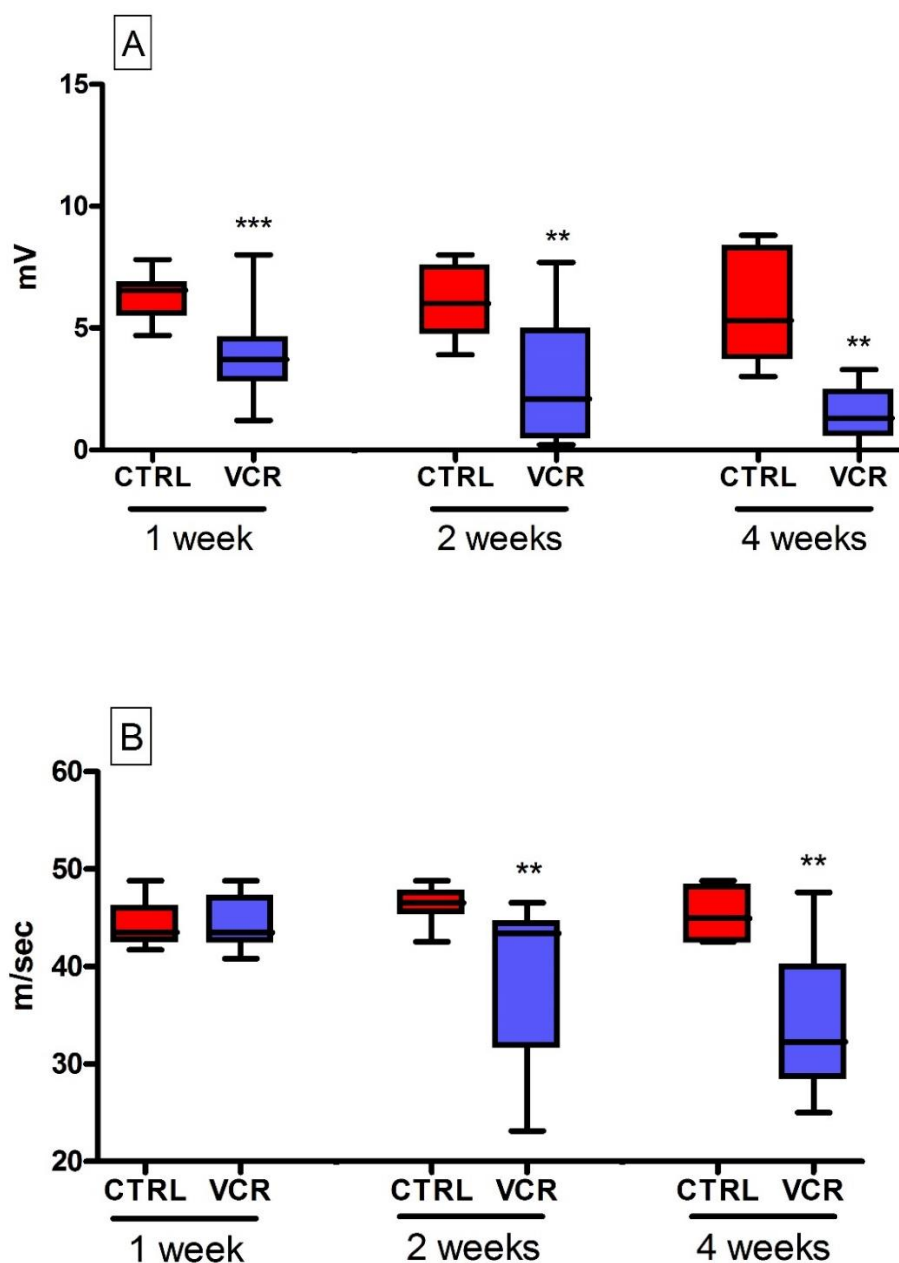

Fig.33. Motor conduction studies. The graph reports a time course of the motor amplitude (A) and NCV (B) of vincristine (VCR)-treated rats compared to controls (CTRL). The graph shows a decrease in amplitude starting from the 1 week of treatment. The NCV was reduced from the 2 weeks of treatment. Statistical evaluations were obtained using the Mann-Whitney test. **p<0.01, ***p<0.001 for VCR vs CTRL.

2.5 Serum NfL concentration

In PTX-treated animals, NfL concentration was increased from the first week of treatment until the 4 weeks, compared to the CTRL arm ($p<0.001$). This concentration was higher in the second week of treatment. In VCR-treated group, NfL concentration started to increase after 1 week of treatment, but it was statistically significant only after 3 weeks of treatment and at the end of treatment ($p<0.05$, $p<0.001$ respectively) (Fig.34).
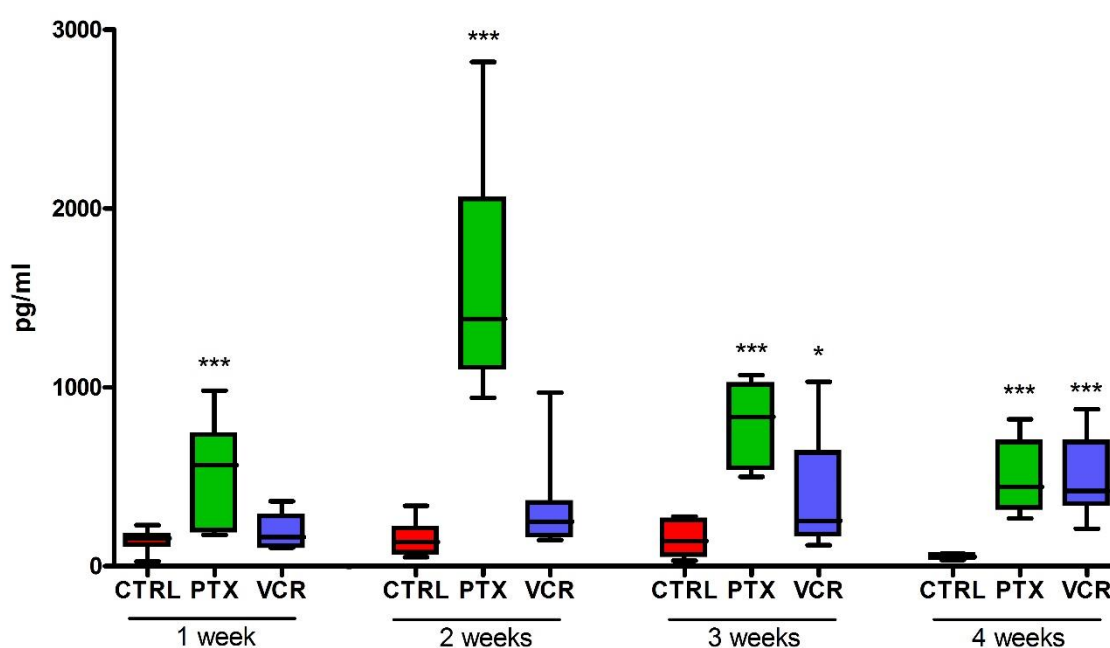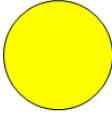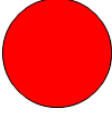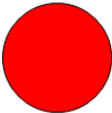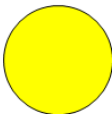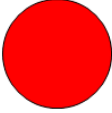

Fig.34. Serum neurofilaments (NfL) concentration. Data collected indicate that paclitaxel (PTX)-treated animals had an important increase in NfL concentration from 1 week of treatment until the end of the experiment. NfL concentration in vincristine (VCR)-treated group started to increase after 3 week of treatment. Data were compared to controls (CTRL).
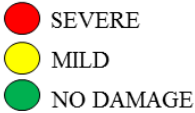
Statistical evaluations were obtained using the Kruskal-Wallis test followed by the Dunn's post-hoc test. *$p<0.05$ for VCR vs CTRL, ***$p<0.001$ for PTX, VCR vs CTRL.

3. SUMMARY OF THE RESULTS

The Fig.35 shows the results of the first experiment. In PTX-treated animals a marked axonal damage was detected compared to CDDP-treated ones. These results were supported by morphological and morphometric analysis, immunohistochemical investigations and neurophysiological studies. The serum NfL concentration resulted higher in PTX-treated group, according to the severe axonal damage.

Fig.35. Study 1 Summary results. The results indicated a more relevant axonal damage in paclitaxel (PTX)-treated animals compared to cisplatin (CDDP)-treated ones, which is correlated with an increase in serum Neurofilament Light (NfL) levels.

The Fig.36 shows the result of the Study 2. The time course evidenced a progressive increase of the axonal damage in PTX- and VCR-treated animals correlated with an increase in NfL concentration. NfL concentration was otherwise higher in PTX-treated group according to the more severe damage.

Fig.36. Study 2 Summary results. The results indicated a more severe axonal damage in paclitaxel (PTX)-treated rats. Also in vincristine (VCR)-treated animals the damage was quite severe. The serum Neurofilament Light (NfL) concentration was correlated to the axonal damage in each time point and it was anyway higher in PTX-treated group.

CONCLUSION

CIPN is the most prevalent neurological complication (Cavaletti et al., 2015) of anticancer therapy. CIPN is predominantly a sensory and length-dependent neuropathy (Brewer et al., 2015).

In this project, three different agents (CDDP, PTX and VCR) belonging respectively to platinum, taxanes and vinca alkaloids classes of antineoplastic agents were used. These drugs have different targets involved in the development of CIPN: for CDDP, neurotoxicity is due to the accumulation of the drug in the cell body of DRG. Otherwise, PTX is a microtubule-binding drug which stabilizes microtubules whereas VCR blocks the polymerization and therefore they act directly on axons (Carozzi et al., 2015).

Nowadays the monitoring of CIPN onset and progression in treated patients represents an unmet clinical need. Several efforts in the identification of risk factors were developed during the recent years: different polymorphisms in several genes were correlated to CIPN severity. However these data are supported by single studies or have contrasting evidence regarding their efficacy (Cavaletti et al., 2011; Cliff et al., 2017). Studies of NGF dosage were also conducted, indicating a dose-dependent reduction of NGF levels in plasma of CIPN models. Despite these interesting results, NGF levels were not efficient predictors of final patient outcome (Cavaletti et al., 2004).

Nfs are specifically expressed in axons and they are released into the interstitial fluid and blood after axonal damage (Al-Chalabi et al., 2003; Perrot et al., 2009). The measurement of NfL concentration is useful for clinical diagnostic evaluation in neurological disorders of the CNS (Perrot et al., 2009; Novakova et al., 2017; Khalil et al., 2018).

A recent work demonstrated a significantly raised plasma NfL concentration in patients with CMT which is an inherited neuropathy that causes a slowly and progressive axonal degeneration (Sandelius et al., 2018).

Since no blood biomarkers are nowadays available for monitoring the damage of PNS in CIPN, our goal was to evaluate the use of NfL serum concentration as a biomarker in preclinical models of peripheral neurotoxicity induced by CDDP, PTX and VCR.

Indeed, the ability to readily detect and supervise axonal damage would be an important advantage in the assessment of CIPN onset and in monitoring treatment response and prognosis. Moreover, serum parameter could be an important indicator due to its feasibility as a routine test.

The measure of NfL concentration was determined using an ultrasensitive Simoa immunoassay technology thanks to the collaboration with The Sahlgrenska Academy at the University of Gothenburg (Mölndal, Sweden) and with Disarm Therapeutics (Cambridge, MA, USA) which both used the home-brew kit Quanterix (Boston, MA, USA). The Simoa technology relies on single-molecule arrays and the simultaneous counting of singulated capture microbeads. This technique restricts the diffusion of the fluorescent molecules by femtoliter-sized wells. A camera counts the active or inactive wells which correspond to the presence or absence of single enzyme molecules. Therefore, this technique allows a remarkable gain in sensivity compared to the other assays (Khalil et al., 2012).

The neuropathy and the examination scores are based on objective evaluations, which include clinical examination and nerve conduction studies (NCS), and on subjective evaluations, which reflect patient symptoms. These subjective evaluations are based on grading scales of neurotoxicity or recently on self-reported questionnaires (Cavaletti et al., 2010; Hershman et al., 2011; Alberti et al., 2014; Miltenburg and Boogerd, 2014).

These scales are simple to use but they usually underestimate the severity and the frequency of symptoms and therefore, they are not satisfactory for evaluating CIPN (Cavaletti et al., 2010).

Dosing serum NfL concentration, we provided for the first time a dynamic measure of axonal damage, in particular a monitoring of the grade of severity in rat preclinical models of CIPN.

Our CIPN animal models lasted 4 weeks: this treatment period allowed to obtain a chronic model, which is able to mimic the features of the pathology in patients. Since previous works (not published) showed no differences between female and male animals, we chose female rats.

In the first experiment, animals were divided in CTRL, CDDP- and PTX-treated group. Neurotoxicity induced by CDDP is due to the accumulation of the drug in DRG, which results in large myelinated axons degeneration and nerve fiber axonopathy (Sharawy et al., 2015). In our CDDP rat model we evidenced a mild axonopathy which was characterized by a significant reduction in caudal amplitude and NCV only at distal level. Regarding to morphological investigations, at distal level only a few degenerated fibers were detected.

On the contrary, PTX is a microtubule-binding drug which stabilizes microtubules and leads to an important sensory axonal neurotoxicity (Carozzi et al., 2015). Rats treated with PTX showed a huge loss of fibers and a very evident axonopathy, confirmed by morphological and nerve conduction studies. Interestingly, the analysis of NfL quantification in serum samples collected at the end of treatment evidenced a significant increase of concentration in PTX samples whereas CDDP ones were similar to the control arm. The mild axonal damage was therefore correlated with the unchanged NfL concentration.

In the second experiment, we performed a time course study using PTX and VCR, which also targets the axons (Mora et al., 2016). The aim of this second experiment was to assess a weekly time course in order to observe the progression of the pathology and correlation with the serum NfL concentration.

The time course showed the onset of a progressive and length-dependent axonopathy, which started after 2 weeks of treatment, but was more severe in PTX-treated animals. In particular,

during the 4 weeks of treatment, we observed a more progressive increase in axonal damage in VCR-treated animals: the morphological analysis indicated a mild loss of fibers from the second week of treatment, which became more evident at the end of treatment. In addition, the reduction of amplitude started at the second week of treatment, and at the end of treatment, the nerves were so severely damaged that no electrical responses could be recorded. These observations were correlated with a progressive increase in serum NfL concentration which started to be statistically significant compared to control animals after three weeks of treatment. The NfL dosage of PTX-treated animals showed a significant increase in all the 4 weeks of treatment, although the concentration after 2 weeks of treatment was the highest one. This high concentration was confirmed by the morphological and neurophysiological investigations, which showed the beginning of an important axonal damage and loss of fibers at the time point of 2 weeks.

Anyway, NfL concentration was higher in PTX samples compared to VCR ones at every time points. These results were in agreement with the severity of the axonal damage, which was more important and marked in PTX-treated animals. Regarding to VCR results, we have recently published on Experimental Neurology the data of the NfL concentration time course (attached at the end of the thesis): for the first time serial results were obtained in a well-established CIPN animal model of repeated VCR administration inducing both sensory and motor nerves damage with the features of distal axonopathy (Meregalli et al., 2018).

Our data confirmed the role of NfL concentration as a biomarker for disease severity. The correlation between NfL and damage severity was also confirmed by other works: Sandelius and colleagues demonstrated that the severity scale for peripheral neuropathy in patients with CMT reflects NfL concentration (Sandelius et al., 2018). Another interesting work investigated NfL levels in ALS patients: they demonstrated that blood NfL levels in ALS-fast

were significantly higher than ALS-slow, thus being related to the course of this disease (Lu et al., 2015).

Other interesting observations concern the NfL concentration detection at early time points: regarding to PTX samples, after 1 week of treatment the NfL levels were significantly higher than in the CTRL group. Nevertheless, the neurophysiological and morphological analysis did not evidence any evident alteration. Regarding VCR sample, after 1 and 2 weeks of treatment the NfL concentration was higher than in the CTRL group. Although this difference was not statistically significant, it suggested a trend in increase. This observation indicates the possible prediction role of NfL concentration, which could evidence the prospective damage although the standard evaluation (e.g. the neurophysiological investigation) results negative. Therefore the advantages of NfL dosage would be several:

- ✓ the blood collection is not an invasive procedure and it is routinely performed in patients undergoing chemotherapy;

- ✓ each subject could be examined before, during and after chemotherapy in order to observe any difference from the baseline value;

- ✓ early detection of CIPN might prevent irreversible nerve damage (Meregalli et al., 2018).

These results indicate a possible role of blood NfL level measurement as a possible valid biomarker for monitoring CIPN and assessing the response to a therapy. In fact, since no effective treatment is currently available for CIPN, NfL dosage will be very useful in order to test any possible therapeutic agent.

Further developments of this project will encompass a pre-clinical study with a possible therapeutic agent for CIPN in order to measure the time course of NfL during the therapy. This

study will allow the assessment of a valid biomarker for readily detect and supervise axonal damage and further for monitoring treatment response and prognosis.

BIBLIOGRAPHY

Alberti P, Rossi E, Cornblath DR, Merkies I.S, Postma TJ, Frigeni B, Bruna J, Velasco R, Argyriou AA, Kalofonos HP, Psimaras D, Ricard D, Pace A, Galiè E, Briani C, Dalla Torre C, Faber CG, Lalisang RI, Boogerd W, Brandsma D, Koeppen S, Hense J, Storey D, Kerrigan S, Schenone A, Fabbri S, Valsecchi MG, Cavaletti G; CI-PeriNomS Group. Physician-assessed and patient-reported outcome measures in chemotherapy-induced sensory peripheral neurotoxicity: two sides of the same coin. Annals of oncology. 2014;25(1):257-64.

Al-Chalabi A, Miller CC. Neurofilaments and neurological disease. Bioessays. 2003 Apr;25(4):346-55.

Allodi I, Udina E, Navarro X. Specificity of peripheral nerve regeneration: interactions at the axon level. Progress in neurobiology. 2012;98(1):16-37.

Argyriou AA, Bruna J, Marmiroli P, Cavaletti G. Chemotherapy-induced peripheral neurotoxicity (CIPN): an update. Crit Rev Oncol Hematol. 2012 Apr;82(1):51-77.

Argyriou AA, Bruna J, Genazzani AA, Cavaletti G. Chemotherapy-induced peripheral neurotoxicity: management informed by pharmacogenetics. Nat Rev Neurol. 2017 Aug;13(8):492-504.

Bakogeorgos M, Georgoulias V. Risk-reduction and treatment of chemotherapy-induced peripheral neuropathy. Expert review of anticancer therapy. 2017;17(11):1045-1060.

Banach M, Juranek JK, Zygulska AL. Chemotherapy-induced neuropathies-a growing problem for patients and health care providers. Brain and Behavior. 2017;7(1):e00558.

Bennett GJ. A neuroimmune interaction in painful peripheral neuropathy. Clin J Pain. 2000 Sep;16(3 Suppl):S139-43. PubMed PMID: 11014458.

Brewer JR, Morrison G, Dolan ME, Fleming GF. Chemotherapy-induced peripheral neuropathy: Current status and progress. Gynecol Oncol. 2016 Jan;140(1):176-83.

Butler JS, Sadler PJ. Targeted delivery of platinum-based anticancer complexes. Curr Opin Chem Biol. 2013 Apr;17(2):175-88.

Canta A, Chiorazzi A, Carozzi VA, Meregalli C, Oggioni N, Bossi M, Rodriguez-Menendez V, Avezza F, Crippa L, Lombardi R, de Vito G, Piazza V, Cavaletti G, Marmiroli P. Age-related changes in the function and structure of the peripheral sensory pathway in mice. Neurobiol Aging. 2016 Sep;45:136-148.

Canta A, Pozzi E, Carozzi VA. Mitochondrial Dysfunction in Chemotherapy-Induced Peripheral Neuropathy (CIPN). Bellinger D, ed. Toxics. 2015;3(2):198-223.

Carozzi VA, Canta A, Chiorazzi A. Chemotherapy-induced peripheral neuropathy: What do we know about mechanisms? Neurosci Lett. 2015 Jun 2;596:90-107.

Cavaletti G, Pezzoni G, Pisano C, Oggioni N, Sala F, Zoia C, Ferrarese C, Marmiroli P, Tredici G. Cisplatin-induced peripheral neurotoxicity in rats reduces the circulating levels of nerve growth factor. Neurosci Lett. 2002 Apr 5;322(2):103-6. **a**

Cavaletti G, Petruccioli MG, Marmiroli P, Rigolio R, Galbiati S, Zoia C, Ferrarese C, Tagliabue E, Dolci C, Bayssas M, Griffon Etienne G, Tredici G. Circulating nerve growth factor level changes during oxaliplatin treatment-induced neurotoxicity in the rat. Anticancer Res. 2002 Nov-Dec;22(6C):4199-204. **b**

Cavaletti G, Bogliun G, Marzorati L, Zincone A, Piatti M, Colombo N, Franchi D, La Presa MT, Lissoni A, Buda A, Fei F, Cundari S, Zanna C. Early predictors of peripheral neurotoxicity in cisplatin and paclitaxel combination chemotherapy. Ann Oncol. 2004 Sep;15(9):1439-42.

Cavaletti G, Frigeni B, Lanzani F, Mattavelli L, Susani E, Alberti P, Cortinovis D, Bidoli P. Chemotherapy-Induced Peripheral Neurotoxicity assessment: a critical revision of the currently available tools. European journal of cancer. 2010;46(3):479-94.

Cavaletti G, Alberti P, Marmiroli P. Chemotherapy-induced peripheral neurotoxicity in the era of pharmacogenomics. Lancet Oncol. 2011 Nov;12(12):1151-61.

Cavaletti G, Marmiroli P. Chemotherapy-induced peripheral neurotoxicity. Curr Opin Neurol. 2015 Oct;28(5):500-7. **a**

Cavaletti G, Alberti P, Marmiroli P. Chemotherapy-induced peripheral neurotoxicity in cancer survivors: an underdiagnosed clinical entity? Am Soc Clin Oncol Educ Book. 2015:e553-60.

b

Chiorazzi A, Wozniak KM, Rais R, Wu Y, Gadiano AJ, Farah MH, Liu Y, Canta A, Alberti P, Rodriguez-Menendez V, Meregalli C, Fumagalli G, Monza L, Pozzi E, Vornov JJ, Polydefkis M, Pietra C, Slusher BS, Cavaletti G. Ghrelin agonist HM01 attenuates chemotherapy-induced neurotoxicity in rodent models. Eur J Pharmacol. 2018 Dec 5;840:89-103.

Cleeland CS, Bennett GJ, Dantzer R, Dougherty PM, Dunn AJ, Meyers CA, Miller AH, Payne R, Reuben JM, Wang XS, Lee BN. Are the symptoms of cancer and cancer treatment due to a shared biologic mechanism? A cytokine-immunologic model of cancer symptoms. Cancer. 2003 Jun 1;97(11):2919-25.

Cliff J, Jorgensen AL, Lord R, Azam F, Cossar L, Carr DF, Pirmohamed M. The molecular genetics of chemotherapy-induced peripheral neuropathy: A systematic review and meta-analysis. Crit Rev Oncol Hematol. 2017 Dec;120:127-140.

Cohlberg JA, Hajarian H, Tran T, Alipourjeddi P, Noveen A. Neurofilament protein heterotetramers as assembly intermediates. J Biol Chem. 1995 Apr 21;270(16):9334-9.

Cornblath DR, Chaudhry V, Carter K, Lee D, Seysedadr M, Miernicki M, Joh T. Total neuropathy score: validation and reliability study. Neurology. 1999;53:1660-1664.

Diaz PL, Furfari A, Wan BA, Lam H, Charames G, Drost L, Fefekos A, Ohearn S, Blake A, Asthana R, Chow E, DeAngelis C. Predictive biomarkers of chemotherapy-induced peripheral neuropathy: a review. Biomark Med. 2018 Aug;12(8):907-916.

Disanto G, Barro C, Benkert P, Naegelin Y, Schädelin S, Giardiello A, Zecca C, Blennow K, Zetterberg H, Leppert D, Kappos L, Gobbi C, Kuhle J; Swiss Multiple Sclerosis Cohort Study Group. Serum Neurofilament light: A biomarker of neuronal damage in multiple sclerosis. Ann Neurol. 2017 Jun;81(6):857-870.

Drobník J, Horácek P. Specific biological activity of platinum complexes. Contribution to the theory of molecular mechanism. Chem Biol Interact. 1973 Oct; 7(4):223-9.

Duggett NA, Griffiths LA, McKenna OE, de Santis V, Yongsanguanchai N, Mokori EB, Flatters SJ. Oxidative stress in the development, maintenance and resolution of paclitaxel-induced painful neuropathy. Neuroscience. 2016 Oct 1;333:13-26.

Englander EW. DNA damage response in peripheral nervous system: coping with cancer therapy-induced DNA lesions. DNA Repair (Amst). 2013 Aug; 12 (8):685-90.

Flatters SJL, Dougherty PM, Colvin LA. Clinical and preclinical perspectives on Chemotherapy-Induced Peripheral Neuropathy (CIPN): a narrative review. Br J Anaesth. 2017 Oct 1;119(4):737-749.

Gaiottino J, Norgren N, Dobson R, Topping J, Nissim A, Malaspina A, Bestwick JP, Monsch AU, Regeniter A, Lindberg RL, Kappos L, Leppert D, Petzold A, Giovannoni G, Kuhle J.

Increased neurofilament light chain blood levels in neurodegenerative neurological diseases. PLoS One. 2013 Sep 20;8(9):e75091.

Gornstein E, Schwarz TL. The paradox of paclitaxel neurotoxicity: Mechanisms and unanswered questions. Neuropharmacology. 2014 Jan;76 Pt A:175-83.

Gornstein EL, Schwarz TL. Neurotoxic mechanisms of paclitaxel are local to the distal axon and independent of transport defects. Exp Neurol. 2017 Feb;288:153-166.

Heins S, Wong PC, Müller S, Goldie K, Cleveland DW, Aebi U. The rod domain of NF-L determines neurofilament architecture, whereas the end domains specify filament assembly and network formation. J Cell Biol. 1993 Dec;123(6 Pt1):1517-33.

Hershman DL, Weimer LH, Wang A, Kranwinkel G, Brafman L, Fuentes D, Awad D, Crew KD. Association between patient reported outcomes and quantitative sensory tests for measuring long-term neurotoxicity in breast cancer survivors treated with adjuvant paclitaxel chemotherapy. Breast cancer research and treatment. 2011;125(3):767-74.

Hirokawa N, Glicksman MA, Willard MB. Organization of mammalian neurofilament polypeptides within the neuronal cytoskeleton. J Cell Biol. 1984 Apr;98(4):1523-36.

Hisanaga S, Hirokawa N. Structure of the peripheral domains of neurofilaments revealed by low angle rotary shadowing. J Mol Biol. 1988 Jul 20;202(2):297-305.

Hopkins HL, Duggett NA, Flatters SJL. Chemotherapy-induced painful neuropathy: pain-like behaviours in rodent models and their response to commonly used analgesics. Curr Opin Support Palliat Care. 2016 Jun;10(2):119-128.

Howle JA, Gale GR. Cis-dichlorodiammineplatinum (II). Persistent and selective inhibition of deoxyribonucleic acid synthesis in vivo. Biochem Pharmacol. 1970 Oct; 19 (10):2757-62.

Lees JG, Makker PG, Tonkin RS, Abdulla M, Park SB, Goldstein D, Moalem-Taylor G. Immune-mediated processes implicated in chemotherapy-induced peripheral neuropathy. Eur J Cancer. 2017 Mar;73:22-29.

Lu CH, Macdonald-Wallis C, Gray E, Pearce N, Petzold A, Norgren N, Giovannoni G, Fratta P, Sidle K, Fish M, Orrell R, Howard R, Talbot K, Greensmith L, Kuhle J, Turner MR, Malaspina A. Neurofilament light chain: A prognostic biomarker in amyotrophic lateral sclerosis. Neurology. 2015 Jun 2;84(22):2247-57.

Lu CH, Petzold A, Topping J, Allen K, Macdonald-Wallis C, Clarke J, Pearce N, Kuhle J, Giovannoni G, Fratta P, Sidle K, Fish M, Orrell R, Howard R, Greensmith L, Malaspina A. Plasma neurofilament heavy chain levels and disease progression in amyotrophic lateral sclerosis: insights from a longitudinal study. J Neurol Neurosurg Psychiatry. 2015 May;86(5):565-73.

Jacobs BC, Willison HJ. Peripheral neuropathies: Biomarkers for axonal damage in immune-mediated neuropathy. Nat Rev Neurol. 2009 Nov;5(11):584-5.

Kampan NC, Madondo MT, McNally OM, Quinn M, Plebanski M. Paclitaxel and Its Evolving Role in the Management of Ovarian Cancer. Biomed Res Int. 2015;2015:413076.

Kim PY, Johnson CE. Chemotherapy-induced peripheral neuropathy: a review of recent findings. Current opinion in anaesthesiology. 2017;30(5):570-576.

Kerckhove N, Collin A, Condé S, Chaleteix C, Pezet D, Balayssac D. Long-term effects, pathophysiological mechanisms, and risk factors of chemotherapy-induced peripheral neuropathies: a comprehensive literature review. Frontiers in Pharmacology. 2017;8:86.

Khalil M, Enzinger C, Langkammer C, Ropele S, Mader A, Trentini A, Vane ML, Wallner-Blazek M, Bachmaier G, Archelos JJ, Koel-Simmelink MJ, Blankenstein MA, Fuchs S, Fazekas F, Teunissen CE. CSF neurofilament and N-acetylaspartate related brain changes in clinically isolated syndrome. Mult Scler. 2013 Apr;19(4):436-42.

Khalil M, Teunissen CE, Otto M, Piehl F, Sormani MP, Gattringer T, Barro C, Kappos L, Comabella M, Fazekas F, Petzold A, Blennow K, Zetterberg H, Kuhle J. Neurofilaments as biomarkers in neurological disorders. Nat Rev Neurol. 2018 Oct;14(10):577-589.

Khalilzadeh M, Panahi G, Rashidian A, Hadian MR, Abdollahi A, Afshari K, Shakiba S, Norouzi-Javidan A, Rahimi N, Momeny M, Dehpour AR. The protective effects of sumatriptan on vincristine - induced peripheral neuropathy in a rat model. Neurotoxicology. 2018 Jul;67:279-286.

Kuhle J, Barro C, Andreasson U, Derfuss T, Lindberg R, Sandelius Å, Liman V, Norgren N, Blennow K, Zetterberg H. Comparison of three analytical platforms for quantification of the neurofilament light chain in blood samples: ELISA, electrochemiluminescence immunoassay and Simoa. Clin Chem Lab Med. 2016 Oct 1;54(10):1655-61.

Kuhle J, Nourbakhsh B, Grant D, Morant S, Barro C, Yaldizli Ö, Pelletier D, Giovannoni G, Waubant E, Gnanapavan S. Serum neurofilament is associated with progression of brain atrophy and disability in early MS. Neurology. 2017 Feb 28;88(9):826-831.

Kuhle J, Plattner K, Bestwick JP, Lindberg RL, Ramagopalan SV, Norgren N, Nissim A, Malaspina A, Leppert D, Giovannoni G, Kappos L. A comparative study of CSF neurofilament light and heavy chain protein in MS. Mult Scler. 2013 Oct;19(12):1597-603.

Madsen ML, Due H, Ejskjær N, Jensen P, Madsen J, Dybkær K. Aspects of vincristine-induced neuropathy in hematologic malignancies: a systematic review. Cancer Chemother Pharmacol. 2019 Sep;84(3):471-485.

Maheswari KU, Ramachandran T, Rajaji D. Interaction of cisplatin with planar model membranes - dose dependent change in electrical characteristics. Biochim Biophys Acta. 2000 Feb 15;1463 (2):230-40.

Meregalli C, Marjanovic I, Scali C, Monza L, Spinoni N, Galliani C, Brivio R, Chiorazzi A, Ballarini E, Rodriguez-Menendez V, Carozzi VA, Alberti P, Fumagalli G, Pozzi E, Canta A, Quartu M, Briani C, Oggioni N, Marmiroli P, Cavaletti G. High-dose intravenous

immunoglobulins reduce nerve macrophage infiltration and the severity of bortezomib-induced peripheral neurotoxicity in rats. J Neuroinflammation. 2018 Aug 21;15(1):232. **a**

Meregalli C, Fumagalli G, Alberti P, Canta A, Carozzi VA, Chiorazzi A, Monza L, Pozzi E, Sandelius Å, Blennow K, Zetterberg H, Marmiroli P, Cavaletti G. Neurofilament light chain as disease biomarker in a rodent model of chemotherapy induced peripheral neuropathy. Exp Neurol. 2018 Sep;307:129-132. **b**

Miltenburg NC, Boogerd W. Chemotherapy-induced neuropathy: A comprehensive survey. Cancer Treat Rev. 2014 Aug;40(7):872-82.

Mora E, Smith EM, Donohoe C, Hertz DL. Vincristine-induced peripheral neuropathy in pediatric cancer patients. Am J Cancer Res. 2016 Nov 1;6(11):2416-2430. eCollection 2016.

Nelson WJ, Traub P. Intermediate (10 nm) filament proteins and the Ca2+-activated proteinase specific for vimentin and desmin in the cells from fish to man: an example of evolutionary conservation. J Cell Sci. 1982 Oct;57:25-49.

Norgren N, Rosengren L, Stigbrand T. Elevated neurofilament levels in neurological diseases. Brain Res. 2003 Oct 10;987(1):25-31.

Notturno F, Caporale CM, De Lauretis A, Uncini A. Glial fibrillary acidic protein: a marker of axonal Guillain-Barrè syndrome and outcome. Muscle Nerve. 2008 Jul;38(1):899-903.

Novakova L, Zetterberg H, Sundström P, Axelsson M, Khademi M, Gunnarsson M, Malmeström C, Svenningsson A, Olsson T, Piehl F, Blennow K, Lycke J. Monitoring disease activity in multiple sclerosis using serum neurofilament light protein. Neurology. 2017 Nov 28;89(22):2230-2237.

Park SB, Goldstein D, Krishnan AV, Lin CS, Friedlander ML, Cassidy J, Koltzenburg M, Kiernan MC. Chemotherapy-induced peripheral neurotoxicity: a critical analysis. CA: A cancer journal for clinicians. 2013;63(6):419-37.

Perrot R, Berges R, Bocquet A, Eyer J. Review of the multiple aspects of neurofilament functions, and their possible contribution to neurodegeneration. Mol Neurobiol. 2008 Aug;38(1):27-65.

Perrot R, Eyer J. Neuronal intermediate filaments and neurodegenerative disorders. Brain Res Bull. 2009 Oct 28;80(4-5):282-95.

Petzold A. Neurofilament phosphoforms: surrogate markers for axonal injury, degeneration and loss. J Neurol Sci. 2005 Jun 15;233(1-2):183-98.

Petzold A, Brettschneider J, Jin K, Keir G, Murray NM, Hirsch NP, Itoyama Y, Reilly MM, Takeda A, Tumani H. CSF protein biomarkers for proximal axonal damage improve prognostic accuracy in the acute phase of Guillain-Barré syndrome. Muscle Nerve. 2009 Jul;40(1):42-9.

Petzold A, Keir G, Green AJ, Giovannoni G, Thompson EJ. A specific ELISA for measuring neurofilament heavy chain phosphoforms. J Immunol Methods. 2003 Jul;278(1-2):179-90.

Podratz JL, Knight AM, Ta LE, Staff NP, Gass JM, Genelin K, Schlattau A, Lathroum L, Windebank AJ. Cisplatin induced mitochondrial DNA damage in dorsal root ganglion neurons. Neurobiol Dis. 2011 Mar;41(3):661-8.

Rabik CA, Dolan ME. Molecular mechanisms of resistance and toxicity associated with platinating agents. Cancer Treat Rev. 2007 Feb; 33 (1):9-23.

Renshaw E, Thomson AJ. Tracer studies to locate the site of platinum ions within filamentous and inhibited cells of Escherichia coli. J Bacteriol. 1967 Dec; 94 (6):1915-8.

Rohrer JD, Woollacott IO, Dick KM, Brotherhood E, Gordon E, Fellows A, Toombs J, Druyeh R, Cardoso MJ, Ourselin S, Nicholas JM, Norgren N, Mead S, Andreasson U, Blennow K, Schott JM, Fox NC, Warren JD, Zetterberg H. Serum neurofilament light chain protein is a measure of disease intensity in frontotemporal dementia. Neurology. 2016 Sep 27;87(13):1329-36.

Sandelius Å, Zetterberg H, Blennow K, Adiutori R, Malaspina A, Laura M, Reilly MM, Rossor AM. Plasma neurofilament light chain concentration in the inherited peripheral neuropathies. Neurology. 2018 Feb 6;90(6):e518-e524.

Seretny M, Currie GL, Sena ES, Ramnarine S, Grant R, MacLeod MR, Colvin LA, Fallon M. Incidence, prevalence, and predictors of chemotherapy-induced peripheral neuropathy: A systematic review and meta-analysis. Pain. 2014 Dec;155(12):2461-70.

Sharawy N, Rashed L, Youakim MF. Evaluation of multi-neuroprotective effects of erythropoietin using cisplatin induced peripheral neurotoxicity model. Exp Toxicol Pathol. 2015 Apr;67(4):315-22.

Soylu-Kucharz R, Sandelius Å, Sjögren M, Blennow K, Wild EJ, Zetterberg H, Björkqvist M. Neurofilament light protein in CSF and blood is associated with neurodegeneration and disease severity in Huntington's disease R6/2 mice. Sci Rep. 2017 Oct 26;7(1):14114.

Starobova H, Vetter I. Pathophysiology of Chemotherapy-Induced Peripheral Neuropathy. Front Mol Neurosci. 2017 May 31; 10:174.

Stillman M, Cata JP. Management of chemotherapy-induced peripheral neuropathy. Curr Pain Headache Rep. 2006 Aug;10(4):279-87.

Themistocleous AC, Ramirez JD, Serra J, Bennett DL. The clinical approach to small fibre neuropathy and painful channelopathy. Practical Neurology. 2014;14:368–379.

Trostchansky A. Overview of Lipid Biomarkers in Amyotrophic Lateral Sclerosis (ALS). Adv Exp Med Biol. 2019;1161:233-241.

Üstün R, Oğuz EK, Şeker A, Korkaya H. Thymoquinone prevents cisplatin neurotoxicity in primary DRG neurons. Neurotoxicology. 2018 Dec;69:68-76.

Vakilian A, Masoumi J, Mirzaee S, Khorramdelazad H. Expression analysis of beta-secretase 1 (BACE1) enzyme in peripheral blood of patients with Alzheimer's disease. Caspian J Intern Med. 2019 Summer;10(3):276-280.

van de Velde ME, Kaspers GL, Abbink FCH, Wilhelm AJ, Ket JCF, van den Berg MH. Vincristine-induced peripheral neuropathy in children with cancer: A systematic review. Crit Rev Oncol Hematol. 2017 Jun;114:114-130.

Velasco R, Bruna J. [Chemotherapy-induced peripheral neuropathy: an unresolved issue]. Neurologia. 2010 Mar;25(2):116-31.

Velasco R, Navarro X, Gil-Gil M, Herrando-Grabulosa M, Calls A, Bruna J. Neuropathic Pain and Nerve Growth Factor in Chemotherapy-Induced Peripheral Neuropathy: Prospective Clinical-Pathological Study. J Pain Symptom Manage. 2017 Dec;54(6):815-825.

Wessig C, Bendszus M, Reiners K, Pham M. Lesions of the peripheral nerves: MR neurography as an innovative supplement to electrodiagnostics. Klinische Neurophysiologie. 2011;42:231-238.

WHO, International programme on chemical safety. Biomarkers in risk assessment: validity and validation. www.inchem.org/documents/ehc/ehc/ehc222.htm.

Wolf S, Barton D, Kottschade L, Grothey A, Loprinzi C. Chemotherapy-induced peripheral neuropathy: prevention and treatment strategies. Eur J Cancer. 2008 Jul;44(11):1507-15.

Yang L, Yu L, Chen X, Hu Y, Wang B. Clinical Analysis of Adverse Drug Reactions between Vincristine and Triazoles in Children with Acute Lymphoblastic Leukemia. Med Sci Monit. 2015 Jun 7;21:1656-61.

Yuan A, Rao MV, Veeranna, Nixon RA. Neurofilaments at a glance. J Cell Sci. 2012 Jul 15;125(Pt 14):3257-63.
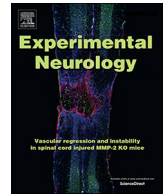
Short Communication

Neurofilament light chain as disease biomarker in a rodent model of chemotherapy induced peripheral neuropathy

Cristina Meregalli[a,*], Giulia Fumagalli[a,b], Paola Alberti[a,b], Annalisa Canta[a], Valentina Alda Carozzi[a], Alessia Chiorazzi[a], Laura Monza[a,c], Eleonora Pozzi[a,b], Åsa Sandelius[d,e], Kaj Blennow[d,e], Henrik Zetterberg[d,e,f,g], Paola Marmiroli[a], Guido Cavaletti[a]

[a] School of Medicine and Surgery, Experimental Neurology Unit and NeuroMI, University of Milano-Bicocca, Monza, Italy
[b] PhD program in Neuroscience, University of Milano-Bicocca, Monza, Italy
[c] PhD program in Translational and Molecular Medicine (Dimet), University of Milano-Bicocca, Monza, Italy
[d] Department of Psychiatry and Neurochemistry, The Sahlgrenska Academy at the University of Gothenburg, Mölndal, Sweden
[e] Clinical Neurochemistry Laboratory, Sahlgrenska University Hospital, Mölndal, Sweden
[f] Department of Molecular Neuroscience, UCL Institute of Neurology, Queen Square, London, United Kingdom
[g] UK Dementia Research Institute at UCL, London, United Kingdom

ARTICLE INFO

ABSTRACT

The objective of this study is to test the feasibility of using serum neurofilament light chain (NfL) as a disease biomarker in Chemotherapy Induced Peripheral Neuropathy (CIPN) since this easy accessible biological test may have a large impact on clinical management and safety of cancer patients.

We performed this preclinical study using a well-characterized rat model based on repeated administration of the cytostatic drug vincristine (VCR, 0.2 mg/kg intravenously via the tail vein once/week for 4 times). Serial NfL serum concentration was measured using the in-house Simoa NfL assay and peripheral neuropathy onset was measured by sensory and motor nerve conduction studies.

Serum NfL measure in untreated and VCR-treated rats demonstrated a steady, and significant increase during the course of VCR administration, with a final 4-fold increase with respect to controls ($p < .001$) when sign of axonopathy and loss of intraepidermal nerve fibers were clearly evident and verified by behavioral, neurophysiological and pathological examination.

This simple monitoring approach based on serum NfL concentration measures may be easily translated to clinical practice and should be considered as a putative marker of CIPN severity in a typical oncology outpatient setting. Further studies are needed to validate its utility in cancer patients treated with different neurotoxic drugs.

1. Introduction

Neurofilament light chain (NfL) is a neuron-specific cytoskeletal protein important for cell structural stability. Damage of axons releases NfL into the interstitial fluid and increased concentrations of NfL can be detected in blood samples. Recently, increased NfL concentration has been demonstrated in a cross-sectional study performed in inherited peripheral neuropathies, and their levels correlated with the severity of nerve impairment (Sandelius et al., 2018).

Chemotherapy Induced Peripheral Neurotoxicity (CIPN) is a potentially dose-limiting side effect of chemotherapy treatments of several common forms of cancer. Several highly active and widely used

antineoplastic drugs belonging to different classes (platinum-based agents, antitubulins, proteasome inhibitors) share the common feature represented by CIPN. Although the neuronal target might be different according to the neurotoxic agent administered, the main clinical features of CIPN are those of a length dependent axonopathy (Cavaletti et al. 2015). CIPN onset and course require close monitoring, since delayed recognition or improper management (for instance missing adequate chemotherapy schedule modification) can lead to permanent nerve damage, with severe effects of patients' quality of life. However, careful monitoring of CIPN is frequently problematic, since the scales commonly used by oncologists in daily clinical practice (e.g. National Cancer Institute Common Toxicity Criteria) are not sufficiently sensitive

and reliable (Cavaletti et al., 2013), and in most cases a formal neurological assessment is not easily available.

For these reasons, the availability of a simple, fast, effective and reliable biomarker obtained from an easy accessible biological matrix might have a large impact on the clinical management and safety of cancer patients treated with neurotoxic drugs. Moreover, this putative biomarker might be used in the context of neuroprotection clinical trials, and used as a surrogate endpoint to strengthen the validity of the results based on patient reported outcomes.

To test the possibility to use NfL as a CIPN biomarker we performed this preclinical study using a well-characterized rat model based on repeated administration of the cytostatic drug vincristine, where axonopathy and sensorimotor damage are clearly evident and measurable (VIPN).

2. Materials and methods

The study was approved by Animal Care and Use Committee of the University of Milano-Bicocca and adhered to all guidelines for humane treatment of laboratory animals set forth in the Guide for the Care and Use of Laboratory Animals (Office of Laboratory Animal Welfare) as well as to the Italian D.L.vo n. 26/2014 in compliance with the European Union directive 2010/63/UE.

Adult female Wistar rats (n. 8/group, 175-200 g at the beginning of the study, Envigo, Udine, Italy) were randomly assigned to be left untreated or received vincristine 0.2 mg/kg (VCR) (EVA Pharma B.V., Mijdrecht, Olanda) intravenously via the tail vein once/week for 4 times. The number of animals/group was based on a pre-study statistical analysis using the sensory conduction velocity as the calculation basis (20% decrease in treated vs. control rats, alpha = 0.05, beta = 80%, www.clinicalc.com). The animals were housed 2/cage in a certified animal facility under constant temperature (21 °C +/− 2) and humidity (50% +/− 20) and a 12:12 h light cycle (12 AM:12 PM). Animals health status was monitored daily and body weight was recorded twice weekly to monitor general conditions and VCR dose adjustment.

At baseline and at the end of treatment the animals were tested by a blinded examiner and in random fashion with behavioral methods to assess their mechanical and thermal sensory thresholds (Dynamic and Plantar test), as previously described (Carozzi et al., 2010). Moreover, at the end of treatment, sensory conduction studies (Sensory Nerve Action Potential [SAP] and conduction velocity) of caudal and hind limb digital nerves were obtained through an orthodromic stimulation; motor conduction studies of caudal nerve (Compound Motor Action Potential [CMAP] and conduction velocity) were also performed. In the sensory caudal nerve set up recording cathode and anode, ground electrode and stimulating anode and cathode were placed respectively at 1 cm, 2 cm, 3 cm, 5 cm 6 cm from the base of the tail. In the hind limb digital nerve set up recording cathode and anode were placed in front of the patellar bone and behind the ankle bone, respectively; stimulating anode and cathode were placed at the tip and base of the fourth toe, respectively; the ground electrode was placed in the sole. In the motor caudal nerve set up recording anode and cathode were placed in the caudal muscle at 11 and 12 cm respectively from the base of the tail; ground electrode was placed at 6 cm from the base of the tail; distal stimulation was performed placing cathode and anode respectively at 5 and 6 cm from the base of the tail and proximal stimulation was then obtained repositioning them at 1 cm and 2 cm, respectively. Filters were kept between 20 Hz and 3 KHz for sensory recordings and between 20 Hz and 2 KHz for motor recordings; sweep was kept at 0.5 msec. A Myto II EMG apparatus (EBN Neuro, Florence, Italy) and subdermal needle electrodes (Ambu Neuroline, Ambu, Ballerup, Denmark) were employed for all recordings. Nerve conduction studies were performed under deep isoflurane anesthesia and body temperature was kept constant (37° ± 0.5) using a heating pad.

At the end of the treatment period, sciatic and caudal nerves were obtained for pathological examination and morphometry (Carozzi et al., 2010); moreover in order to include in the assessment a pathology readout already used in clinical practice, an analysis of intraepidermal nerve fiber (IENF) density was been performed on skin samples of control and VCR-treated animals collected at sacrifice (Canta et al., 2016).

On days 7, 14, 21, and 28 blood samples were withdrawn from control and treated rats and serum was obtained through centrifugation at 4°, 3500 g for 15 min. Serum was then aliquoted and stored at −80 °C until NfL measurements.

Serum NfL concentration were determined using the in-house Simoa Nfl assay which has been previously described (Rohrer et al., 2016). Samples were analyzed using one batch of reagents and animal treatment information was blinded to the examiner performing the analysis. The average repeatability of the assay was assessed by measurements of quality control samples and the coefficient of variation was 6.2% for a sample with a mean NfL concentration of 50.7 pg/ml, and 12.3% for a sample with a mean NfL concentration of 22.6 pg/ml.

Statistical analyses were carried out on raw data using GraphPad Prism4 (GraphPad, La Jolla, CA). To compare the behavioral and IENF density assessments Student's t-test was used, while NfL and neurophysiological data were analyzed using the 2-sided Mann-Whitney U test.

3. Results

The administration of VCR was well tolerated by the animals, with a normal weight gain (baseline: CTRL mean ± SEM 199.7 g ± 4.03 and VCR 194.3 g ± 3.48; end of treatment: CTRL mean ± SEM 218.2 g ± 5.2 and VCR 212.3 g ± 4.2); no behavioral signs of distress and no mortality were reported. The onset of VIPN was confirmed at the end of treatment by the results of the Dynamic test indicating significant mechanical allodynia (baseline: CTRL mean ± SEM 32.04 g ± 1.11 and VCR 31.72 g ± 0.75; end of treatment: CTRL mean ± SEM 30.17 g ± 0.87 and VCR 25.04 g ± 1.21; $p < .01$). By contrast, the change in the Plantar test results for thermal threshold induced by VCR treatment was not statistically significant (baseline: CTRL mean ± SEM 11.49 s ± 0.48 and VCR 10.81 s ± 0.294; end of treatment: CTRL 11.02 s ± 0.65; VCR 9.708 s ± 0.69; $p = .19$).

No significant changes were observed at the neurophysiological examination of digital nerves in VRC-treated rats. The examination of the caudal nerves evidenced at the end of treatment significant reduction in conduction velocity, SAP and CMAP potential amplitude in VCR-treated rats with respect to control animals ($p < .01$, Figs. 1A-F).

At the pathologic examination performed on samples obtained at the end of VCR administration, axonopathy was evident, particularly in the caudal nerve (Figs. 1G-I), while changes in the sciatic nerve were milder. Moreover, at the end of experiment VCR-treated animals had significant decrease of IENF density in comparison to control rats (CTRL mean ± SEM 29.77 fibers/mm ± 0.66 and VCR 21.64 fibers/mm ± 1.12; $p < .0001$). Serial NfL serum concentration measured in untreated and VCR-treated rats demonstrated a steady, significant increase during the course of VCR administration (Fig. 1L-O), with a final 4-fold increase vs. controls ($p < .001$).

4. Discussion

Elevated concentrations of blood NfL have already been demonstrated to occur in several central nervous system diseases (e.g. dementia, multiple sclerosis, motor neuron disease) (Sandelius et al., 2018; Rohrer et al., 2016; Bacioglu et al., 2016; Oeckl et al., 2016), where NfL are considered a biomarker of axonal damage. Moreover, in central nervous system diseases, NfL may also represent a possible biomarker of disease activity. In fact, in multiple sclerosis patients NfL levels correlate with treatment response and relapses (Varhaug et al., 2018), thus adding additional relevance to their measurement. One of
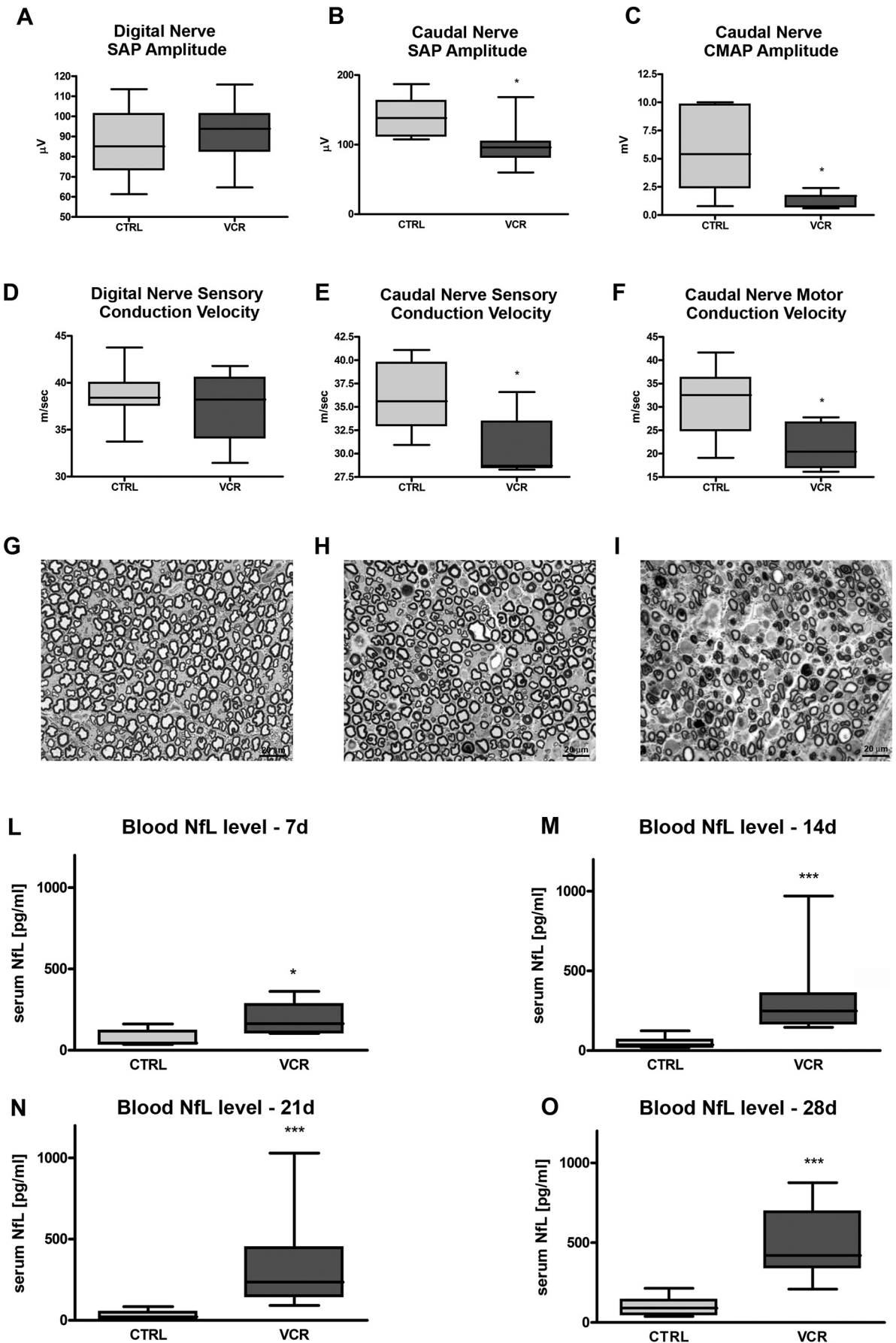
Fig. 1. Summary of the results indicating that neurofilament light (NfL) levels are increased in the vincristine (VCR)-induced peripheral neuropathy model used in the study. Neurophysiological results obtained at the end of treatment in digital and caudal nerves in nerve Sensory Action Potential (SAP) amplitude, Compound Muscle Action Potential (CMAP) amplitude, Sensory and Motor Conduction Velocities indicate that VCR administration induced sensorimotor peripheral neuropathy (A-F, $*p < .01.$). Semithin sections of caudal nerves collected from a control animal (G), and proximal and distal caudal nerves from a representative VCR-treated rat (respectively, H and I) show severe distal axonopathy, with milder axonopathy in the more proximal part of the caudal nerve. NfL analyses performed after 1 (L), 2 (M) 3 (N) and 4 weeks of treatment in VCR-treated rats (O) demonstrated steady, significant increase in serum levels (boxplots report median concentrations and interquartile range, $*p < .05$; $***p < .001$).

the major limitations in NfL measurement was represented by insufficient standardization and methodological differences in different studies, so that their changes were inconsistent.

Recently, a highly sensitive and reliable method to measure NfL concentrations was reported and tested in peripheral neuropathies, showing elevated levels and significant correlation with disease severity (Sandelius et al., 2018). These results obtained in Charcot Marie Tooth (CMT) disease are particularly important since no effective serological disease biomarkers are available for peripheral neuropathies. Although CMT results were achieved in a cross-sectional study, the hypothesis that NfL levels might be used not only to assess the *presence* of peripheral nerve damage, but also to *monitor* the course of peripheral neuropathies deserves to be explored, particularly when monitoring is not performed by neurologists.

CIPN represents an ideal model to test this hypothesis since a) each subject can be examined before, during and after chemotherapy, so that individual baseline concentrations could be used as a very precise reference for subsequent samples; b) blood testing are routinely performed in cancer patients undergoing chemotherapy, and therefore no additional invasive procedure would be requested to obtain suitable samples, c) CIPN monitoring is a major challenge for oncologists, particularly when they are not supported by neurologists as is common in daily clinical practice, d) early detection of CIPN might prevent irreversible nerve damage, e) CIPN severity is extremely variable among patients, and the time course of NfL changes might allow for early detection of high-risk patients.

This latter point is particularly relevant since no effective treatment is currently available for CIPN once it has ensued (Cavaletti et al. 2015), and treatment schedule modification is at present the only effective option to limit its severity and prevent the occurrence of long-term/permanent, debilitating CIPN-related side effects (Mustafa et al. 2017).

In the present study, serial results were obtained in a well-established animal model of repeated VCR administration inducing both sensory and motor nerves damage with the features of distal axonopathy confirmed by reduction in IENF density and relative sparing of more proximal nerves (i.e. mimicking mild-to-moderate peripheral neuropathy).

Using the same highly sensitive method used in the cross-sectional human CMT study we have demonstrated a progressive increase in serum NfL levels, that is closely correlated to pathologically-confirmed axonopathy and reflects progressive damage.

Despite additional studies including other antineoplastic drugs able to induce peripheral neurotoxicity are needed in order to verify if the results obtained in the VCR model can be reproduced in different settings, this simple monitoring approach that might be easily translated in clinical practice should be considered as a putative marker of CIPN severity in a typical oncology outpatient setting, and deserve to be tested in cancer patients treated with peripheral neurotoxic drugs.

Acknowledgement

Author contributions statement

G. C., C. M., Å. S., K. B., H. Z. designed the study. C. M., G. F., P. A., A. C., V. A. C., A. C., L. M., E. P. performed the animal study. Å. S., K. B., H. Z. performed the NfL measurements. G. C., C. M., G. F., P. A, P. M. prepared the first draft of the manuscript. A. C., V. A. C.; A. C., L. M., E. P., Å. S., K. B., H. Z., P.M. contributed to results interpretation and critically revised the manuscript. C. M., G. F., P. A., A. C., V. A. C., A. C., L. M., E. P., Å. S., K. B., H. Z., P. M. G. C. approved the final version of the manuscript.

Disclosures

C. Meregalli, G. Fumagalli, P. Alberti, A. Canta, V.A. Carozzi, A. Chiorazzi, L. Monza, E. Pozzi, P. Marmiroli and G. Cavaletti report no disclosures relevant to the manuscript.

H. Zetterberg has served at advisory boards of Eli Lilly, Roche Diagnostics and Wave, has received travel support from Teva and is a co-founder of Brain Biomarker Solutions in Gothenburg AB, a GU Ventures-based platform company at the University of Gothenburg.

K. Blennoe has served as a consultant or at advisory boards for Alzheon, BioArctic, Biogen, Eli Lilly, Fujirebio Europe, IBL International, Merck, Novartis, Pfizer, and Roche Diagnostics, and is a co-founder of Brain Biomarker Solutions in Gothenburg AB, a GU Venture-based platform company at the University of Gothenburg.

References

Bacioglu, M., Maia, L.F., Preische, O., Schelle, J., Apel, A., Kaeser, S.A., Schweighauser, M., Eninger, T., Lambert, M., Pilotto, A., Shimshek, D.R., Neumann, U., Kahle, P.J., Staufenbiel, M., Neumann, M., Maetzler, W., Kuhle, J., Jucker, M., 2016. Neurofilament light chain in blood and CSF as marker of disease progression in mouse models and in neurodegenerative diseases. Neuron 91, 494–496.

Canta, A., Chiorazzi, A., Carozzi, V.A., Meregalli, C., Oggioni, N., Bossi, M., Rodriguez-Menendez, V., Avezza, F., Crippa, L., Lombardi, R., et al., 2016. Age-related changes in the function and structure of the peripheral sensory pathway in mice. Neurobiol. Aging 45, 136–148.

Carozzi, V.A., Canta, A., Oggioni, N., Sala, B., Chiorazzi, A., Meregalli, C., Bossi, M., Marmiroli, P., Cavaletti, G., 2010. Neurophysiological and neuropathological characterization of new murine models of chemotherapy-induced chronic peripheral neuropathies. Exp. Neurol. 226, 301–309.

Cavaletti, G., Marmiroli, P., 2015. Chemotherapy-induced peripheral neurotoxicity. Curr. Opin. Neurol. 28, 500–507.

Cavaletti, G., Cornblath, D.R., Merkies, I.S.J., Postma, T.J., Rossi, E., Frigeni, B., Alberti, P., Bruna, J., Velasco, R., Argyriou, A.A., Kalofonos, H.P., Psimaras, D., Ricard, D., Pacem, A., Galiè, E., Briani, C., Dalla Torre, C., Faber, C.G., Lalisang, R.I., Boogerd, W., Brandsma, D., Koeppen, S., Hense, J., Storey, D., Kerrigan, S., Schenone, A., Fabbri, S., Valsecchi, M.G., CI-PeriNomS Group, 2013. The chemotherapy-induced peripheral neuropathy outcome measures standardization study: from consensus to the first validity and reliability findings. Ann. Oncol. 24, 454–462.

Mustafa Ali, M., Moeller, M., Rybicki, L., Moore, H.C.F., 2017. Long-term peripheral neuropathy symptoms in breast cancer survivors. Breast Cancer Res. Treat. 166, 519–526.

Oeckl, P., Jardel, C., Salachas, F., Lamari, F., Andersen, P.M., Bowser, R., de Carvalho, M., Costa, J., van Damme, P., Gray, E., Grosskreutz, J., Hernández-Barral, M., Herukka, S.K., Huss, A., Jeromin, A., Kirby, J., Kuzma-Kozakiewicz, M., Amador Mdel, M., Mora, J.S., Morelli, C., Muckova, P., Petri, S., Poesen, K., Rhode, H., Rikardsson, A.K., Robberecht, W., Rodríguez Mahillo, A., Shaw, P., Silani, V., Steinacker, P., Turner, M.R., Tüzün, E., Yetimler, B., Ludolph, A.C., Otto, M., 2016. Multicenter validation of CSF neurofilaments as diagnostic biomarkers for ALS. Amyotroph. Lateral Scler. Frontotemporal. Degener. 17, 404–413.

Rohrer, J.D., Woollacott, I.O., Dick, K.M., Brotherhood, E., Gordon, E., Fellows, A., Toombs, J., Druyeh, R., Cardoso, M.J., Ourselin, S., Nicholas, J.M., Norgren, N., Mead, S., Andreasson, U., Blennow, K., Schott, J.M., Fox, N.C., Warren, J.D., Zetterberg, H., 2016. Serum neurofilament light chain protein is a measure of disease intensity in frontotemporal dementia. Neurology 87, 1329–1336.

Sandelius, Å., Zetterberg, H., Blennow, K., Diutori, R., Malaspina, A., Laura, M., Reilly, M.M., Rossor, A.M., 2018. Plasma neurofilament light chain concentration in the inherited peripheral neuropathies. Neurology 90, e518–e524.

Varhaug, K.N., Barro, C., Bjørnevik, K., Myhr, K.M., Torkildsen, Ø., Wergeland, S., Bindoff, L.A., Kuhle, J., Vedeler, C., 2018. Neurofilament light chain predicts disease activity in relapsing-remitting MS. Neurol. Neuroimmunol. Neuroinflamm. 5, e422.

Neuropharmacology and analgesia

Ghrelin agonist HM01 attenuates chemotherapy-induced neurotoxicity in rodent models

Alessia Chiorazzi[a,1], Krystyna M. Wozniak[b,1], Rana Rais[b,c], Ying Wu[b], Alexandra J. Gadiano[b], Mohamed H. Farah[c], Ying Liu[c,d], Annalisa Canta[a], Paola Alberti[a,e], Virginia Rodriguez-Menendez[a], Cristina Meregalli[a], Giulia Fumagalli[a,e], Laura Monza[a,f], Eleonora Pozzi[a,e], James J. Vornov[g], Michael Polydefkis[c,d], Claudio Pietra[h], Barbara S. Slusher[b,c,i,*], Guido Cavaletti[a,**]

[a] Experimental Neurology Unit and Milan Center for Neuroscience, University of Milano-Bicocca, 20900 Monza, Italy
[b] Johns Hopkins Drug Discovery, Johns Hopkins School of Medicine, Baltimore, MD 21205, USA
[c] Department of Neurology, Johns Hopkins School of Medicine, Baltimore, MD 21205, USA
[d] Department of Neuromuscular Medicine and Pathology, Johns Hopkins School of Medicine, Baltimore, MD 21205, USA
[e] PhD Program in Neuroscience, University of Milano-Bicocca, 20900 Monza, Italy
[f] PhD Program DIMET, University of Milano-Bicocca, 20900 Monza, Italy
[g] Medpace, Cincinnati, OH 45227, USA
[h] Helsinn Healthcare SA, 6915 Lugano, Switzerland
[i] Department of Neuroscience, Medicine, Psychiatry and Oncology, Johns Hopkins School of Medicine, Baltimore, MD 21205, USA

ARTICLE INFO

ABSTRACT

Chemotherapy-Induced Peripheral Neurotoxicity (CIPN) is often dose-limiting and impacts life quality and survival of cancer patients. Ghrelin agonists have neuroprotectant effects and may have a role in treating or preventing CIPN. We evaluated the CNS-penetrant ghrelin agonist HM01 in three experimental models of CIPN at doses of 3–30 mg/kg p.o. daily monitoring orexigenic properties, nerve conduction, mechanical allodynia, and intra-epidermal nerve fiber density (IENFD). In a cisplatin-based study, rats were dosed daily for 3 days (0.5 mg/kg i.p.) + HM01. Cisplatin treatment induced mechanical hypersensitivity which was significantly reduced by HM01. In a second study, oxaliplatin was administered to mice (6 mg/kg i.p. 3 times/week for 4 weeks) resulting in significant digital nerve conduction velocity (NCV) deficits and reduction of IENFD. Concurrent HM01 dose dependently prevented the decline in NCV and attenuated the reduction in IENFD. Pharmacokinetic studies showed HM01 accumulation in the dorsal root ganglia and sciatic nerves which reached concentrations > 10 fold that of plasma. In a third model, HM01 was tested in preventive and therapeutic paradigms in a bortezomib-based rat model (0.2 mg/kg i.v., 3 times/week for 8 weeks). In the preventive setting, HM01 blocked bortezomib-induced hyperalgesia and IENFD reduction at all doses tested. In the therapeutic setting, significant effect was observed, but only at the highest dose. Altogether, the robust peripheral nervous system penetration of HM01 and its ability to improve multiple oxaliplatin-, cisplatin-, and bortezomib-induced neurotoxicities suggest that HM01 may be a useful neuroprotective adjuvant for CIPN.

1. Introduction

The G protein-coupled growth hormone secretagogue receptor (GHSR) was cloned in 1996 (Howard et al., 1996), and 3 years later, ghrelin was discovered as its natural ligand (Kojima et al., 1999). Two receptor subtypes have been described, 1a and 1b, but only the former is capable of activating signal transduction (Kojima et al., 1999). GHSR is expressed primarily in the nervous system as well as in multiple non-nervous organs where it is involved in diverse physiological processes (Kojima et al., 1999; Nakazato et al., 2001; Tschop et al., 2000). Clinical trials have evaluated the therapeutic potential of ghrelin in multiple disease states including anorexia nervosa (Hotta et al., 2009),

---

cancer cachexia (Collden et al., 2017; Temel et al., 2016), sleep-wake regulation (Kluge et al., 2011), chronic heart failure (Nagaya et al., 2004) and gastro-intestinal mobility disturbances (Sanger and Furness, 2016). Despite these efforts and the recent discovery of small molecule agonists that are potent and bioavailable, none have been approved for clinical use.

In animals, ghrelin promotes cell proliferation and neurogenesis (Steculorum and Bouret, 2011). Ghrelin has also been shown to possess neuroprotective properties and to prevent apoptosis (Chung et al., 2007). GHSRs have been located in several distinct regions of the central nervous system (CNS), even though the presence of ghrelin itself in CNS areas outside of the hypothalamus is controversial (Ferrini et al., 2009; Furness et al., 2011). Exogenous ghrelin administration ameliorates experimental encephalomyelitis (Theil et al., 2009), Parkinson's (Moon et al., 2009) and Alzheimer's disease (Gahete et al., 2011) in preclinical models. In addition, ghrelin has been proposed to possess direct neural repair properties after central or peripheral nervous system injury (Raimondo et al., 2013).

Neuropathic pain has an important inflammatory component, with sustained activation of neuroglial cells and increased production of pro-inflammatory cytokines. Thus, ghrelin's inhibitory effects on neuroglial activation and inflammation (Baatar et al., 2011) have been proposed as being useful for treating neuropathy and neuropathic pain. Moreover, there are reports of ghrelin's therapeutic effects in several neuropathies, including rodent models of diabetic- (Tsuchimochi et al., 2013), chronic constrictive injury- (Zhou et al., 2014) and chemotherapy-induced neurotoxicity (CIPN) (Garcia et al., 2008), as well as in acute pain (Wei et al., 2013), and chronic arthritis (Granado et al., 2005) models.

These neuroprotective, neurotrophic and anti-inflammatory properties of this endogenous peptide render it an ideal candidate as a therapeutic agent. However, ghrelin's limited brain penetration (Banks et al., 2002), lack of oral bioavailability and short half-life of only 8–24 min in rodents (Hosoda and Kangawa, 2012), and 37 min in man (Tong et al., 2013) limit its clinical utility. In fact, demonstration of preclinical efficacy often requires multiple systemic injections or central intrathecal/intraventricular administration, emphasizing the need for continuous infusion of ghrelin or use of agonists with longer half-lives and enhanced nervous system penetration.

The development of small molecule ghrelin agonists with improved pharmacokinetic properties and nervous system penetration would allow full evaluation of this mechanism in preclinical and clinical studies. HM01, a new synthetic brain penetrant ghrelin receptor agonist, was recently identified and shown to alleviate constipation and delay gastric emptying associated with a rodent Parkinson's disease model as well as anorexia/cachexia in rodent tumor-bearing models (Borner et al., 2016; Karasawa et al., 2014), and recently entered into Phase 1.

In this study, we evaluated the efficacy of daily oral HM01 administration in three distinct CIPN experimental models.

2. Materials and methods

2.1. Drugs and formulations

HM01 (Helsinn Healthcare SA, Lugano, Switzerland, Fig. 1) was made as a suspension in 0.5% carboxymethylcellulose solution in dosing volumes of 1 and 10 ml/kg for rats and mice respectively and dosed orally at 3, 10 or 30 mg/kg. Cisplatin (LKT Laboratories, St. Paul, MN) was dosed in saline solution at 0.5 mg/kg intraperitoneally (i.p., 1 ml/kg). Oxaliplatin (LC Laboratories, Woburn, MA) was formulated in 5% dextrose solution and injected i.p. (10 ml/kg) at a concentration of 0.6 mg/ml. Bortezomib (LC Laboratories, Woburn, MA) was prepared in 10% Tween 80, 10% EtOH 100% and 80% saline solution and injected i.v. (1 ml/kg) at 0.2 mg/kg. All dosing solutions were made fresh on each administration day.
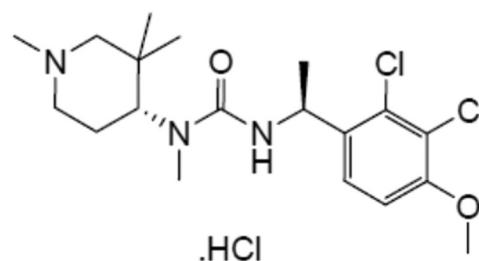
Fig. 1. Chemical structure of HM01 (expressed as hydrochloride salt).

2.2. Animals and dosing schedules

All experimental protocols (Table 1) were approved by the Institutional Animal Care and Use Committee of Johns Hopkins University (cisplatin and oxaliplatin studies) or of University of Milano-Bicocca (bortezomib studies) and adhered to all of the applicable institutional and governmental guidelines for the humane treatment of laboratory animals set forth in the Guide for the Care and Use of Laboratory Animals (Office of Laboratory Animal Welfare) as well as to the Italian D.L.vo n. 26/2014.

2.2.1. Cisplatin study

Fifty male Wistar rats (Harlan Laboratories, Indianapolis, IN) weighing 250–300 g at start of experiment were randomly divided into 5 groups of 10 rats each. Group 1 received daily HM01 vehicle (p.o.) for 6 days and cisplatin vehicle (i.p.) for 3 days. Group 2 received HM01 vehicle (p.o) and 0.5 mg/kg cisplatin (i.p.) for 3 days followed by HM01 vehicle for 3 additional days. Group 3 received daily 3 mg/kg HM01 (p.o.) and 0.5 mg/kg cisplatin (i.p.) for 3 days followed by 3 mg/kg HM01 for an additional 3 days. Group 4 received 10 mg/kg HM01 (p.o.) and 0.5 mg/kg cisplatin (i.p.) for 3 days followed by 10 mg/kg HM01 for an additional 3 days. Group 5 received daily 30 mg/kg HM01 (p.o.) and 0.5 mg/kg cisplatin (i.p.) for 3 days followed by 30 mg/kg HM01 for an additional 3 days. In each case, cisplatin or cisplatin vehicle was dosed 30 min after HM01 or HM01 vehicle, which was dosed 1 h prior to von Frey filament testing. Individual body weights and 24 h food intake were measured daily from just prior to initiation of dosing. This protocol was implemented based on a published study (Garcia et al., 2008) in which hyperalgesia was induced using the same cisplatin dosing regimen in rats and was eliminated by administration of ghrelin peptide. This particular regimen was previously chosen by Garcia et al. (2008) because the total cisplatin dose administered is similar to that given to humans during a typical 'cycle' and was previously determined to produce a mild but significant degree of weight loss and hyperalgesia in rats similar to that induced in humans.

2.2.2. Oxaliplatin study

Sixty female Balb/c mice (Harlan Laboratories, Indianapolis, IN) weighing 20–25 g at start of experiment were used and divided into 4 groups of 15 mice each. Group 1 received HM01 vehicle (p.o.) daily, 60–90 min prior to oxaliplatin vehicle dosing (i.p.) twice weekly for 4 weeks. Group 2 received HM01 vehicle (p.o.) daily, 60–90 min prior to 6 mg/kg oxaliplatin (i.p.) twice weekly for 4 weeks. Group 3 received 10 mg/kg HM01 (p.o.) daily 60–90 min prior to 6 mg/kg oxaliplatin (i.p.) twice weekly for 4 weeks. Group 4 received 30 mg/kg HM01 (p.o.) daily 60–90 min prior to 6 mg/kg oxaliplatin (i.p.) twice weekly for 4 weeks. Body weights were measured daily, immediately prior to the initiation of dosing. Nerve conduction velocity (NCV) and potential amplitude measurements were made 24 h after last oxaliplatin (or vehicle) dose and 1 h after last HM01 (or vehicle) dose, after which blood and tissue samples (dorsal root ganglia [DRG], sciatic nerve [SN], and foot pads) were collected for pharmacokinetic and intra-epidermal nerve fiber density (IENFD) evaluations.

Table 1
Summary of the study plan and of the assessments performed in the three models described in this study.

Neurotoxic drug and schedule	Species	Gender	Body weight	Food intake	Allodynia	NCV amplitude	IENFD	HM01 pharmacokinetic	DRG and nerve pathology	Proteasome inhibition
Cisplatin 0.5 mg/kg i.p. x 3 days	Rat	Male	X	X	X					
Oxaliplatin 6 mg/kg i.p. twice weekly for 4 weeks	Mouse	Female	X			X	X	X	X	
Bortezomib 0.2 mg/kg i.v. 3 times/week for 8 weeks	Rat	Female	X		X	X	X		X	X

NCV = nerve conduction velocity; IENFD = intraepidermal nerve fiber density; DRG = dorsal root ganglia.

2.2.3. Bortezomib studies

Prevention paradigm: Fifty female Wistar rats (Envigo, Bresso, Italy) weighing 200–225 g at start of experiment were randomized into 5 experimental groups of 10 rats each. Group 1 was left untreated (CTRL), Group 2 was treated with bortezomib i.v. 0.2 mg/kg, 3 times/week for 8 weeks (BTZ), Group 3 was co-treated with bortezomib i.v. 0.2 mg/kg, 3 times/week for 8 weeks and HM01 p.o. 3 mg/kg daily 90 min before the i.v. administration (BTZ + HM01 3), Group 4 was co-treated with bortezomib i.v. 0.2 mg/kg, 3 times/week for 8 weeks and HM01 p.o. 10 mg/kg daily 90 min before the i.v. administration (BTZ + HM01 10), Group 5 was co-treated with bortezomib i.v. 0.2 mg/kg, 3 times/week for 8 weeks and HM01 p.o. 30 mg/kg daily 90 min before the i.v. administration (BTZ + HM01 30). At baseline and after 8 weeks of treatment, caudal and digital nerve conduction and potential amplitude studies, behavioral test (Dynamic Aesthesiometer Test) and blood collection to study proteasome inhibition were performed. After 8 weeks of treatment, tissue samples (sciatic and caudal nerves, DRG and foot pads) were collected and analyzed to study morphological parameters and IENFD.

Therapeutic paradigm: Fifty female Wistar rats (Envigo, Bresso, Italy) weighing 200–225 g at start of experiment were randomized into 5 experimental groups of 10 animals each. Group 1 was left untreated (CTRL), Group 2 was treated with bortezomib i.v. 0.2 mg/kg, 3 times/week for 8 weeks (BTZ), Group 3 was treated with bortezomib i.v. 0.2 mg/kg, 3 times/week for 4 weeks and co-treated with bortezomib 0.2 mg/kg, 3 times/week and HM01 p.o. 3 mg/kg daily 90 min before the i.v. administration for other 4 weeks (BTZ + HM01 3), Group 4 was treated with bortezomib i.v. 0.2 mg/kg, 3 times/week for 4 weeks and co-treated with bortezomib 0.2 mg/kg, 3 times/week and HM01 p.o. 10 mg/kg daily 90 min before the i.v. administration for other 4 weeks (BTZ + HM01 10), Group 5 was treated with bortezomib i.v. 0.2 mg/kg, 3 times/week for 4 weeks and co-treated with bortezomib 0.2 mg/kg, 3 times/week and HM01 p.o. 30 mg/kg daily 90 min before the i.v. administration for other 4 weeks (BTZ + HM01 30). At baseline and after 8 weeks of treatment, caudal and digital nerve conduction and potential amplitude studies and blood collection to study proteasome inhibition were performed. Behavioral test (Dynamic Aesthesiometer Test) was performed at baseline, after 4 and 5 weeks and at the end of bortezomib treatment. After 8 weeks of treatment, sciatic nerves, caudal nerves, DRG and foot pads were collected and analyzed to study morphological parameters and IENFDs.

2.3. Assessments

2.3.1. Von Frey testing

In the cisplatin study, rats were individually housed and acclimated to handling and to the Von Frey testing apparatus for several days prior to start of the experiment. Baseline measurements were obtained prior to dosing. Behavioral testing was conducted in a quiet room following procedures previously described (Chaplan et al., 1994). Rats were placed on a wire mesh floor while loosely restrained in a plexiglass compartment and allowed to acclimate for at last 15 min prior to

initiation of testing. For testing, a monofilament was applied perpendicularly to the plantar surface of the hind paw with a constant force for 2–5 s. The starting filament was the n° 10 filament (4.31 marking). Each filament was tested 5 times by applying to the mid-plantar region of each hind paw from beneath the mesh floor and with intervening intervals of a few s. A descending series of the filament was used when the rat responded to the previous filament. A response was considered positive if the animal exhibited any nocifensive behaviors, including brisk paw withdrawal, licking, or shaking of the paw, either during application of the stimulus or immediately after the filament is removed. If a response was observed at least three times, the rat was considered responsive to that filament. The response threshold was defined as the lowest force filament that produced at least three withdrawal responses in five tests. Values for each animal were then used to average across treatment groups to yield a mean group threshold response.

2.3.2. Dynamic aesthesiometer test

In the bortezomib studies, the mechanical nociceptive threshold was assessed using a Dynamic Aesthesiometer Test (model 37450, Ugo Basile Biological Instruments, Comerio, Italy). After the acclimatization period, the animals were placed in a plexiglass cages and a servo-controlled mechanical stimulus was applied to the plantar surface of the hind paw, reaching up to 50 g within 20 s with a linear, constant increase in pressure. A response was considered positive if the animal exhibited any nocifensive behaviors, including brisk paw withdrawal, licking, or shaking of the paw. The mechanical threshold was assessed alternatively on each side every 2 min on 3 occasions to yield a mean value. The results represented the maximal pressure (expressed in grams) tolerated by the animals.

2.3.3. Nerve conduction studies (NCS)

Baseline NCV measurements were performed prior to drug dosing. Animals were then randomly assigned to one of the study treatment groups with similar mean NCV values. NCS measurements were again performed 24 h after completion of the antineoplastic drugs dosing and 1 h after the last HM01 dose. During all recording sessions, animals were anesthetized with 2% isoflurane and placed on a warm heating pad with rectal temperature monitored and maintained between 37.0 and 41.0 °C. Stimulation of each nerve segment was performed, with increasing voltage, until the maximal response had been achieved. Latency measurements were scored to the nearest 0.01 msec and amplitude measurements to the nearest 0.01 µV. NCV was calculated dividing the response latency time by the distance between the anode electrodes of the stimulating and recording dipole. Stimulation of each nerve segment was performed at least 3 times, up to a maximum of 6 times, with increasing voltage, until the maximal response had been achieved as evidenced by no further increase or a reduction in amplitude despite increase in voltage.

In mice, NCS measurements were determined as previously described (Wozniak et al., 2011). Platinum subdermal needle electrodes (Grass Technologies, West Warwick, RI) were used for both recording

and stimulation. Caudal and digital NCV were recorded ortho-dromically with recording sites at the proximal tail and the lateral malleolus, respectively. Caudal NCV was recorded from electrodes in a bipolar configuration at the base of the tail (at the hair line); the sti-mulating cathode being positioned 35 mm further distal. Digital NCV was recorded using stimulation at the base of the second toe and re-cording at the level of the lateral malleolus. The distance travelled was measured for each mouse and was between 9 and 14 mm. Latencies were measured from stimulus onset and baseline-to-peak amplitudes were calculated. Recordings were made using a BIOPAC MP100 and AcqKnowledge software version 3.7.3 (BIOPAC Systems Inc., Goleta, CA).

In rats, stainless-steel electrodes [Ambu Neuroline (Ambu, Ballerup, Denmark)] were employed for both recording and stimulation. NCV and sensory action potential amplitude were assessed orthodromically. Latencies were measured from stimulus onset and peak-to-peak amplitudes were calculated. For caudal NCS recording cathode and anode, ground electrode and stimulating anode and cathode were positioned at 1 cm, 2 cm, 3 cm, 5 cm, and 6 cm from the tail hair line, respectively. The digital nerve response was recorded in the hind limb placing the recording cathode in front of the patellar bone and the recording anode behind the ankle bone; the stimulating anode and cathode were positioned in the fourth toe, in the tip and at its base, respectively; in the sole, the ground electrode was inserted subcutaneously. A Myto2 EMG device (EBN Neuro, Firenze, Italy) was used.

2.3.4. DRG and sciatic nerve histopathology

At the end of the oxaliplatin and bortezomib experiments, animals were killed under deep anesthesia. SN segments and L4 and L5 DRG were dissected from 5 animals/group and embedded for analysis as previously described (Carozzi et al., 2010a; Meregalli et al., 2010). Semithin sections of 1.5 μm thickness were prepared from at least three tissue blocks for each animal and the sections were stained with methylene blue. Morphometric assessment of the g-ratio (calculated as axonal diameter/entire fiber diameter) of myelinated fibers was calculated in bortezomib-treated rats (preventive setting) (Meregalli et al., 2015).

2.3.5. IENFD analysis

IENFD analysis was performed on specimens collected and processed as previously described (Wozniak et al., 2011). Four sections were processed for each biopsy. Intra-epidermal unmyelinated axons were counted in a blinded fashion and the fiber density per mm of skin fibers that cross the dermal/epidermal junction was determined as previously described (Wozniak et al., 2011).

In brief, at sacrifice hind limbs at the ankle were collected. 5-mm round samples from each animal were taken and fixed in 2% paraformaldehyde-lysine-sodium periodate for 24 h at 4 °C. Footpads were dissected out and were washed in phosphate buffer and placed in cryoprotectant (30% glycerol) solution. Tissue blocks were cut by freezing microtome at 50 μm intervals and immunohistochemical staining was performed using rabbit polyclonal antiprotein gene product 9.5 (PGP 9.5; AbD Serotec, a Bio-Rad Company, Kidlington, UK) using a free-floating protocol. Sections were incubated over night at room temperature in 96 well tissue culture plates on a horizontal tabletop shaker at 50 rolls per min. The following day, sections were washed in phosphate buffer and then incubated with biotinylated goat anti-rabbit Ab (Vector Labs, Burlingame, CA) for 3 h. Bound im-munoglobulin was visualized by the ABC kit (Vector labs, Burlinggame, CA). The total number of PGP 9.5-positive IENF in each section was counted, the length of the epidermis was measured and the linear density of IENF/mm was obtained.

2.3.6. HM01 pharmacokinetic analyses

In the oxaliplatin study, a single dose of HM01 at 10 or 30 mg/kg p.o. was administered to mice which were killed 0, 15 min, 30 min, 1 h, 3 h, 6 h, 24 h, 72 h post dose (3 mice per time point). Similarly, in the chronic dosing study, 3 mice per group were killed 1 h post last HM01 administration. Plasma samples were derived from whole blood

removed by cardiac puncture centrifuged at 1,000g at 4 °C in plasma separator tubes for 10 min and stored at −80 °C until analysis. DRG (L4, L5 and L6) and SN were dissected and immediately frozen in dry ice. SN and DRG were pooled from 3 mice per treatment and time point.

2.3.7. Bioanalysis of HM01

For plasma analysis, standards and quality control samples were prepared by spiking known amounts of HM01 in mouse plasma (5–5000 nM). For extraction, 50 μl of each standard, unknown and quality control sample was added to the low retention micro-centrifuge tube and extracted in 300 μl acetonitrile containing internal standard (500 nM losartan). Extracts were vortexed and centrifuged (16,000g for 10 min) and supernatant analyzed using LC/MS/MS methods. Similarly, for analysis of tissue samples, standard curve and quality control samples were prepared using tissue matrix (10–5000 nM). Tissue samples were weighed and extracted by single one-step protein precipitation with acetonitrile. Samples and standards were pulverized, followed by vortexing and centrifugation 16,000g at 4 °C for 10 min and supernatants were analyzed via LC/MS/MS.

Briefly, the mass spectrometer was operated with an ESI interface in positive ionization mode for HM01. Separation was achieved on a C_{18} Agilent Eclipse Plus column (100 × 2.1 mm i.d, 1.8 μm.) with 0.1% formic acid in acetonitrile and 0.1% formic acid in H_2O using gradient elution. The [M + H] + ion transitions of HM01 at m/z 401.481 → 125.638, 156.859 and that of the internal standard at m/z 423.129→ 179.981, 206.994 were monitored. Correlation coefficient > 0.99 was obtained in all analytical runs. The mean-predicted concentration accuracy ranged between 98% and 117% for HM01 standards and 102–110% for quality control samples.

2.3.8. Proteasome inhibition assay in Bortezomib-treated rats

Whole blood was taken from the tail vein and collected in EDTA heparinized tube and processed for proteasome inhibition assay. Peripheral blood mononuclear cells (PBMC) were isolated using a Ficoll–Hypaque density separation. Later, PBMCs were added with lysis solution (50 mM Hepes, 5 mM EDTA, 150 mM NaCl, 1% Triton-X100 in H_2O) and extracted. The lysates obtained were then centrifuged at 17,000g for 15 min at 4 °C. Protein concentration was determined by the Bradford assay using a Coomassie® Protein Assay Reagent Kit (Pierce, Thermo Scientific, Rockford, IL). To evaluate the proteasomal activity a fluorometric assay was used, and the protein extract from tissue was incubated with the N-succinyl-Leu-Leu-Val-Tyr-7-Amido-4-Methylcoumarin substrate (Sigma Aldrich, Milano, Italy) for 2 h, as previously reported (Meregalli et al., 2014). The proteasome activity was detected as the relative light unit generated from the cleaved substrate in the reagent. Fluorescence generated from each reaction was detected with a fluorometer (Wallac 1420 multilabel counter, PerkinElmer Italia SPA, Monza, Italy). The proteasome activity (A) was calculated as following: % $A = F_{BTZ}-F_{SUBSTRATE}/F_{CTRL}-F_{SUBSTRATE}$ and the inhibition obtained was 100*(1-A).

2.3.9. Statistical analysis

For all statistical analysis, data were analyzed comparing mean group responses using two way ANOVA followed by Tukey's or Dunnet's post-hoc comparisons, made using Prism GraphPad software Version 4.03 (GraphPad Inc, La Jolla, CA), with significance being defined at $P < 0.05$.

3. Results

3.1. Cisplatin study

3.1.1. Body weight changes and food intake

Cisplatin treatment induced significant decrease in daily body weight and food intake ($P < 0.05$, Fig. 2A and B) compared to vehicle-treated rats. HM01 treatment at 3, 10 and 30 mg/kg increased overall food intake and body weight ($P < 0.05$) compared to cisplatin alone.
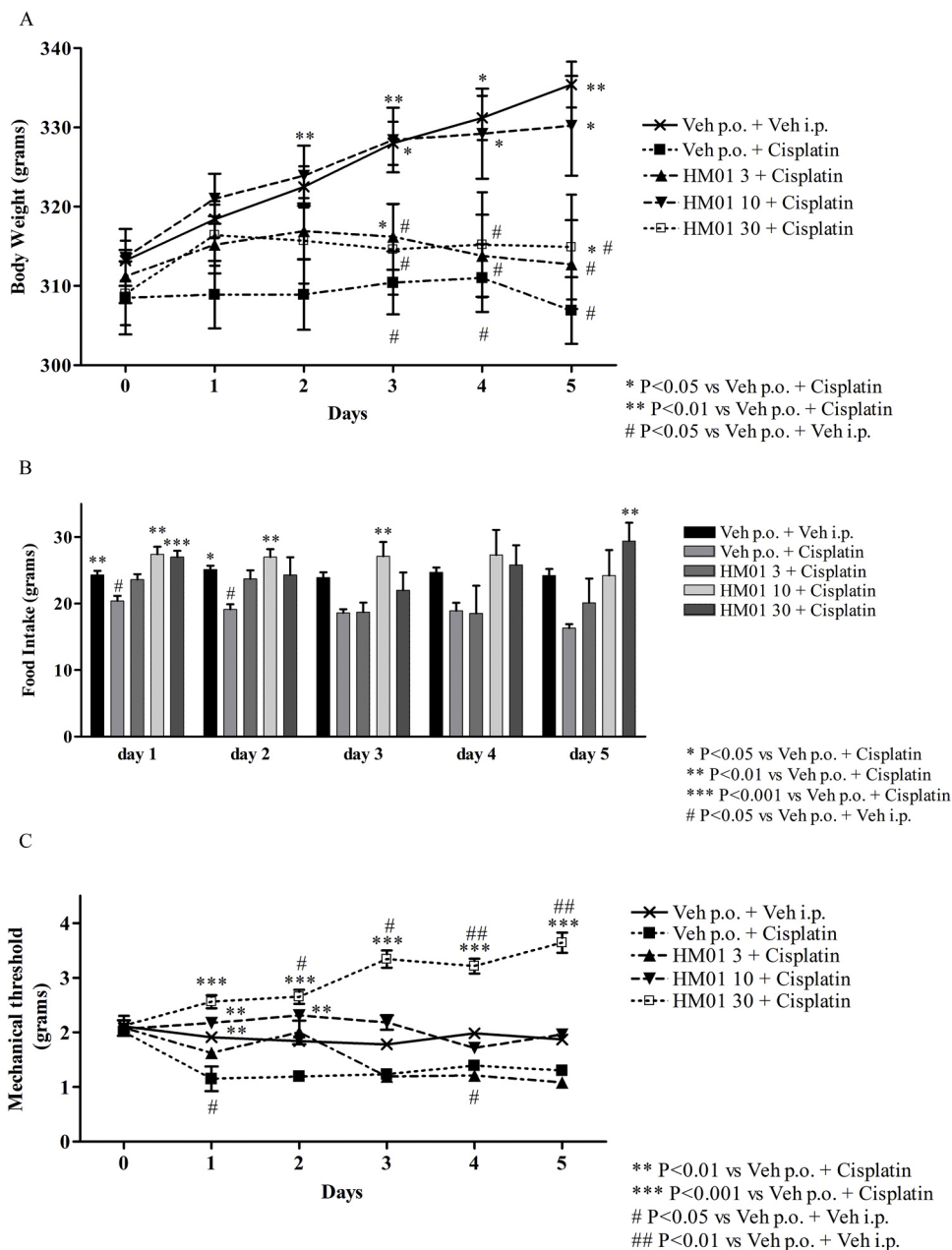
Fig. 2. Effect of HM01 treatment on body weight, food intake and mechanical hyperalgesia induced by cisplatin injection into rats. Cisplatin (0.5 mg/kg), administered i.p. once daily for 3 days (day 0 thru day 2), resulted in a decrease in body weight and daily food intake and development of mechanical hyperalgesia. A) One way ANOVA followed by post hoc Tukey multi-comparison test found a significant overall effect of cisplatin on body weight (P < 0.05) which was improved by HM01 treatment at 10 and 30 mg/kg (P < 0.05). B) Food intake was significantly reduced by cisplatin (P < 0.05) and this was improved by 10 and 30 mg/kg HM01 (both P < 0.05). C) Mechanical hyperalgesia was induced by cisplatin and at the determination performed 1 day after cisplatin administration this effect was significantly improved by 10 and 30 mg/kg HM01 (P < 0.05), but not 3 mg/kg HM01 (mechanical threshold was tested using Von Frey filaments).

3.1.2. Allodynia

Treatment with cisplatin decreased the paw withdrawal threshold in rats compared to vehicle-treated rats (P < 0.01), indicating development of mechanical hypersensitivity. Pre-treatment with HM01 at 10 and 30 mg/kg significantly reduced this hyperalgesia at the determination performed 1 day after cisplatin administration. HM01 treatment at 30 mg/kg resulted in overall significantly increased paw withdrawal thresholds compared to vehicle-treated rats (P < 0.05) on days 3 thru 5. HM01 at 3 mg/kg had no significant effect on cisplatin-induced hyperalgesia (Fig. 2C).

3.2. Oxaliplatin study

3.2.1. Body weight changes

Oxaliplatin-treated mice showed significant loss of body weight from day 10 to the end of the study vs vehicle-treated mice (P < 0.01). The animals co-treated with oxaliplatin and 10 or 30 mg/kg HM01 showed less weight loss than oxaliplatin treated mice (P < 0.01). This effect reached statistical significance (P < 0.05) on multiple test days, with 10 mg/kg HM01 having the most robust effect (data not shown).

3.2.2. Nerve conduction studies

Oxaliplatin administration caused a significant decrease in digital

Fig. 3. Effect of HM01 on nerve conduction velocity (NCV) and potential amplitude in oxaliplatin-treated mice. All the parameters were measured prior to and 24 h after completion of dosing regimen consisting of vehicle or HM01 (10 or 30 mg/kg) p.o. daily, followed by oxaliplatin (6 mg/kg) or vehicle (every 4 days for a total of 8 administrations) i.p. Last HM01 dose was administered 1 h before recording. (*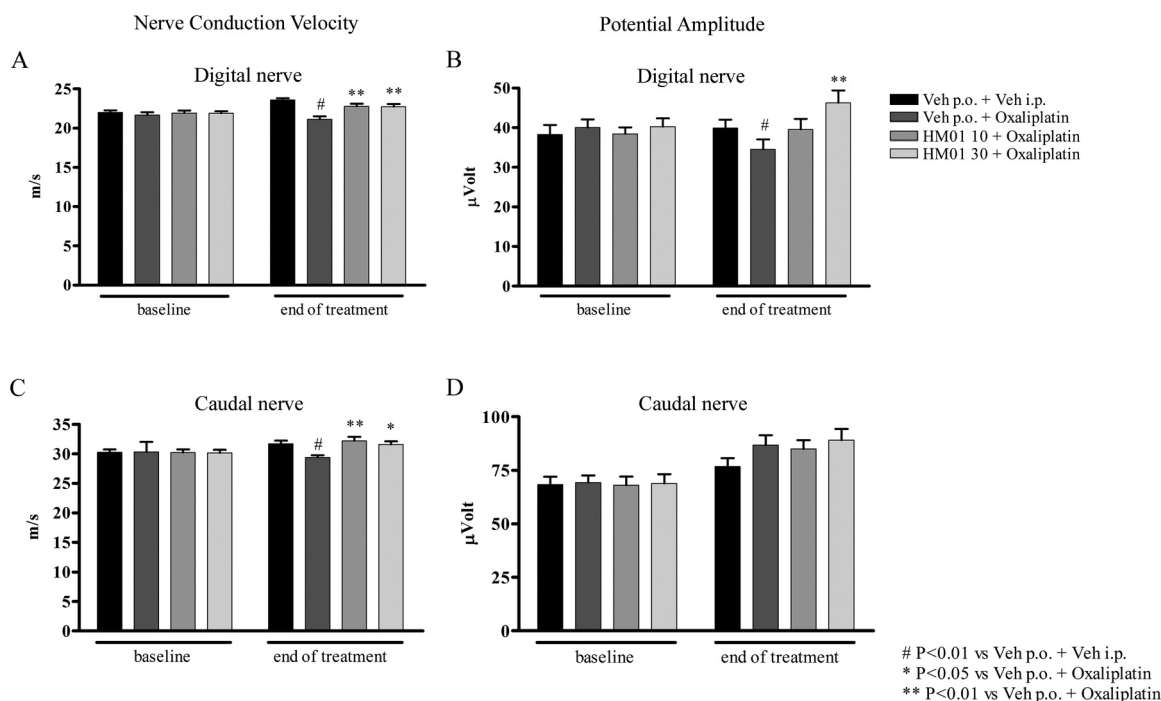 denotes $P < 0.05$ vs veh/oxaliplatin; # $P < 0.05$ vs veh/veh). A) and C) The administration of HM01 at 10 and 30 mg/kg significantly prevented the decrease in digital and caudal NCV observed in oxaliplatin-treated mice. B) Digital potential amplitude was decreased by oxaliplatin administration and the HM01 treatment trended to normalize the potential amplitude, but only the administration of HM01 30 mg/kg was able to normalize this data. D) Caudal nerve potential amplitude was not significantly affected by oxaliplatin treatment.

and caudal NCV (reduced by $10.6 \pm 1.6\%$ and $8 \pm 1.1\%$ respectively, $P < 0.01$) vs vehicle-treated mice. Concurrent treatment with HM01 at both 10 and 30 mg/kg significantly prevented both these impairments (Fig. 3A and C). Digital potential amplitude was also decreased by oxaliplatin ($13.5 \pm 6.4\%$), although given the variability the effect did not reach statistical significance. HM01 treatment trended to normalize the potential amplitude decrease, so that at 30 mg/kg digital potential amplitude was significantly improved vs oxaliplatin-treated mice (by $33 \pm 9\%$; $P < 0.01$; Fig. 3B). Caudal nerve potential amplitude was not significantly affected by oxaliplatin treatment (Fig. 3D).

3.2.3. Pathological examination

No degenerative changes in the DRG neuronal cell bodies or satellite cells or in the sciatic nerve from oxaliplatin-treated mice were observed, and HM01 treatment itself did not cause any degenerative changes (data not shown).

In the footpads, oxaliplatin treatment produced a significant reduction in IENFD ($-31.7 \pm 3.5\%$, $P < 0.01$ vs vehicle-treated mice). Concurrent HM01 treatment completely normalized IENFD to vehicle treated mouse values at both 10 and 30 mg/kg ($P < 0.01$; Fig. 4).

3.2.4. HM01 pharmacokinetics following acute and chronic administration

HM01 demonstrated very high and dose dependent sciatic nerve and DRG exposure. After a single oral dose of 10 and 30 mg/kg, HM01 was readily absorbed and distributed in plasma and nerve tissues with peak concentrations within 0.25–0.5 h post dose. The terminal half-life of HM01

in plasma was short (approximately 1 h), but significantly longer in sciatic nerve (approximately 4.7 h). The area under the concentration-time curve extrapolated to infinity ($AUC_{0-\infty}$) was lowest in plasma and almost 3–4 fold higher in sciatic nerve and DRG, and correlated with administered doses, suggesting enhanced penetration of HM01 into the peripheral nervous system (Table 2, Fig. 5A and B). After 30 days of daily dosing, the tissue penetration index (ratio of tissue/plasma) of HM01 was further enhanced to about 9–12 fold in SN and 18–19 fold in DRG suggesting marked accumulation of HM01 in these tissues (Table 2 and Fig. 5C).

3.3. Bortezomib studies

3.3.1. Body weight changes

In the preventive study, during the first few weeks and until day 21 the animals co-treated with bortezomib and HM01 at different doses showed a significant increase in body weight vs CTRL and bortezomib groups at several time points. This difference, however, was not significant at the end of treatment (data not shown).

In the therapeutic setting, following 10 days co-treatment of bortezomib with HM01, animals showed a significant increase of body weight vs CTRL and bortezomib groups. At the end of treatment only the animals treated with BTZ + HM01 30 showed a significant increase in body weight vs CTRL and bortezomib groups ($P < 0.01$, data not shown).
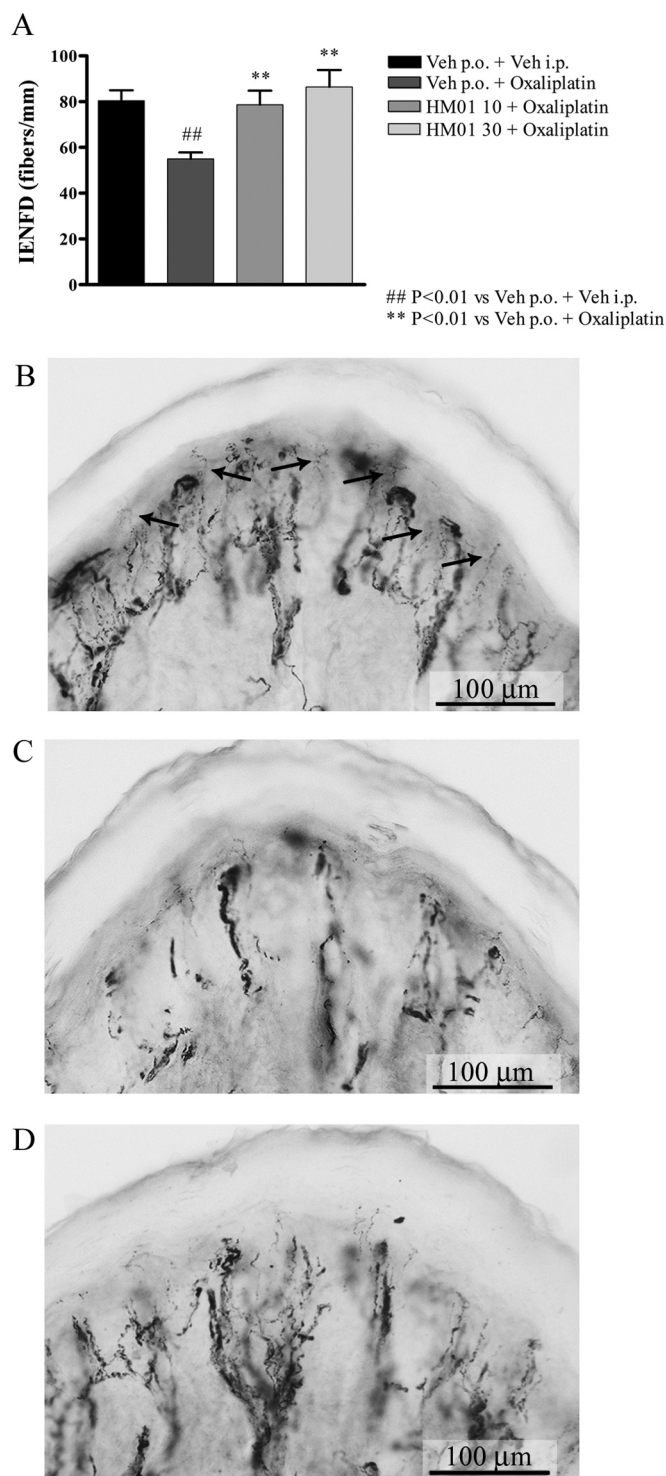
A

B

C

D

Fig. 4. HM01 reverses the reduction of intra-epidermal nerve fiber density (IENFD) in oxaliplatin-treated mice. IENFD was measured 24 h after last HM01 dose. Oxaliplatin produced a significant decrease in fiber number which was completely normalized by treatment with HM01 at 10 or 30 mg/kg daily (P < 0.01). A) The administration of HM01 at both 10 and 30 mg/kg was able to normalize IENFD to vehicle-treated mouse. Images B), C) and D) show representative pictures of skin biopsies obtained from mice treated with vehicle, oxaliplatin and oxaliplatin + HM01 30 mg/kg, respectively (arrows in panel B) indicate IENF).

3.3.2. Mechanical threshold

In both bortezomib studies, mechanical threshold was reduced by antineoplastic drug administration. At the end of treatment, in the preventive setting, the groups treated with bortezomib in combination with HM01 did not show allodynia vs CTRL, while this was observed in the bortezomib group (P < 0.001, Fig. 6A).

In the therapeutic setting (Fig. 6B), after 4 weeks all groups treated with bortezomib showed the development of allodynia with a reduction in the latency until withdrawal vs CTRL (P < 0.001). After 5 weeks (1 week of co-treatment) and at the end of treatment, only the groups treated with bortezomib alone had allodynia vs CTRL, while all the groups co-treated with HM01 were protected (P < 0.001).

3.3.3. Nerve conduction studies

In digital NCV the groups treated with bortezomib alone or in combination with HM01 3 and 10 mg/kg in the preventive setting showed a statistically significant reduction (P < 0.01 vs CTRL), while the group co-treated with BTZ + HM01 30 mg/kg had no alteration vs CTRL (Fig. 7A). No changes in digital potential amplitude were observed in all groups vs CTRL at the end of treatment (Fig. 7B).

All groups treated with bortezomib alone or in combination with HM01 in the preventive setting showed a statistically significant reduction in caudal NCV (P < 0.05 vs CTRL) as well as in caudal potential amplitude (P < 0.01 vs CTRL, Fig. 7C and D).

In the therapeutic setting, digital nerve NCV showed a statistically significant reduction only in the animals treated with bortezomib alone (P < 0.05 vs CTRL, Fig. 7E), while a reduction in potential amplitude was observed in the group co-treated with the highest dose of HM01 (P < 0.05 vs CTRL, Fig. 7F). All groups treated with bortezomib alone or in combination with HM01 showed a statistically significant reduction in caudal NCV and potential amplitude (P < 0.001 vs CTRL, Fig. 7G and H).

3.3.4. Pathological examination

Bortezomib-treated rats showed occasional degeneration of DRG sensory neurons and vacuolization of cytoplasm of satellite cells. The co-administration of HM01 in the preventive setting produced incomplete protection from these alterations (Fig. 8A-C). In the sciatic nerve mild axonal changes were evident in all the bortezomib-treated groups, and the co-administration of HM01 at different doses did not alter these changes (data not shown).

In the caudal nerve, the animals treated with bortezomib alone had reduced fiber density with axonal and Schwann cells degeneration while the animals co-treated with bortezomib and HM01 at different doses showed a mild, non-dose-dependent reduction in these pathological changes (Fig. 8D-F). The g-ratio assessment demonstrated significant (P < 0.001) axonopathy after bortezomib administration, and this effect was significantly prevented by HM01 co-treatment (Fig. S1).

These protective effects were not present when HM01 was delivered in the therapeutic setting.

Chronic treatment with bortezomib induced a statistically significant reduction of IENFD when compared to CTRL (P < 0.001). All doses of HM01 significantly prevented the reduction of IENFD induced by bortezomib in the preventive (Fig. 9), but not in the therapeutic setting, although an inhibitory trend was observed.

3.3.5. Proteasome inhibition study

Chronic treatment with bortezomib induced a statistically significant inhibition of proteasome activity; the co-administration of HM01 at different doses did not impair bortezomib-induced proteasome inhibition either in preventive or therapeutic settings (data not shown).

Table 2
HM01 Pharmacokinetic parameters following acute and chronic dosing.

Acute dosing

	C_{max} (pmol/ml or pmol/g)	T_{max} (h)	$t_{1/2}$ (h)	AUC_{0-t} (h x pmol/ml or h x pmol/g)	$AUC_{0-\infty}$ (h x pmol/ml or h x pmol/g)	Tissue penetration index (Tissue/plasma ratio)
10 mg/kg						
Plasma	1150	0.25	0.90	945.2	960.7	1
Sciatic nerve	1550	0.25	4.7	2923	2984.3	3.1
DRG	1713	0.25	NR	4296	4357.8	4.5
30 mg/kg						
Plasma	2726.8	0.25	1.1	4335.9	4375.2	1
Sciatic nerve	4966.1	0.5	4.7	14,220.3	14,546.6	3.3
DRG	4406.7	0.5	NR	12,247.3	12,380.6	2.8

Chronic dosing

Dose	Plasma pmol/ml	Sciatic Nerve pmol/g (pooled)	DRG pmol/g (pooled)	Tissue penetration index (SN/plasma ratio)	Tissue penetration index (DRG/plasma ratio)
10 mg/kg	703 (± 52)	6274	12,386	8.9	17.6
30 mg/kg	3113 (± 548)	37,346	58,819	12.0	18.9

NR (not reported) when correlation coefficient for terminal elimination < 0.9.

SN = sciatic nerve; DRG = dorsal root ganglia.
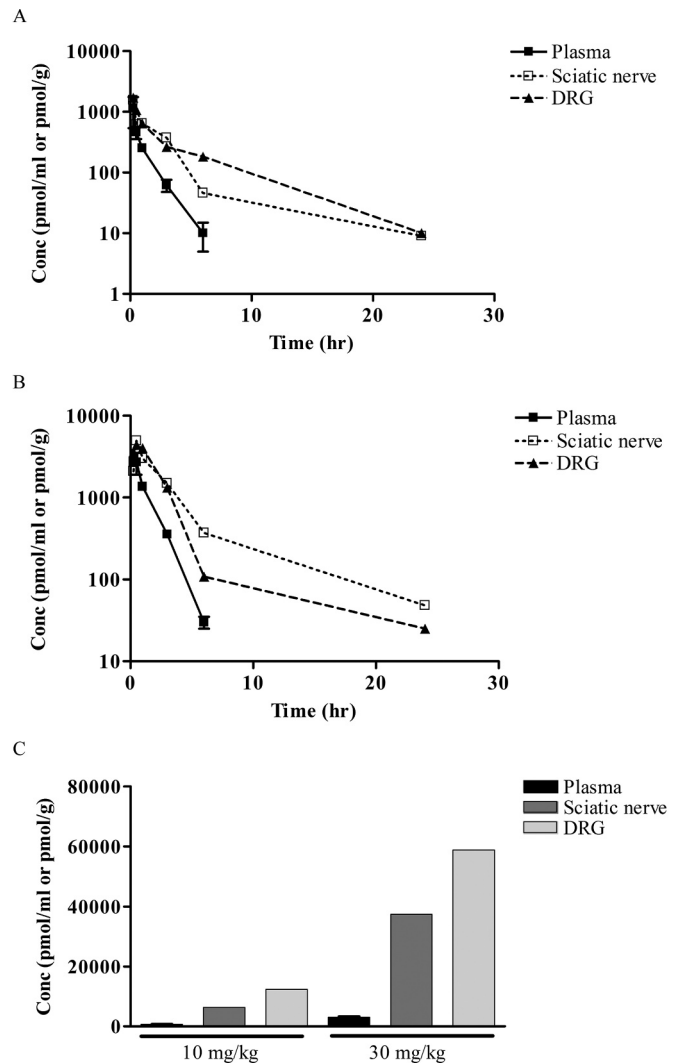
Fig. 5. Plasma, DRG and sciatic nerve concentrations of HM01. A) and B) After a single oral dose of HM01 at both 10 and 30 mg/kg the compound was readily absorbed and distributed in plasma and nerve tissues with peak concentrations within 0.25–0.5 h. The terminal half-life was short in plasma, but significantly longer in sciatic nerve and DRG; the compound showed excellent tissue penetration into both the sciatic nerves and DRG. C) After 30 days of daily dosing, the concentration of HM01 was very low in plasma but elevated in sciatic nerve and DRG suggesting marked accumulation of HM01 in these tissues.

4. Discussion

Ghrelin, is an endogenous ligand of the GHSR, which was originally identified in stomach and found to influence many metabolic processes, including growth hormone secretion, food intake and energy balance (Kojima et al., 1999; Tschop et al., 2000; Nakazato et al., 2001). Ghrelin and its functional receptor GHSR-1a are expressed in several CNS areas in rats including regions controlling pain transmission (Ferrini et al., 2009). Several studies have demonstrated that ghrelin can inhibit activation of microglia and secretion of proinflammatory cytokines (Moon et al., 2009; Theil et al., 2009), both processes involved in the development and maintenance of neuropathic pain in animal models. In a rat chronic constrictive injury model, intrathecal administration of ghrelin for 7 days attenuated signs of neuropathic pain and reduced inflammatory cytokines TNF-alpha, IL-1beta and IL-6, which in turn was attenuated by treatment with the ghrelin receptor antagonist [D-Lys3] GHRP-6 (Zhou et al., 2014). Ghrelins show acute anti-nociceptive

Fig. 6. HM01 administration reverted the allodynia induced by bortezomib. <u>Preventive setting.</u> A) At the end of treatment the groups treated with bo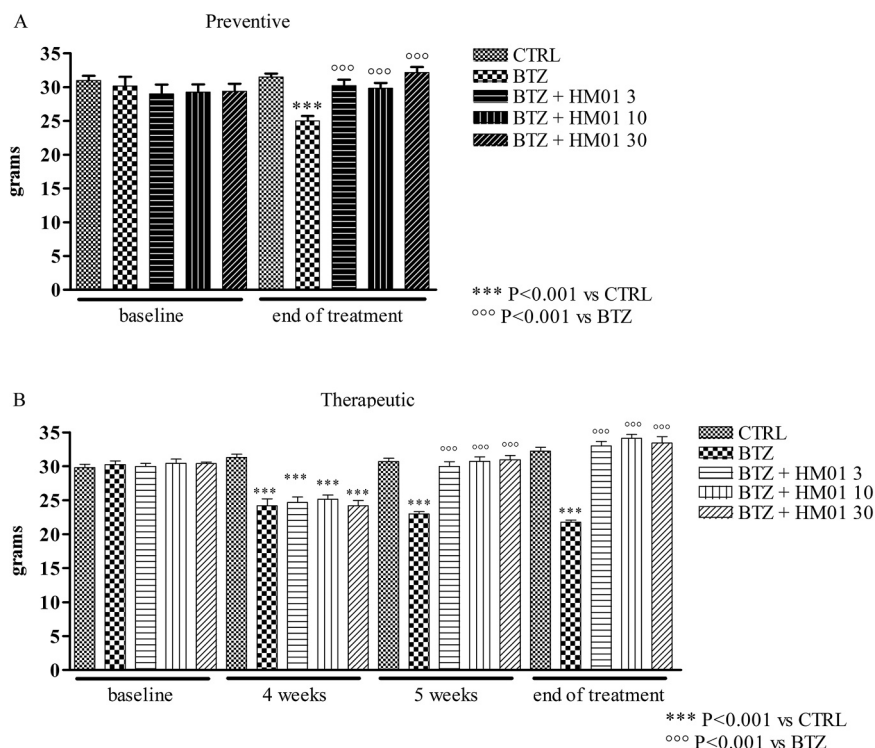rtezomib in combination with all doses of HM01 did not show allodynia, while this was observed in the rats treated with bortezomib alone. <u>Therapeutic setting.</u> B) Before the beginning of co-administration with HM01 (4weeks) all bortezomib-treated animals developed allodynia. After one week from the start of the co-treatment and at the end of treatment, only the groups treated with bortezomib alone had allodynia, while all the groups co-treated with HM01 were protected. (mechanical threshold was tested using the Dynamic Aesthesiometer, model 37450, Ugo Basile Biological Instruments, Comerio, Italy).

effects following intracerebroventricular injection (Wei et al., 2013) that are hypothesized to be mediated via direct activity at GHSR receptors and indirectly via delta and kappa opioid receptors.

HM01, a synthetic, brain penetrable, non-peptidic, ghrelin receptor agonist, was recently obtained with high binding affinity (K_i: $1.42 \pm 0.35\,nM$), excellent oral bioavailability (F% = 70.6%), significant brain penetration (brain/plasma ratio = 0.8) and a half-life after oral gavage in rats of 4.3 h (Karasawa et al., 2014). Moreover, we previously tested if any pathological effect on the nervous system could be produced by prolonged administration of HM01 in rats and the treatment at the maximum dose of 160 mg/kg p.o. (i.e. much higher than any dose used in the present studies) did not induce any change on peripheral nerves or spinal cord after 28 days repeated daily dosing (personal observation, unpublished data).

In this study we showed that once daily dosing of oral HM01 reverses chemotherapy-induced weight loss and decreased food intake in rats and mice (Table 3). These findings are consistent with previously reported effects of ghrelin in normal, as well as in tumor-bearing rodents (Tschop et al., 2000). HM01 reportedly mimics the neuronal effects of ghrelin in the arcuate nucleus (Borner et al., 2016) and promotes weight gain and stimulates food intake in normal and hepatoma tumor-bearing rats and mice (Villars et al., 2017). All these activities are consistent with the anti-cachexia effect observed with ghrelin agonists, in preclinical and clinical settings (Takayama et al., 2016; Temel et al., 2016; Villars et al., 2017).

Using mechanistically distinct, well-accepted acute and chronic preclinical CIPN models we tested the effect of HM01 administration on peripheral nerve structure and function. Moreover, in the bortezomib

models we also verified that no interference with the antineoplastic mechanism of action of the drug occurred (Kaplan et al., 2017). These animal models have been extensively used to test the effectiveness of putative neuroprotective treatments, thus providing the rationale for their use in our study.

In agreement with the results obtained using ghrelin injected systemically twice daily (Garcia et al., 2008), in all the tested conditions we consistently observed reduction in mechanical allodynia. The results obtained in the bortezomib models are particularly important, since this is the antineoplastic drug that induces the most painful, dose-limiting CIPN. These data are in line with previous results showing that ghrelin and/or another synthetic ghrelin agonist GHRP2, are effective in reducing hyperalgesia in preclinical models following cisplatin treatment, chronic constrictive injury or induction of diabetic neuropathy (Garcia et al., 2008; Tsuchimochi et al., 2013; Zhou et al., 2014), actions that are blocked by the ghrelin antagonist, [d-Lys3]-GHRP6 (Smith et al., 1993). These results are further supported by the demonstration in a rat model of visceral pain that the ghrelin antagonist H0900 was able to prevent the anti-nocifensive effect of HM01 as well as of the other ghrelin agonist ipamorelin (personal observation, unpublished data). The anti-nocifensive effects observed in our study was very rapid, as demonstrated by the results of the cisplatin study, and are likely centrally mediated since HM01 is highly brain penetrable.

Chemotherapy administration has been demonstrated to result in structural and functional changes in peripheral nerve, both in clinical and preclinical settings. Here, we observed that HM01 treatment prevented IENFD loss in oxaliplatin treated animals and ameliorated IENFD loss in bortezomib-treated animals in a preventive paradigm, but
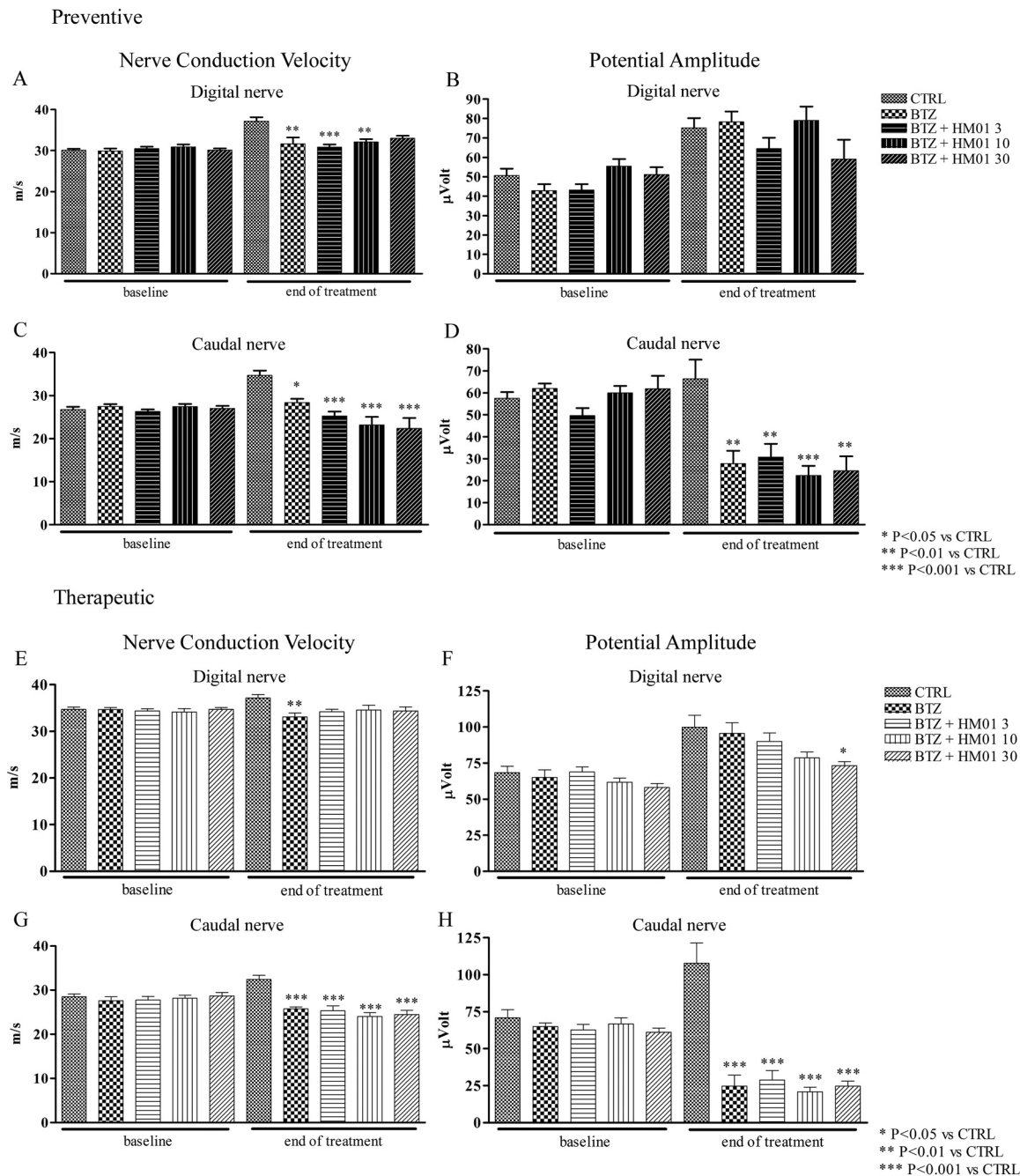
Fig. 7. Effect of HM01 on nerve conduction velocity (NCV) and potential amplitude in bortezomib-treated rats. Preventive setting. A) The treatment with bortezomib alone or in combination with HM01 at the doses of 3 and 10 mg/kg showed a statistically significant reduction in digital NCV, while the group co-treated with the highest dose of HM01 had no alteration if compared to CTRL. B) No changes in digital potential amplitude were observed in all groups. C) and D) All groups treated with bortezomib alone or in combination with all doses of HM01 showed a significant reduction in caudal NCV and potential amplitude. Therapeutic setting. E) and F) Only the animals treated with bortezomib alone showed a significant reduction in digital NCV, while a reduction in potential amplitude was observed only in the group co-treated with the highest dose of HM01. G) and H) As shown in preventive setting, all groups treated with bortezomib alone or in combination with all doses of HM01 had a significant reduction in caudal NCV and potential amplitude.

not a therapeutic one (Siau et al., 2006; Boyette-Davis et al., 2011; Boros et al., 2016). Similar patterns were seen for independently assessed electrophysiology parameters (nerve conduction velocity and amplitude) further supporting these conclusions. Together, these findings support that HM01 acts on both myelinated and unmyelinated axons, preventing both axonal loss as well as myelin alterations. However, the results obtained using long-term administration suggest that HM01 also has some peripheral trophic effect, since it provides a significant protection from drug-induced reduction in IENFD in both oxaliplatin and bortezomib models. The same result was recently also

observed in a paclitaxel animal model, where the co-administration of paclitaxel and ghrelin prevented the loss of IENFD induced by paclitaxel alone (Ishii et al., 2018). Importantly, in the therapeutic setting, reduction in allodynia was still significant, but it was not associated with any effect on IENFD, thus further supporting the hypothesis of a central analgesic effect that is dissociated from the peripheral neuroprotection and that the latter can occur only if HM01 treatment is started before small fiber depletion.

Besides this effect, additional activity of HM01 on myelinated sensory fibers of the peripheral nervous system is supported by the
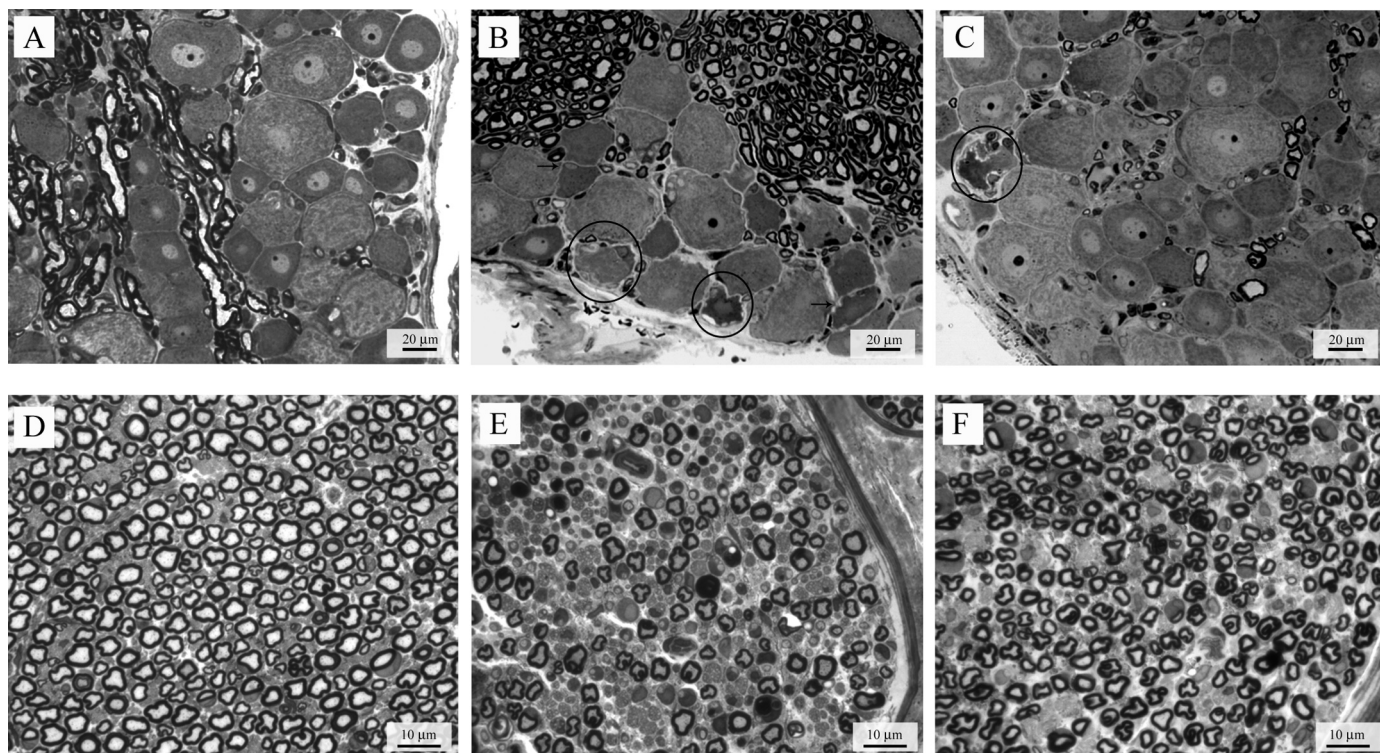
Fig. 8. Morphological examination of DRG and caudal nerve. <u>DRG.</u> The animals treated with bortezomib alone (B) showed occasional degeneration of DRG sensory neurons (circle) and vacuolization of cytoplasm of satellite cells (arrow) while the co-administration of HM01 (C) provided partial protection. <u>Caudal nerve.</u> The animals treated with bortezomib alone (E) showed a reduction in fiber density while the co-administration of HM01 (F) reduced the severity of these pathological changes. A) and D) show representative images obtained from control animals.
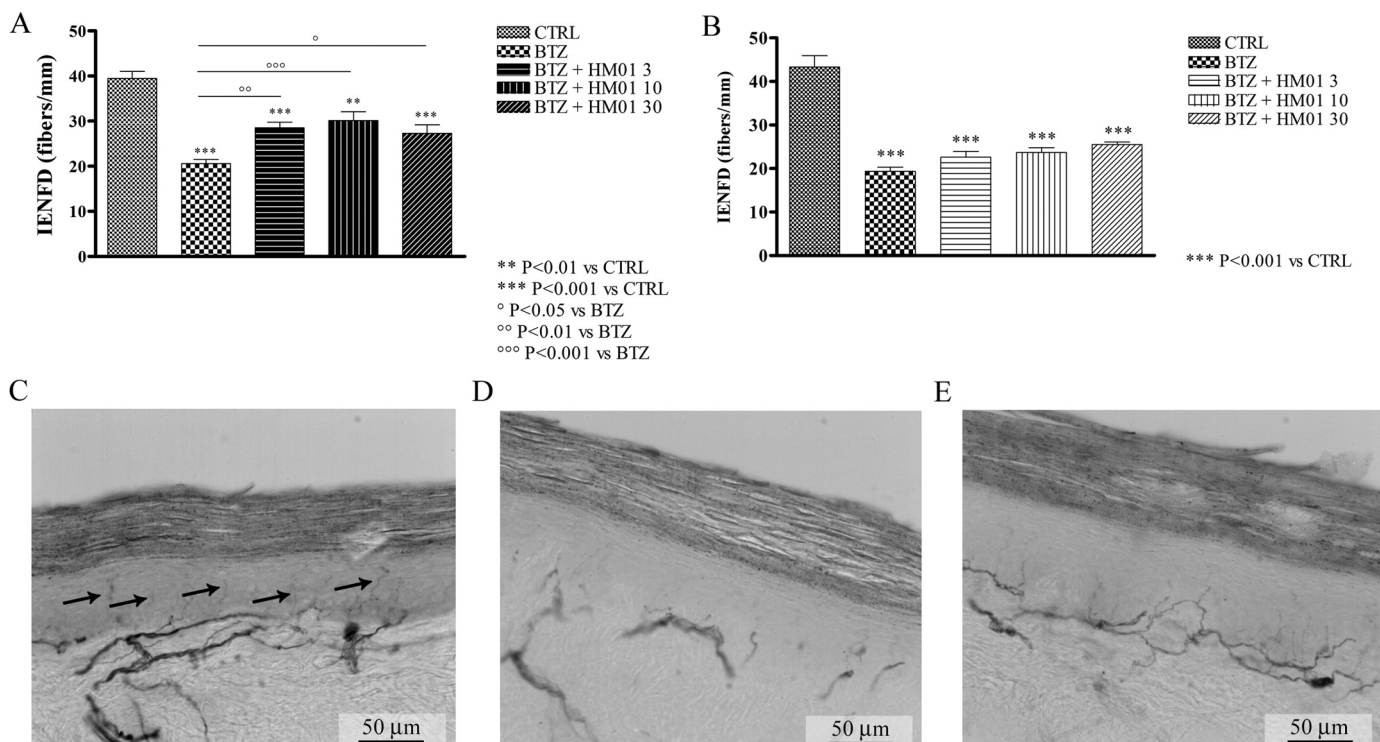
Fig. 9. Co-administration of HM01 limits the reduction of intra-epidermal nerve fiber density (IENFD) in bortezomib-treated rats. Chronic treatment with bortezomib induced a statistically significant reduction in IENFD; in the preventive setting (A), but not in the therapeutic setting (B), all doses of HM01 significantly ameliorated this reduction. Images C), D) and E) show representative pictures of skin biopsies obtained from control, bortezomib and bortezomib + HM01 30 mg/kg mice treated from the beginning of bortezomib administration (preventive setting), respectively (arrows in panel C) indicate IENF).

demonstration that HM01 attenuates some of the neurophysiologic deficits induced by chronic multiple dosing of oxaliplatin and, to a lesser extent, of bortezomib. In fact, the neurophysiological effect directly measured in peripheral nerves cannot be attributed to a central event, but rather to preservation in the responding number of peripheral axons. The presence of a bell shaped dose-response to HM01, where 10 mg/kg was generally more effective than 30 mg/kg, has also been noted previously for antinociceptive effects of ghrelin and the ghrelin agonist GHRP-2 given intracerebroventricularly (Wei et al., 2013; Zeng et al., 2014).

Despite consistent evidence of HM01 effectiveness at the behavioral and neurophysiologic levels, in our study pathological confirmation in the sciatic nerve and DRG of the protective effect of HM01 was partial and evidenced only in bortezomib CIPN, despite marked accumulation of HM01 in peripheral nerve and DRG (9–12 fold of that in plasma after chronic systemic dosing in mice).

Although ghrelin and HM01 have therapeutic potential for cancer cachexia (Collden et al., 2017), ghrelin treatment may raise concern about accelerating cancer progression, even in the absence of a direct interference with antineoplastic drugs in view of the well-demonstrated effect of ghrelin in the regulation of several processes related to cancer progression, especially in metastasis and proliferation (Lin and Hsiao, 2017). This concern could be correlated to the well-known increase of GH and IGF-1 induced by administration of ghrelin and ghrelin agonists. However, the increase is pulsatile in nature and in preclinical studies performed in nude mice implanted with A549 human NSCLC adenocarcinoma tumor cell line, both ghrelin and the ghrelin agonist Anamorelin after 28 consecutive days of treatment had no effect on tumor growth (Northrup et al., 2013). Moreover, concern regarding any increased risk of tumor formation from increased GH and IGF-1 levels was addressed in formal 2-year rodent carcinogenicity studies (Farris et al., 2007).

These studies demonstrated that prolonged administration of recombinant rat and recombinant mouse growth hormone (rmGH), sufficient to produce ~ 10-fold increases in GH levels and moderate increases in IGF-1 (~ 22%) in rats and mice compared vs control animals produced no increase in the incidence of tumor formation. However, in previous studies in rat we have reported that HM01 30 mg/kg p.o. produced 2.5 fold increase of the basal plasma GH (data not shown). These reassuring results are consistent with those of a recent systematic review on this topic (Sever et al., 2016).

The exact mechanisms underlying the ameliorative effects of HM01 against CIPN are unclear, although its effectiveness in very different models indicates that effects are not drug-specific and limited to a single toxicity mechanism, but rather suggest a widespread supportive, neurotrophic effect, in line with ghrelin's reported ability to promote peripheral nerve regeneration after injury (Raimondo et al., 2013). For instance, transgenic mice (Myh6/Ghrl) developed with cardiac specific ghrelin gene expression, reportedly displayed enhanced functional recovery over their wildtype counterparts after transection of their forelimb median nerves, although this may also be a reflection of direct anti-atrophic activity on skeletal muscle, independent of GHSR1a stimulation (Porporato et al., 2013). Ghrelin might also provide nerve protection by decreasing glutamate-mediated nerve toxicity, since ghrelin and its mimetics protect against glutamate excitotoxicity (Lim et al., 2011) and ischemia-induced injury, thought to be at least partially glutamate-mediated.

Indeed, glutamate-mediated toxicity appears to play a role in CIPN and an inhibitor of glutamate carboxypeptidase (an enzyme associated with glutamate release) protected against damage following cisplatin, paclitaxel or bortezomib treatment (Carozzi et al., 2010b). Moreover, bortezomib, paclitaxel and vincristine-induced hyperalgesia have all been associated with decreased expression of glutamate transporters in spinal astrocytes (Robinson and Dougherty, 2015). Given that spinal neurons show pronounced after-discharges that appear related to the downregulation of glutamate transporters and that similar changes in spinal neuron physiology are observed in vincristine and cisplatin neuropathies (Cata et al., 2008; Weng et al., 2003), downregulation of glutamate transporters may be a common mechanism across CIPN and a target for ghrelin or ghrelin agonists.

Another hypothesis behind the effect of HM01 could be related to the increase of IGF-1 which can counterbalance the same reduction of IGF-1 observed after chemotherapy treatment (Smith et al., 1993; Garcia et al., 2008).

Overall, there is a wealth of literature suggesting that ghrelin and the ghrelin receptor, GHSR1a, may be a novel target for therapy of various diseases. Our data with the ghrelin agonist HM01 in several different CIPN models, added to those already existing with ghrelin and other ghrelin agonists, support its potential utility as adjuvant in chemotherapy. The capacity of HM01 to penetrate in the CNS, coupled with its peripheral neurotrophic activity, the capacity to protect from different neurotoxic agents and its possible use to treat cancer cachexia makes this compound a unique putative neuroprotectant in cancer patients treated with neurotoxic chemotherapy.

Table 3
Summary of the assessment results in multiple neurotoxicity models.

Drug and schedule	HM01 dose	Body Weight	Allodynia	NCS	IENFD	DRG/nerve pathology
Cisplatin	3	+	ND	ND	ND	ND
0.5 mg/kg (i.p.) for three days	10	+	+	ND	ND	ND
	30	+	+	ND	ND	ND
Oxaliplatin	10	+	ND	+	+	=
6 mg/kg (i.p.) twice weekly for 4 weeks	30	+	ND	+	+	=
Bortezomib	3	+/-	+	–	+	–
Preventive setting	10	+/-	+	–	+	+/-
0.2 mg/kg (i.v.) 3 times/week for 8 weeks	30	+/-	+	+/-	+	+/-
Bortezomib	3	+/-	+	+/-	–	–
Therapeutic setting	10	+/-	+	+/-	–	+/-
0.2 mg/kg (i.v.) 3 times/week for 8 weeks	30	+/-	+	–	–	+/-

+ significant effect of HM01 vs antineoplastic drug; +/- partial effect of HM01 vs antineoplastic drug;- no effect of HM01 vs antineoplastic drug; = no effect of the antineoplastic drug; ND not done.

Acknowledgments

Author contribution

Name	Location	Role	Contribution
Alessia Chiorazzi	University of Milano-Bicocca, Italy	Author	Revised and approved the manuscript; drafted the manuscript; interpreted the data
Krystyna M. Wozniak	Johns Hopkins School of Medicine, USA	Author	Revised and approved the manuscript; designed the experiment; interpreted the data
Rana Rais	Johns Hopkins School of Medicine, USA	Author	Revised and approved the manuscript; drafted the manuscript; interpreted the data
Ying Wu	Johns Hopkins School of Medicine, USA	Author	Revised and approved the manuscript; performed the animal studies
Alexandra J. Gadiano	Johns Hopkins School of Medicine, USA	Author	Revised and approved the manuscript; performed the animal studies
Mohamed H. Farah	Johns Hopkins School of Medicine, USA	Author	Revised and approved the manuscript; performed the animal studies; interpreted the data
Ying Liu	Johns Hopkins School of Medicine, USA	Author	Revised and approved the manuscript; performed the animal studies
Annalisa Canta	University of Milano-Bicocca, Italy	Author	Revised and approved the manuscript; performed the animal studies; interpreted the data
Paola Alberti	University of Milano-Bicocca, Italy	Author	Revised and approved the manuscript; performed the animal studies
Virginia Rodriguez-Menendez	University of Milano-Bicocca, Italy	Author	Revised and approved the manuscript; performed the animal studies; interpreted the data
Cristina Meregalli	University of Milano-Bicocca, Italy	Author	Revised and approved the manuscript; performed the animal studies; interpreted the data
Giulia Fumagalli	University of Milano-Bicocca, Italy	Author	Revised and approved the manuscript; performed the animal studies
Laura Monza	University of Milano-Bicocca, Italy	Author	Revised and approved the manuscript; performed the animal studies
Eleonora Pozzi	University of Milano-Bicocca, Italy	Author	Revised and approved the manuscript; performed the animal studies
James J. Vornov	Medpace, USA	Author	Revised and approved the manuscript; performed the animal studies
Michael Polydefkis	Johns Hopkins School of Medicine, USA	Author	Revised and approved the manuscript; performed the animal studies; interpreted the data
Claudio Pietra	Helsinn Healthcare SA, Switzerland	Author	Revised and approved the manuscript; designed the experiment; interpreted the data
Barbara S. Slusher	Johns Hopkins School of Medicine, USA	Author	Revised and approved the manuscript; designed the experiment; interpreted the data
Guido Cavaletti	University of Milano-Bicocca, Italy	Author	Revised and approved the manuscript; designed the experiment; interpreted the data

Appendix A. Supporting information

Supplementary data associated with this article can be found in the online version at doi:10.1016/j.ejphar.2018.09.029

References

Baatar, D., Patel, K., Taub, D.D., 2011. The effects of ghrelin on inflammation and the immune system. Mol. Cell Endocrinol. 340, 44–58.

Banks, W.A., Tschop, M., Robinson, S.M., Heiman, M.L., 2002. Extent and direction of ghrelin transport across the blood-brain barrier is determined by its unique primary structure. J. Pharmacol. Exp. Ther. 302, 822–827.

Borner, T., Loi, L., Pietra, C., Giuliano, C., Lutz, T.A., Riediger, T., 2016. The ghrelin receptor agonist HM01 mimics the neuronal effects of ghrelin in the arcuate nucleus and attenuates anorexia-cachexia syndrome in tumor-bearing rats. Am. J. Physiol. Regul. Integr. Comp. Physiol. ajpregu 2016 (00044).

Boros, K., Jancsó, G., Dux, M., Fekécs, Z., Bencsik, P., Oszlács, O., Katona, M., Ferdinandy, P., Nógrádi, A., Sántha, P., 2016. Multiple impairments of cutaneous nociceptor function induced by cardiotoxic doses of Adriamycin in the rat. Naunyn Schmiede. Arch. Parmacol. 389, 1009–1020.

Boyette-Davis, J., Xin, W., Zhang, H., Dougherty, P., M., 2011. Intraepidermal nerve fiber loss corresponds to the development of Taxol-induced hyperalgesia and can be prevented by treatment with minocycline. Pain 152, 308–313.

Carozzi, V.A., Canta, A., Oggioni, N., Sala, B., Chiorazzi, A., Meregalli, C., Bossi, M., Marmiroli, P., Cavaletti, G., 2010a. Neurophysiological and neuropathological characterization of new murine models of chemotherapy-induced chronic peripheral neuropathies. Exp. Neurol. 226, 301–309.

Carozzi, V.A., Chiorazzi, A., Canta, A., Lapidus, R.G., Slusher, B.S., Wozniak, K.M., Cavaletti, G., 2010b. Glutamate carboxypeptidase inhibition reduces the severity of chemotherapy-induced peripheral neurotoxicity in rat. Neurotox. Res. 17, 380–391.

Cata, J.P., Weng, H.R., Dougherty, P.M., 2008. Behavioral and electrophysiological studies in rats with cisplatin-induced chemoneuropathy. Brain Res. 1230, 91–98.

Chaplan, S.R., Bach, F.W., Pogrel, J.W., Chung, J.M., Yaksh, T.L., 1994. Quantitative assessment of tactile allodynia in the rat paw. J. Neurosci. Methods 53, 55–63.

Chung, H., Kim, E., Lee, D.H., Seo, S., Ju, S., Lee, D., Kim, H., Park, S., 2007. Ghrelin inhibits apoptosis in hypothalamic neuronal cells during oxygen-glucose deprivation. Endocrinology 148, 148–159.

Collden, G., Tschop, M.H., Muller, T.D., 2017. Therapeutic potential of targeting the ghrelin pathway. Int. J. Mol. Sci. 18.

Farris, G.M., Miller, G.K., Wollenberg, G.K., Molon-Noblot, S., Chan, C., Prahalada, S., 2007. Recombinant rat and mouse growth hormones: risk assessment of carcinogenic potential in 2-year bioassays in rats and mice. Toxicol. Sci. 97, 548–561.

Ferrini, F., Salio, C., Lossi, L., Merighi, A., 2009. Ghrelin in central neurons. Curr. Neuropharmacol. 7, 37–49.

Furness, J.B., Hunne, B., Matsuda, N., Yin, L., Russo, D., Kato, I., Fujimiya, M., Patterson, M., McLeod, J., Andrews, Z.B., Bron, R., 2011. Investigation of the presence of ghrelin in the central nervous system of the rat and mouse. Neuroscience 193, 1–9.

Gahete, M.D., Cordoba-Chacon, J., Kineman, R.D., Luque, R.M., Castano, J.P., 2011. Role of ghrelin system in neuroprotection and cognitive functions: implications in Alzheimer's disease. Peptides 32, 2225–2228.

Garcia, J.M., Cata, J.P., Dougherty, P.M., Smith, R.G., 2008. Ghrelin prevents cisplatin-induced mechanical hyperalgesia and cachexia. Endocrinology 149, 455–460.

Granado, M., Priego, T., Martin, A.I., Villanua, M.A., Lopez-Calderon, A., 2005. Anti-inflammatory effect of the ghrelin agonist growth hormone-releasing peptide-2 (GHRP-2) in arthritic rats. Am. J. Physiol. Endocrinol. Metab. 288, E486–E492.

Hosoda, H., Kangawa, K., 2012. Standard sample collections for blood ghrelin measurements. Methods Enzymol. 514, 113–126.

Hotta, M., Ohwada, R., Akamizu, T., Shibasaki, T., Takano, K., Kangawa, K., 2009. Ghrelin increases hunger and food intake in patients with restricting-type anorexia nervosa: a pilot study. Endocr. J. 56, 1119–1128.

Howard, A.D., Feighner, S.D., Cully, D.F., Arena, J.P., Liberator, P.A., Rosenblum, C.I., Hamelin, M., Hreniuk, D.L., Palyha, O.C., Anderson, J., Paress, P.S., Diaz, C., Chou, M., Liu, K.K., McKee, K.K., Pong, S.S., Chaung, L.Y., Elbrecht, A., Dashkevicz, M., Heavens, R., Rigby, M., Sirinathsinghji, D.J., Dean, D.C., Melillo, D.G., Patchett, A.A., Nargund, R., Griffin, P.R., DeMartino, J.A., Gupta, S.K., Schaeffer, J.M., Smith, R.G., Van der Ploeg, L.H., 1996. A receptor in pituitary and hypothalamus that functions in growth hormone release. Science 273, 974–977.

Ishii, N., Tsubouchi, H., Miura, A., Yanagi, S., Ueno, H., Shiomi, K., Nakazato, M., 2018. Ghrelin alleviates paclitaxel-induced peripheral neuropathy by reducing oxidative stress and enhancing mitochondrial anti-oxidant functions in mice. Eur. J. Pharmacol. 819, 35–42.

Kaplan, G.S., Torcun, C.C., Grune, T., Ozer, N.K., Karademir, B., 2017. Proteasome inhibitors in cancer therapy: treatment regimen and peripheral neuropathy as a side effect. Free Radic. Biol. Med. 103, 1–13.

Karasawa, H., Pietra, C., Giuliano, C., Garcia-Rubio, S., Xu, X., Yakabi, S., Taché, Y., Wang, L., 2014. New ghrelin agonist, HM01 alleviates constipation and L-dopa-delayed gastric emptying in 6-hydroxydopamine rat model of Parkinson's disease. Neurogastroenterol. Motil. 26, 1771–1782.

Kluge, M., Schussler, P., Dresler, M., Schmidt, D., Yassouridis, A., Uhr, M., Steiger, A., 2011. Effects of ghrelin on psychopathology, sleep and secretion of cortisol and growth hormone in patients with major depression. J. Psychiatr. Res. 45, 421–426.

Kojima, M., Hosoda, H., Date, Y., Nakazato, M., Matsuo, H., Kangawa, K., 1999. Ghrelin is a growth-hormone-releasing acylated peptide from stomach. Nature 402, 656–660.

Lim, E., Lee, S., Li, E., Kim, Y., Park, S., 2011. Ghrelin protects spinal cord motoneurons against chronic glutamate-induced excitotoxicity via ERK1/2 and phosphatidylinositol-3-kinase/Akt/glycogen synthase kinase-3beta pathways. Exp. Neurol. 230, 114–122.

Lin, T.C., Hsiao, M., 2017. Ghrelin and cancer progression. Biochim. Biophys. Acta 1868, 51–57.

Meregalli, C., Canta, A., Carozzi, V.A., Chiorazzi, A., Oggioni, N., Gilardini, A., Ceresa, C., Avezza, F., Crippa, L., Marmiroli, P., Cavaletti, G., 2010. Bortezomib-induced painful neuropathy in rats: a behavioral, neurophysiological and pathological study in rats. Eur. J. Pain 14, 343–350.

Meregalli, C., Chiorazzi, A., Carozzi, V.A., Canta, A., Sala, B., Colombo, M., Oggioni, N., Ceresa, C., Foudah, D., La Russa, F., Miloso, M., Nicolini, G., Marmiroli, P., Bennett, D.L., Cavaletti, G., 2014. Evaluation of tubulin polymerization and chronic inhibition of proteasome as citotoxicity mechanisms in bortezomib-induced peripheral neuropathy. Cell Cycle 13, 612–621.

Meregalli, C., Carozzi, V.,A., Sala, B., Chiorazzi, A., Canta, A., Oggioni, N., Rodriguez-Menendez, V., Ballarini, E., Ceresa, C., Nicolini, G., Crippa, L., Orciani, M., Cavaletti, G., Marmiroli, P., 2015. Bortezomib-induced peripheral neurotoxicity in human multiple myeloma-bearing mice. J. Biol. Regul. Homeost. Agents 2015 (29), 115–124.

Moon, M., Kim, H.G., Hwang, L., Seo, J.H., Kim, S., Hwang, S., Kim, S., Lee, D., Chung, H., Oh, M.S., Lee, K.T., Park, S., 2009. Neuroprotective effect of ghrelin in the 1-methyl-4-phenyl-1,2,3,6-tetrahydropyridine mouse model of Parkinson's disease by blocking microglial activation. Neurotox. Res. 15, 332–347.

Nagaya, N., Moriya, J., Yasumura, Y., Uematsu, M., Ono, F., Shimizu, W., Ueno, K., Kitakaze, M., Miyatake, K., Kangawa, K., 2004. Effects of ghrelin administration on left ventricular function, exercise capacity, and muscle wasting in patients with chronic heart failure. Circulation 110, 3674–3679.

Nakazato, M., Murakami, N., Date, Y., Kojima, M., Matsuo, H., Kangawa, K., Matsukura, S., 2001. A role for ghrelin in the central regulation of feeding. Nature 409, 194–198.

Northrup, R., Kuroda, K., Duus, E.M., Barnes, S.R., Cheatham, L., Wiley, T., Pietra, C., 2013. Effect of ghrelin and anamorelin (ONO-7643), a selective ghrelin receptor agonist, on tumor growth in a lung cancer mouse xenograft model. Support Care Cancer 21, 2409–2415.

Porporato, P.E., Filigheddu, N., Reano, S., Ferrara, M., Angelino, E., Gnocchi, V.F., Prodam, F., Ronchi, G., Fagoonee, S., Fornaro, M., Chianale, F., Baldanzi, G., Surico, N., Sinigaglia, F., Perroteau, I., Smith, R.G., Sun, Y., Geuna, S., Graziani, A., 2013. Acylated and unacylated ghrelin impair skeletal muscle atrophy in mice. J. Clin. Invest. 123, 611–622.

Raimondo, S., Ronchi, G., Geuna, S., Pascal, D., Reano, S., Filigheddu, N., Graziani, A., 2013. Ghrelin: a novel neuromuscular recovery promoting factor? Int. Rev. Neurobiol. 108, 207–221.

Robinson, C.R., Dougherty, P.M., 2015. Spinal astrocyte gap junction and glutamate transporter expression contributes to a rat model of bortezomib-induced peripheral neuropathy. Neuroscience 285, 1–10.

Sanger, G.J., Furness, J.B., 2016. Ghrelin and motilin receptors as drug targets for gastrointestinal disorders. Nat. Rev. Gastroenterol. Hepatol. 13, 38–48.

Sever, S., White, D.L., Garcia, J.M., 2016. Is there an effect of ghrelin/ghrelin analogs on cancer? A systematic review. Endocr. Relat. Cancer 23, R393–R409.

Siau, C., Xiao, W., Bennett, G., J., 2006. Paclitaxel- and vincristine-evoked painful peripheral neuropathies: loss of epidermal innervation and activation of Langerhans cells. Exp. Neurol. 201, 507–514.

Smith, R.G., Cheng, K., Schoen, W.R., Pong, S.S., Hickey, G., Jacks, T., Butler, B., Chan, W.W., Chaung, L.Y., Judith, F., Taylor, J., Wyvratt, M.J., Fisher, M.H., 1993. A nonpeptidyl growth hormone secretagogue. Science 260, 1640–1643.

Steculorum, S.M., Bouret, S.G., 2011. Developmental effects of ghrelin. Peptides 32, 2362–2366.

Takayama, K., Katakami, N., Yokoyama, T., Atagi, S., Yoshimori, K., Kagamu, H., Saito, H., Takiguchi, Y., Aoe, K., Koyama, A., Komura, N., Eguchi, K., 2016. Anamorelin (ONO-7643) in Japanese patients with non-small cell lung cancer and cachexia: results of a randomized phase 2 trial. Support Care Cancer 24, 3495–3505.

Temel, J.S., Abernethy, A.P., Currow, D.C., Friend, J., Duus, E.M., Yan, Y., Fearon, K.C., 2016. Anamorelin in patients with non-small-cell lung cancer and cachexia (ROMANA 1 and ROMANA 2): results from two randomised, double-blind, phase 3 trials. Lancet Oncol. 17, 519–531.

Theil, M.M., Miyake, S., Mizuno, M., Tomi, C., Croxford, J.L., Hosoda, H., Theil, J., von Hörsten, S., Yokote, H., Chiba, A., Lin, Y., Oki, S., Akamizu, T., Kangawa, K., Yamamura, T., 2009. Suppression of experimental autoimmune encephalomyelitis by ghrelin. J. Immunol. 183, 2859–2866.

Tong, J., Dave, N., Mugundu, G.M., Davis, H.W., Gaylinn, B.D., Thorner, M.O., Tschöp, M.H., D'Alessio, D., Desai, P.B., 2013. The pharmacokinetics of acyl, des-acyl, and total ghrelin in healthy human subjects. Eur. J. Endocrinol. 168, 821–828.

Tschop, M., Smiley, D.L., Heiman, M.L., 2000. Ghrelin induces adiposity in rodents. Nature 407, 908–913.

Tsuchimochi, W., Kyoraku, I., Yamaguchi, H., Toshinai, K., Shiomi, K., Kangawa, K., Nakazato, M., 2013. Ghrelin prevents the development of experimental diabetic neuropathy in rodents. Eur. J. Pharmacol. 702, 187–193.

Villars, F.O., Pietra, C., Giuliano, C., Lutz, T.A., Riediger, T., 2017. Oral treatment with the ghrelin receptor agonist HM01 attenuates cachexia in mice bearing colon-26 (C26) tumors. Int. J. Mol. Sci. 18.

Wei, J., Zhi, X., Wang, X.L., Zeng, P., Zou, T., Yang, B., Wang, J.L., 2013. In vivo characterization of the effects of ghrelin on the modulation of acute pain at the supraspinal level in mice. Peptides 43, 76–82.

Weng, H.R., Cordella, J.V., Dougherty, P.M., 2003. Changes in sensory processing in the spinal dorsal horn accompany vincristine-induced hyperalgesia and allodynia. Pain 103, 131–138.

Wozniak, K.M., Nomoto, K., Lapidus, R.G., Wu, Y., Carozzi, V., Cavaletti, G., Hayakawa,

K., Hosokawa, S., Towle, M.J., Littlefield, B.A., Slusher, B.S., 2011. Comparison of neuropathy-inducing effects of eribulin mesylate, paclitaxel, and ixabepilone in mice. Cancer Res. 71, 3952–3962.

Zeng, P., Li, S., Zheng, Y.H., Liu, F.Y., Wang, J.L., Zhang, D.L., Wei, J., 2014. Ghrelin receptor agonist, GHRP-2, produces antinociceptive effects at the supraspinal level via the opioid receptor in mice. Peptides 55, 103–109.

Zhou, C.H., Li, X., Zhu, Y.Z., Huang, H., Li, J., Liu, L., Hu, Q., Ma, T.F., Shao, Y., Wu, Y.Q., 2014. Ghrelin alleviates neuropathic pain through GHSR-1a-mediated suppression of the p38 MAPK/NF-kappaB pathway in a rat chronic constriction injury model. Reg. Anesth. Pain. Med. 39, 137–148.